REPORT SERIES IN AEROSOL SCIENCE
N:o 150 (2014)

SULFURIC ACID AND AMINES IN ATMOSPHERIC CLUSTERING: FIRST-PRINCIPLES INVESTIGATIONS

VILLE LOUKONEN

Division of Atmospheric Sciences
Department of Physics
Faculty of Science
University of Helsinki
Helsinki, Finland

Academic dissertation

To be presented, with the permission of the Faculty of Science of the University of Helsinki, for public criticism in auditorium E204, Gustaf Hällströmin katu 2, on May 9th, 2014, at 12 o'clock noon.

Helsinki 2014

Author's Address: Department of Physics
P.O. Box 64
FI-00014 University of Helsinki
ville.loukonen@helsinki.fi

Supervisors: Professor Hanna Vehkamäki, Ph.D.
Department of Physics
University of Helsinki

Docent Theo Kurtén, Ph.D.
Department of Chemistry
University of Helsinki

Reviewers: Professor David Reguera, Ph.D.
Departament de Física Fonamental
Universitat de Barcelona

Senior application specialist Atte Sillanpää, Ph.D.
CSC – IT Center for Science Ltd.
Espoo, Finland

Opponent: Senior research scientist Shawn M. Kathmann, Ph.D.
Physical Science Division
Pacific Northwest National Laboratory
Richland, WA, USA

ISBN 978-952-5822-92-2 (printed version)
ISSN 0784-3496
Helsinki 2014
Unigrafia Oy

ISBN 978-952-5822-93-9 (pdf version)
http://ethesis.helsinki.fi
Helsinki 2014
Helsingin yliopiston verkkojulkaisut

Acknowledgements

First and foremost, I thank my two supervisors, Prof. Hanna Vehkamäki and Doc. Theo Kurtén – your support, guidance and friendship ever since my sophomore university year are deeply appreciated.

The research presented in this thesis was carried out at the Division of Atmospheric Sciences of the Department of Physics of the University of Helsinki. I thank Prof. Markku Kulmala for the opportunity to work here and Prof. Juhani Keinonen and Prof. Hannu Koskinen for providing the working facilities.

I thank my coauthors for their contributions to the research of this thesis. I am especially thankful to Dr. I-Feng William Kuo for hosting my research visit at the Lawrence Livermore National Laboratory.

Maj and Tor Nessling Foundation and Academy of Finland are acknowledged for financial support, CSC – IT Center for Science, Ltd. and Livermore Computing Center for providing computational resources.

I am grateful to Prof. David Reguera and Dr. Atte Sillanpää for reviewing this thesis.

I thank my colleagues at the Division of Atmospheric Sciences, especially the past and present members of the computational aerosol physics group, for providing a pleasant and inspiring working atmosphere. I also thank Prof. R. Benny Gerber for reminding me why physics is fun.

I thank my friends and family for their mostly indirect contributions, and especially Dr. Niko Aarne for the extended loan of his keyboard. Lastly, I thank my spouse Niina for sharing her life with me throughout these years and often enough reminding me that there is much besides physics in the world.

"I have approximate answers and possible beliefs, in different degrees of certainty, about different things. But I'm not absolutely sure of anything and of many things I don't know anything about, such as whether it means anything to ask why we're here and what the question might mean. I might think about it a little bit, if I can't figure it out, then I go onto something else. But I don't have to know an answer. I don't feel frightened by not knowing things, by being lost in the mysterious universe without having any purpose, which is the way it really is, as far as I can tell, possibly. It doesn't frighten me." – R. P. F.

Ville Anton Loukonen
University of Helsinki, 2014

Abstract

The physical phenomena involving minuscule atmospheric aerosol particles pose many important and currently unresolved questions. The research presented in this doctoral dissertation concentrates on one of the most fundamental of these questions: where do the smallest particles come from? This thesis investigates the *very* first steps of new-particle formation, that is, atmospherically relevant molecular clustering. The main tools used in the research were electronic structure calculations and first-principles molecular dynamics simulations – basically, applied quantum mechanics.

The lead role in the presented cluster studies is played by sulfuric acid. Sulfuric acid is known to correlate well with the aerosol particle formation observations in most locations. However, it is further known that sulfuric acid alone cannot be responsible for the ambient observations. In the past, various formation mechanisms to explain the observations have been suggested, most popular being those involving some combination of water, ammonia, oxidized organics or ions together with sulfuric acid. Although all of these agents have a stabilizing effect on the clustering of sulfuric acid, in general the magnitude of the stabilization is too weak to account for most of the atmospheric measurements.

In this thesis, the role of various amine compounds (especially that of dimethylamine) in sulfuric acid driven clustering is investigated. Amines are some of the few basic compounds that are known to exist in the atmosphere. According to the electronic structure calculations, amines stabilize the smallest sulfuric acid clusters much more strongly than the earlier standard candidate ammonia. Further calculations suggest that dimethylamine also enhances the growth of the small clusters with respect to sulfuric acid much more effectively than ammonia. Based on the electronic structure calculations, the stabilizing effect of the amines is strong enough, so that even relatively small concentrations can be expected to significantly enhance the sulfuric acid driven new-particle formation. This theoretical prediction has later been confirmed experimentally.

The dynamics and stability of the small sulfuric acid and dimethylamine clusters were further studied by first-principles molecular dynamics simulations. In equilibrium, the clusters exhibited pronounced thermal molecular motion, which was observed to be anharmonic. Direct collision simulations revealed rich dynamical behavior, leading to cluster structures differing from both the equilibrium simulations and the static electronic structure calculations. The performed first-principles molecular dynamics simulations demonstrate that the method is well fitted to investigate the atmospheric molecular clustering, and suggest that in future formation free energy calculations, the entropic contributions merit a more detailed treatment.

Keywords: sulfuric acid, dimethylamine, molecular clustering, applied quantum mechanics

Contents

List of publications

This thesis consists of an introductory review, followed by four research articles. In the introductory part, these papers are cited according to their roman numerals. Papers **I** and **II** are reprinted under the Creative Commons Attribution 3.0 License. Papers **III** and **IV** are reproduced with permissions from Elsevier Ltd. and Taylor & Francis publishing companies, respectively.

I Kurtén, T., Loukonen, V., Vehkamäki, H., and Kulmala, M. (2008). Amines are likely to enhance neutral and ion-induced sulfuric acid-water nucleation in the atmosphere more effectively than ammonia. *Atmos. Chem. Phys.*, 8: 4095–4103.

II Loukonen, V., Kurtén, T., Ortega, I. K., Vehkamäki, H., Pádua, A. A. H., Sellegri, K., and Kulmala, M. (2010). Enhancing effect of dimethylamine in sulfuric acid nucleation in the presence of water – a computational study. *Atmos. Chem. Phys.*, 10: 4961–4974.

III Loukonen, V., Kuo, I-F., W., McGrath, M. J., and Vehkamäki, H. (2014). On the stability and dynamics of (sulfuric acid)(ammonia) and (sulfuric acid)(dimethylamine) clusters: A first-principles molecular dynamics investigation. *Chem. Phys.*, 428: 164–174.

IV Loukonen, V., Bork, N., and Vehkamäki, H. (2014). From collisions to clusters: first steps of sulphuric acid nanocluster formation dynamics. *Mol. Phys.*, published online, http://dx.doi.org/10.1080/00268976.2013.877167.

1 From quantum mechanics to air quality and climate change

From the redshifted starlight in our expanding universe to dew in the morning light, Nature simply bewilders the willing: the alert observer is charmed with a plethora of phenomena. Over hundreds of millennia, the awed wondering slowly shaped into a language – a language with which we are finally able to discuss the world we experience in detail. This language is physics.

The present doctoral dissertation with its extended context provides one particular example of the *dulce et utile* of the physical sciences. The theoretical and computational work presented here deals with a handful of small molecular clusters, and thus concentrates on the phenomena taking place at the Ångström and picosecond scales – near the bottom of the fathomable spatial and temporal scales. However, the context and the main motivation behind the investigations is the phenomenon of aerosol particle formation in the Earth's atmosphere. These aerosol particles can be solid, liquid or amorphous agglomerations of molecules, which nevertheless are clumped together in such a way that they can be distinguished from their carrier gas as "particles". The particles and the carrier gas together constitute the definition of "aerosols" (Hinds, 1999). This is a very general definition and it is immediately clear that the concept of aerosols encompasses a large amount of interesting and important features of the physical world. Beside the everyday examples of dust, mist and pressurized spray-can products, aerosols also participate in much more grievous processes. Strikingly, aerosol particles directly affect the daily lives of millions of people in the form of deteriorated air quality: air pollution by particulate matter was recently assessed to be one of the leading global causes of death and disability (Lim et al., 2012). Although particulate matter is most strongly associated with serious health effects such as heart failure, also the gaseous air pollutants ozone, carbon monoxide, nitrogen dioxide and sulfur dioxide have a negative impact (Shah et al., 2013). Sulfur dioxide (SO_2) is an important compound in many ways: in addition to causing health effects, it is the main source for sulfuric acid (H_2SO_4) production in the atmosphere (Seinfeld and Pandis, 2006). This is significant, as sulfuric acid is one of the main drivers of atmospheric new-particle formation (Kuang et al., 2008).

It turns out that without the aerosol particles, we would not have clouds in the atmospheric boundary layer: there simply is not enough water for it to condense by itself

to form clouds (Seinfeld and Pandis, 2006). Pre-existing surfaces are needed to help water condense. This surface often comes in the form of cloud condensation nuclei, which essentially are large aerosol particles (on the order of 0.1 to 0.3μm) (Seinfeld and Pandis, 2006). To make this chain of physical processes even more interesting, current estimates state that up to half of the cloud condensation nuclei form around aerosol particles which are formed in the atmosphere (Merikanto et al., 2009). Clouds, in turn, have a paramount global significance by regulating Earth's radiative budget – and thus, the global temperature (Seinfeld and Pandis, 2006).

Even though the research presented in this dissertation concentrates on molecular clustering on sub-nanometer scale, it has serious ramifications on regional and global scales.

1.1 Sulfuric acid, atmospheric new-particle formation — and the amines

It is a well-established experimental fact that sulfuric acid is a central player in atmospheric new-particle formation, at least over the continental boundary layer[1] (see for example Kulmala et al., 2004; Kuang et al., 2008; Kerminen et al., 2010; Chen et al., 2012). It is equally well known that sulfuric acid alone, even with the ubiquitous water, cannot explain the observed ambient particle formation events. The reason for this is simple: there is not nearly enough sulfuric acid in the air to produce the observed particle formation rates by itself. Typically, the atmospheric sulfuric acid concentration is 10^6–10^7 $\#/\mathrm{cm}^3$ on relatively pristine locations and 10^7–10^8 $\#/\mathrm{cm}^3$ at more polluted sites (Kuang et al., 2008). Recent ultraclean state-of-the-art laboratory experiments demonstrated that with these sulfuric acid concentrations, the binary sulfuric acid - water particle formation mechanism yields particle formation rates of 10^{-1} $\#/\mathrm{cm}^3\mathrm{s}$ at maximum — several orders of magnitude smaller than the ambient rates at the same concentrations (Kirkby et al., 2011). The conclusion is clear: something else besides sulfuric acid and water is needed to explain the atmospheric observations.

In the real atmosphere there are myriads of compounds other than sulfuric acid and water. Many of these have a biological origin. It would seem likely that at least a

[1]This thesis concentrates only on sulfuric acid driven new-particle formation. However, sulfuric acid is not the only player in the game. For example, in Mace Head, Ireland, iodine compounds have been strongly connected to the new-particle formation (O'Dowd et al., 2002).

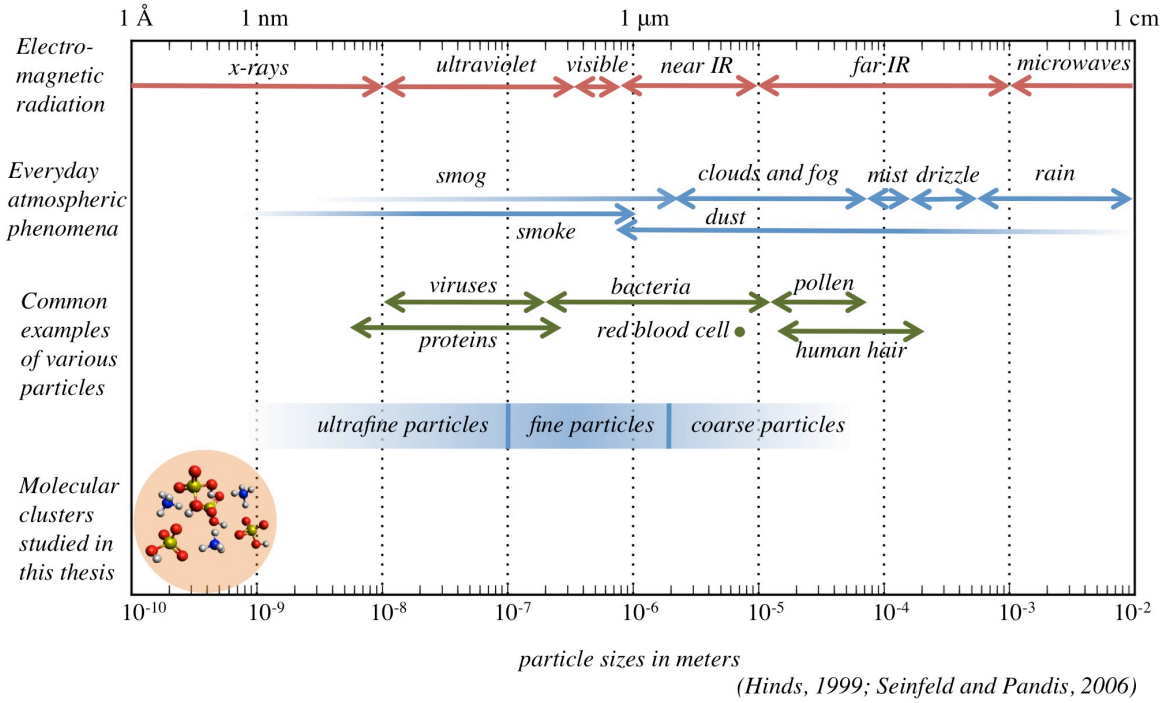

Figure 1: Aerosol physics related phenomena cover size ranges of several orders of magnitude. The molecular clusters investigated in this thesis represent the small end of the spectrum.

fraction of these compounds took part in the aerosol formation processes. Indeed, it is currently believed that much of the aerosol particle growth comes from various organic compounds (see for example Yli-Juuti, 2013). However, the role of the organics in the very first steps of particle formation is still largely unknown (Schobesberger et al., 2013; Ehn et al., 2014). In the past, attention has been given to the role of ammonia in the new-particle formation. There are good reasons for this: (a) ammonia is a *base* compound — it is likely to cluster effectively with sulfuric *acid*; and, (b) it is known to exist in the atmosphere and to find its way into the aerosol particles — there are numerous observations of ammonium sulfate and bisulfate aerosols (Seinfeld and Pandis, 2006). Indeed, the ternary mechanism of sulfuric acid - ammonia - water has been the "standard candidate" to explain atmospheric aerosol particle formation for many years. Consequently, the importance of the mechanism has been discussed extensively (Coffman and Hegg, 1995; Ball et al., 1999; Ianni and Bandy, 1999; Larson et al., 1999; Korhonen et al., 1999; Anttila et al., 2005; Kurtén et al., 2007a; Torpo et al., 2007; Nadykto and Yu, 2007; Kirkby et al., 2011). In addition to ammonia, also

the role of ions in the process has roused heated debate (Raes et al., 1986; Turco et al., 1998; Lovejoy et al., 2004; Kazil et al., 2006; Iida et al., 2006; Sorokin and Arnold, 2007; Manninen et al., 2009; Kulmala et al., 2010; Kirkby et al., 2011). According to the argument, ions enhance sulfuric acid driven new-particle formation enough to explain the ambient observations. Recently, based on detailed experimental and theoretical work (Kirkby et al., 2011; Almeida et al., 2013), the community is reaching towards consensus on the roles of ammonia and ions: they both do enhance the particle formation in comparison to the pure binary sulfuric acid - water mechanism, but still not strongly enough to explain most of the observed ambient particle formation rates. There are of course exceptions. For example, in polluted environments with high ammonia and sulfuric acid concentrations the standard ternary mechanism seems to explain the observations quite well (Jung et al., 2009; Chen et al., 2012). However, to understand the formation mechanisms at work on more pristine locations, something is still missing. This dissertation considers one possible explanation: *the amines.*

Amines are species derived from ammonia (NH_3) by replacing one or more of ammonia's hydrogen atoms with some (organic) functional groups. This thesis concentrates on alkyl amines where the hydrogens have been substituted by simple alkyl groups. The main emphasis is on dimethylamine ($(CH_3)_2NH$) where two of the hydrogens have been replaced by methyl groups. Like ammonia, amines are base molecules, and are thus expected to bind readily to sulfuric acid. In fact, judging from the proton affinity and gas phase basicity, amines considered here are much stronger bases than ammonia (Hunter and Lias, 1998; Ruusuvuori et al., 2013). Various amines are also known to exist in the atmosphere. Amines have both anthropogenic and natural sources, the former dominating (Ge et al., 2011). For example, dimethylamine emissions have been reported from such human activities as animal husbandry, fish processing, sewers, landfills and various industries. The concentrations of different amines in the atmosphere vary greatly. In general, the concentrations are likely to be quite local as the atmospheric lifetimes of the amines are typically short, on the order of few hours. Unfortunately, the literature on amine concentration measurements is rather scarce. For dimethylamine, concentrations of few parts per trillion in volume have been reported (Hanson et al., 2011; Yu et al., 2012). Dimethylamine has also been found in larger particles detected via filter samples. In one particular study (Mäkelä et al., 2001), the dimethylamine concentrations were 50-fold on new-particle formation event days as compared to non-event days, thus strongly suggesting that the amine might have something to do with particle formation and/or growth. This finding was one of the

motivating experimental results behind this thesis.

1.1.1 This thesis: review of papers and author's contribution

The research presented in this thesis seeks to illuminate the role of amines in sulfuric acid driven atmospheric new-particle formation, using a variety of computational methods.

Paper I applies *ab initio* electronic structure calculations to investigate the structures and formation energetics of dimer clusters containing either sulfuric acid or bisulfate ion together with an ammonia molecule or seven different amines possibly present in the atmosphere. According to the calculations, all the studied sulfuric acid - amine clusters are significantly more strongly bound than the sulfuric acid - ammonia cluster, whereas the binding in most of the bisulfate - amine clusters is only moderately stronger than the binding between ammonia and bisulfate. Further calculations, studying the addition of sulfuric acid to the dimer complexes of sulfuric acid or bisulfate ion with ammonia or dimethylamine, demonstrate that the amine enhances the acid addition much more efficiently than ammonia, both in the electrically neutral and negative cases. Although there probably is much more ammonia than amines in the atmosphere, the differences in the calculated formation free energies are large enough to overcome the differences in the concentrations, implying that the amines might have an important role in enhancing the sulfuric acid driven new-particle formation. The author is responsible for performing most of the calculations and data analysis, and writing a significant part of the paper.

Paper II studies explicitly the effect of hydration on the roles of ammonia and dimethylamine in sulfuric acid driven clustering. A variety of computational tools are applied: pair potential molecular dynamics are used to obtain initial cluster structures, which are then optimized using density functional theory, and the final electronic energies are calculated using wavefunction based electronic correlation method. The calculated formation free energies of one to two sulfuric acids with either ammonia or dimethylamine and from zero to five water molecules show that the amine enhances acid addition to the one-acid complexes much more efficiently than ammonia, when there are zero or more than two water molecules in the cluster. Further sensitivity analysis based on hydrate distribution calculations suggests that, within tropospherically relevant relative humidity and concentration ranges, dimethylamine promotes the clustering along the

sulfuric acid axis much more efficiently than ammonia. The author is responsible for part of the initial planning, performing all the molecular dynamics simulations and the electronic structure calculations, analyzing the data, and writing most of the paper.

Paper III investigates the stability and dynamics of various sulfuric acid - ammonia and sulfuric acid - dimethylamine clusters using first-principles molecular dynamics simulations. The simulations, driven by density functional theory, are performed in the $NVT(T = 300$ K) ensemble to explicitly study the role of the kinetic energy at non-zero temperatures. In the 35 ps long equilibrium simulations the clusters are found to exhibit quite pronounced thermal movement. Regardless of this motion, the clusters are observed to stay bound together. However, due to the thermal motion the calculated electric dipole moments show large fluctuations. The molecular movement of the clusters is further investigated by determining the vibrational spectra from the autocorrelation function of the electric dipole moment. The thermal motion of the clusters is found to be anharmonic. The author is responsible for the original idea, performing all the first-principles molecular dynamics simulations, electric dipole moment and vibrational spectra calculations, analyzing the data, and writing most of the paper.

Paper IV presents direct first-principles molecular dynamics collision simulations investigating the very first steps of dimethylamine enhanced sulfuric acid clustering. Both the collisions between sulfuric acid and dimethylamine, and between sulfuric acid monohydrate and dimethylamine are studied using density functional theory driven simulations. The sticking factor in the head-on collisions is found to be unity: the interaction between the molecules is strong enough to overcome the possible non-optimal initial collision geometries. Furthermore, no post-collisional cluster break-up is observed. The efficient clustering is likely due to the proton transfer from the acid to the amine, which is observed to take place in each of the collisions, and due to the subsequent competition over the proton control. This mechanism is found to lead to very dynamic cluster structures, differing from the static optimized clusters and from the dynamical equilibrium clusters. It is also observed from the simulations that the water molecule is able stabilize the formed clusters by accommodating a fraction of the released clustering energy. The author is responsible for the original idea, performing most of the collision simulations and all of the equilibrium simulations, analyzing the data, and writing most of the paper.

The author is solely responsible for the introductory review of this thesis, rest of which

is organized as follows: in sections 2 and 3, the computational methods used in the research are reviewed. Then, in section 4, it is outlined how these methods can be used to study atmospheric clustering and new-particle formation. Finally, section 5, discussing the impact and significance of the presented work in a larger context, closes the introductory part of this doctoral thesis.

2 Electronic structure methods: *solving the Schrödinger!*

The vast majority of the numerous computer hours spent during the research of this thesis was used to solve the time-independent Schrödinger equation

$$\hat{H}\Psi = E\Psi \tag{1}$$

of the studied molecules or molecular clusters. Here E is the ground state energy of the system and Ψ is the corresponding wavefunction. The physics, which ultimately determines both E and Ψ, is encoded in the Hamiltonian operator $\hat{H}$ (shown here in atomic units)

$$\hat{H} = \underbrace{-\sum_{i=1}^{N}\frac{1}{2}\nabla_i^2}_{\equiv\hat{T}_\mathrm{e}} \underbrace{-\sum_{\alpha=1}^{N_\mathrm{nuclei}}\frac{1}{2M_\alpha}\nabla_\alpha^2}_{\equiv\hat{T}_\mathrm{n}} \underbrace{-\sum_{i=1}^{N}\sum_{\alpha=1}^{N_\mathrm{nuclei}}\frac{Q_\alpha}{\hat{r}_{i\alpha}}}_{\equiv\hat{V}_\mathrm{ne}} + \underbrace{\sum_{i=1}^{N}\sum_{j>i}^{N}\frac{1}{\hat{r}_{ij}}}_{\equiv\hat{V}_\mathrm{ee}} + \underbrace{\sum_{\alpha=1}^{N_\mathrm{nuclei}}\sum_{\beta>\alpha}^{N_\mathrm{nuclei}}\frac{Q_\alpha Q_\beta}{\hat{R}_{\alpha\beta}}}_{\equiv\hat{V}_\mathrm{nn}}. \tag{2}$$

$\hat{T}_\mathrm{e}$ and $\hat{T}_\mathrm{n}$ are the kinetic energy operators of the electrons and the atomic nuclei, and $\hat{V}_\mathrm{ee}$, $\hat{V}_\mathrm{ne}$ and $\hat{V}_\mathrm{nn}$ describe the interactions between the electrons, the electrons and the nuclei, and between the nuclei, respectively. The operator ∇_i^2 operates on the electronic and the ∇_α^2 on the nuclear coordinates, M_α is the mass and Q_α is the atomic number of the nucleus α and $\hat{r}_{i\alpha} = |\hat{r}_i - \hat{R}_\alpha|$, $\hat{r}_{ij} = |\hat{r}_i - \hat{r}_j|$ and $\hat{R}_{\alpha\beta} = |\hat{R}_\alpha - \hat{R}_\beta|$ are operators between the electron i and the nucleus α, the electrons i and j, and between the nuclei α and β, respectively. This is a general non-relativistic Hamiltonian applicable to many-atom systems (Szabo and Ostlund, 1996). Concentrating on fairly light species at atmospherically relevant energies renders the relativistic corrections unnecessary, especially as in this thesis the main interest is on the energetic differences, not on the absolute values. The fine and hyperfine structure can also be neglected.

Born-Oppenheimer approximation To solve equation (1) for a molecule or a molecular cluster is a very non-trivial task. Further approximations are necessarily needed. Usually, the first approximation called on is the Born-Oppenheimer approximation – this is also the case in all of the calculations performed in this thesis. The Born-Oppenheimer approximation formalizes the colloquial notion that the atomic nuclei are much heavier than the electrons and consequently their dynamics take place in vastly different time scales. Thus, under the approximation, the total wavefunction describing the whole system can be factorised into a product of the nuclear $\chi(R)$

and electronic $\psi(r)$ contributions (Leach, 2001). The main gain behind this separation is the possibility to solve only the electronic wavefunction with fixed nuclear positions: the nuclear coordinates are only parameters in the electronic Hamiltonian $\hat{H}_{\text{elec}} \equiv \hat{T}_{\text{e}} + \hat{V}_{\text{ne}} + \hat{V}_{\text{ee}} + \hat{V}_{\text{nn}}$ and in the corresponding wavefunction. Solving the electronic Hamiltonian for various nuclear configurations yields a set of ground state electronic energies as a function of the nuclear coordinates[2]. Even though the nuclear positions are only constant parameters in the electronic Hamiltonian, they specify the locations of the positive charge in the system, and thus have an important role in defining the electron distributions. Theoretically, collecting a very large number N_{VL} of electronic energies E_{elec} constructs an effective nuclear potential: $\{E^{(i)}_{\text{elec}}(R)\}_{i=1,\ldots,N_{VL}} \rightarrow V_{\text{eff}}(R)$. The effective nuclear potential V_{eff} is often called *the potential energy surface*. Incorporating the potential V_{eff} with the nuclear kinetic energy operator $\hat{T}_{\text{n}}$ produces the so-called nuclear Schrödinger equation

$$\left(\hat{T}_{\text{n}} + V_{\text{eff}}(R)\right) \chi(R) = E\chi(R). \tag{3}$$

Solving equation (3) would give all the details of the quantized vibrational and rotational nuclear motion, under the assumption that the electronic and nuclear degrees of freedom are decoupled. In theory, that is. Solving the nuclear Schrödinger equation for even the smallest cluster considered in this thesis, the clusters of $(\text{sulfuric acid})_1(\text{water})_1$ (see paper **II**), is a tremendous amount of work, even with further approximations (see for example Partanen et al., 2012).

Although the effective nuclear potential V_{eff} appears to be an attractive idea only theoretically, there are some useful practical corollaries. As suggested by equation (3), one can think of the atomic nuclei as points "moving" on the potential energy surface (hence the name). Mapping the complete surface for the clusters under investigation in this thesis is beyond the current computational capabilities, but one can hope to find some minima on the surface. The minima correspond to more or less stable configurations of the nuclear coordinates: the force exerted by the atomic nuclei on each other in the molecule/cluster is proportional to the gradient of the potential – which vanishes at the minima. In general, for any molecular cluster there are several local minima on the potential energy surface, and thus there are several stable cluster structures. It is evident, then, that the important task is to find the *global* minimum on the surface: the minimum energy cluster.

[2]Of course, solving the electronic Hamiltonian yields *all* the electronic states of the system. However, only the ground state energy has relevance in the cluster studies discussed here.

The search for the global minimum, or structure optimization, poses a large challenge in all fields involving molecules or other many-atom systems. The sulfuric acid clusters studied in this thesis are particularly difficult to optimize. The clusters are bound only via hydrogen bonds, and correspondingly, the potential energy surface is often fairly flat and contains several local minima. The high acidity of sulfuric acid also complicates the situation: the acid can form bisulfate (HSO_4^-) or even sulfate (SO_4^{2-}) ions, depending on the close chemical environment, that is, what else is in the cluster. This renders the global optimization schemes relying on random sampling or on evolutionary mutations quite inefficient. Typically, the search for the global minimum energy cluster is at least a two-step process. First, using for example physical intuition or lower-level computational methods, plausible candidates for the minimum configurations are obtained. Then, these candidate structures are optimized at the chosen level of electronic structure theory using a *local optimizer algorithm*. It should be emphasized that a robust local optimizer is invaluable in the electronic structure calculations based on minimum energy geometries. It is the local optimizer which fine-tunes the bond lengths and angles and ultimately decides for example whether or not a proton transfer happens. These optimizers come in many forms and shapes, but common to all of them is the necessity to solve the electronic Schrödinger equation

$$\hat{H}_{\text{elec}}\psi(r) = E_{\text{elec}}\psi(r). \tag{4}$$

The optimizers try to find the minimum of the ground state energy by moving the atomic nuclei. Often the moves are guided by the forces acting on the system, which are obtained by the gradients of the electronic energy (the forces can also be used to integrate the nuclear equations of motion, see section 3). There is no way around it: one needs to solve the equation (4) many, many times during a typical computational cluster investigation. In the papers **I** and **II** this equation is solved during the optimization process, and in the papers **III** and **IV** during each timestep (see section 3).

Wavefunction methods The smallest cluster studied in this thesis is the cluster of one sulfuric acid and one water molecule, $(H_2SO_4)_1(H_2O)_1$. Already this small cluster contains 60 electrons. These 60 electrons interact with each other and with the ten atomic nuclei. The coordinates of the atomic nuclei are "frozen" in space according to the Born-Oppenheimer approximation, but still, it is a 60-body problem with an external potential. Considering only the valence electrons, as is typically done, reduces this to a 40-body problem. Still, $\mathcal{N}$-body problems with $\mathcal{N} \geq 3$ interacting particles are rather difficult to solve, and one must invoke more approximations. As

often as the Born-Oppenheimer is the first approximation, in wavefunction based electronic structure methods the second one is the so-called *Hartree-Fock approximation*. In the Hartree-Fock approximation one makes the drastic assumption that the electrons do not interact directly with each other, but feel only an average potential due to the other electrons (Szabo and Ostlund, 1996). The total N-electron wavefunction is approximated by some combination of products of the N independent 1-electron wavefunctions: $\psi(\vec{r}_1, \vec{r}_2, \ldots, \vec{r}_N) \propto \varphi_1(\vec{r}_1)\varphi_2(\vec{r}_2)\cdots\varphi_N(\vec{r}_N)$. Electrons are fermions, so the wavefunction must be antisymmetric under the interchange of any two electron coordinates in the system. Furthermore, the wavefunction must obey the Pauli exclusion principle. Both of these conditions are satisfied if the wavefunction takes the form of a Slater determinant:

$$\psi^{SD}(\vec{r}_1, \vec{r}_2, \ldots, \vec{r}_N) = \frac{1}{\sqrt{N!}} \begin{vmatrix} \varphi_1(\vec{r}_1) & \varphi_2(\vec{r}_1) & \ldots & \varphi_N(\vec{r}_1) \\ \varphi_1(\vec{r}_2) & \varphi_2(\vec{r}_2) & \ldots & \varphi_N(\vec{r}_2) \\ \vdots & \vdots & \ddots & \vdots \\ \varphi_1(\vec{r}_N) & \varphi_2(\vec{r}_N) & \ldots & \varphi_N(\vec{r}_N) \end{vmatrix}. \tag{5}$$

The 1-electron functions φ_i are often called *spin orbitals*, due to historical reasons. In the non-relativistic approach the spin degree of freedom is taken into account in an *ad hoc* fashion, where each spin orbital consists of a spatial orbital which can accommodate two spin states. The results obtained crucially depend on how well the spin orbitals are able to describe the physics of the system. However, to obtain any results at all, the electronic Schrödinger equation must be manipulated into a form somewhat more susceptible for computation. This can be done with the help of variational calculus. By minimizing the expectation value of the electronic energy, $\langle\psi^{SD}|\hat{H}_{\text{elec}}|\psi^{SD}\rangle$, with respect to the 1-electron functions φ_i, one can turn the N-electron Schrödinger equation into N *Hartree-Fock equations*:

$$\begin{aligned} \Big(\frac{1}{2}\nabla_i^2 - \sum_{\alpha=1}^{M}\frac{Q_\alpha}{\hat{r}_{i\alpha}}\Big)\varphi_i(\vec{r}_1) + \sum_{j=1}^{N}\Big(\int \varphi_j^*(\vec{r}_2)\frac{1}{\hat{r}_{12}}\varphi_j(\vec{r}_2)\varphi_i(\vec{r}_1)\, d\vec{r}_2 \\ - \int \varphi_j^*(\vec{r}_2)\frac{1}{\hat{r}_{12}}\varphi_i(\vec{r}_2)\varphi_j(\vec{r}_1)\, d\vec{r}_2\Big) = \epsilon_i\varphi_i(\vec{r}_1) \qquad i = 1...N. \end{aligned} \tag{6}$$

The Hartree-Fock equations are a set of coupled, non-local, non-linear integro-differential equations. It is worth noting that the solution for any φ_i depends on the solutions of all the other φ_j's. Thus, the equations must be solved iteratively. In practice, typically the equations are converted into a matrix form and solved via quite

sophisticated matrix manipulation routines (Szabo and Ostlund, 1996). The Hartree-Fock energy is obtained as:

$$E_{\text{elec}}^{\text{HF}} = \sum_{i}^{N} \epsilon_i - \frac{1}{2} \sum_{i=1}^{N} \sum_{j=1}^{N} \Big(\int \varphi_i^*(\vec{r}_1) \varphi_j^*(\vec{r}_2) \frac{1}{\hat{r}_{12}} \varphi_i(\vec{r}_1) \varphi_j(\vec{r}_2) \; d\vec{r}_1 \; d\vec{r}_2 - \int \varphi_i^*(\vec{r}_1) \varphi_j^*(\vec{r}_2) \frac{1}{\hat{r}_{12}} \varphi_j(\vec{r}_1) \varphi_i(\vec{r}_2) \; d\vec{r}_1 \; d\vec{r}_2 \Big), \tag{7}$$

where the energy ϵ_i corresponds to the energy of an electron described by the 1-electron wavefunction φ_i. The Hartee-Fock equations were derived by variational calculus, and as a consequence, the solution will provide the best possible one-determinant, non-interacting, independent particle approximation wavefunction ψ^{SD} in the average static Coulomb field, with the corresponding ground state energy $E_{\text{elec}}^{\text{HF}}$.

Electron correlation It turns out that this scheme can attain around 99% of the total electronic energy. However, it is the missing one percent of the electronic energy that is often very important for chemical bonding, especially in the case of weakly-bound molecular clusters. Intuitively, this makes sense: electron-electron correlation should have a role in the bonding of the clusters. In the literature, there are numerous methods building on the Hartree-Fock solution which are devised to capture at least part of the correlation energy. In a way or another, all these methods extend the Hartree-Fock solution by taking into account some number and combination of excited Slater determinants (Jensen, 2007). It is evident that for all but the smallest of systems, the possible combinations of the excitations is huge, and correspondingly, most of the post–Hartree-Fock methods are computationally very intensive. Currently, the "gold standard" in the electron correlation of closed-shell systems is the so-called CCSD(T) coupled cluster method, which considers both the single and double excitations explicitly and the triple excitations perturbatively (Pople et al., 1987). Unfortunately, the computational burden of CCSD(T) is too heavy for most of the clusters under study here. Instead, two more affordable electron correlation methods were used in papers **I** and **II**: the RI-CC2 coupled cluster method (Hättig and Weigend, 2000) and the second-order Møller-Plesset perturbation theory RI-MP2 (Weigend and Häser, 1997). The former takes into account the double excitations in an approximative manner, and in the latter the electron correlation is treated as a small perturbation on top of the Hartree-Fock solution. Both of the methods further accelerate the calculations by using the resolution of the identity (RI) approximation. These methods represent first level of improvement on the Hartree-Fock energies, and are able to obtain roughly 80-90 % of the electron correlation energy (Jensen, 2007).

Density functional theory In addition to the wavefunction based electronic structure methods, also *density functional theory* was used to solve the electronic Schrödinger equation in paper **II**, and exclusively in papers **III** and **IV**. Density functional theory (henceforth DFT) is a very elegant reformulation of the general electronic structure problem. As can be seen from the Hamiltonian (2), in wavefunction based methods the key quantities defining the physics are the number of electrons and the "external potential": the number, the type and the location of atomic nuclei. In DFT the key quantity is the total electron density ρ:

$$\rho(\vec{r}_1) = \int |\Psi(\vec{r}_1, \vec{r}_2, \ldots \vec{r}_N)|^2 \, d\vec{r}_2 \cdots d\vec{r}_N, \tag{8}$$

where Ψ is the total wavefunction of the system[3]. The number of electrons N is then obtained as:

$$N = \int \rho(\vec{r}_1) \, d\vec{r}_1. \tag{9}$$

It turns out that the electron density determines the external potential (Hohenberg and Kohn, 1964). As the electron density also determines the number of electrons, it then determines the ground state wavefunction, and with that, the physics of the system – in the ground state (Parr and Yang, 1989). The physical property which interests us here is the ground state electronic energy. Now, DFT states that for an *interacting* many-electron system, the ground state energy is unambiguously determined by the electron density. Furthermore, as an N-electron system has $3N$ degrees of freedom, the total density is *always* just a three-dimensional function (neglecting spin). Unfortunately, there is a catch: although it can be shown that the ground state energy is a functional of the electron density, this functional is not known. Thus, to make any use of DFT, one needs to develop approximative energy functionals. In addition to this, typically the electron density is expressed with the help of auxiliary functions – often with the very same functions which are used with the wavefunction based methods:

$$\rho(\vec{r}) = \sum_{i=1}^{N} |\varphi_i(\vec{r})|^2. \tag{10}$$

Within the Born-Oppenheimer approximation, the general form of the electronic energy functional can be expressed as:

$$E[\rho(\vec{r})] = T_\mathrm{e}[\rho] + V_\mathrm{ext}[\rho] + V_\mathrm{ee}[\rho] + E_\mathrm{XC}[\rho], \tag{11}$$

[3]We assume here that the ground state is non-degenerate and shall not consider the spin degree of freedom explicitly; neither of these is a problem in DFT, but they make some of the equations more cumbersome.

where T_e is the kinetic energy functional

$$T_\mathrm{e}[\rho(\vec{r})] = -\frac{1}{2}\sum_{i=1}^{N}\int \varphi_i^*(\vec{r})\nabla^2\varphi_i(\vec{r})\; d\vec{r}, \tag{12}$$

V_ext describes in general the interaction between the electrons and some "external potential" – in this thesis it is the Coulomb potential between the electrons and the atomic nuclei

$$V_\mathrm{ext}[\rho(\vec{r})] = \int v_\mathrm{ext}(\vec{r})\rho(\vec{r})\; d\vec{r}, \tag{13}$$

V_ee is the Coulombic repulsion between the electrons

$$V_\mathrm{ee}[\rho(\vec{r})] = \frac{1}{2}\int \frac{\rho(\vec{r})\rho(\vec{r\prime})}{|\vec{r}-\vec{r\prime}|}\; d\vec{r}\, d\vec{r\prime}, \tag{14}$$

and the last term, E_XC, takes care of all the exchange and correlation effects – this is the only unknown term and must be approximated in one way or another. Looking at expression (11), one realizes that the energy can be readily evaluated once the functions φ_i are known and the functional E_XC chosen. Similarly to the wavefunction based methods, these functions are found iteratively by solving the *Kohn-Sham equations*:

$$\Big(-\frac{1}{2}\nabla^2 + \int \frac{\rho(\vec{r\prime})}{|\vec{r}-\vec{r\prime}|}\; d\vec{r\prime} + v_\mathrm{ext}(\vec{r}) + \epsilon_\mathrm{XC}(\vec{r})\Big)\varphi_i(\vec{r}) = \epsilon_i\varphi_i(\vec{r}), \tag{15}$$

which are derived by variational calculus from the energy expression above. The Kohn-Sham equations are quite similar to the Hartree-Fock equations (see equation (6)): both describe the electronic energy of the system, they both are derived in similar ways, and they must be solved similarly. However, there is one important difference between the equations. The solution to the Hartree-Fock equations is the ideal non-interacting, mean field solution, which serves as a starting point for post–Hartree-Fock methods estimating the electronic correlation. On the other hand, the solution to the Kohn-Sham equations already contains all the energetic contributions, and consequently, there is no systematic way to improve the results. From the applicative point-of-view, this is the main difference between the two electronic structure methods. This also highlights the role and importance of the exchange-correlation potential

$$\epsilon_\mathrm{XC}(\vec{r}) = \frac{\delta E_\mathrm{XC}[\rho]}{\delta\rho(\vec{r})}. \tag{16}$$

in Kohn-Sham equations. Currently, developing and benchmarking exchange-correlation functionals is an active subdiscipline in the field of electronic structure

methods. In the literature, there exist truly myriads of functionals, some claimed by the authors to be very accurate for very specific applications, others more general. It is indeed a very challenging task to construct a transferable functional which would perform well throughout the whole spectrum of electronic structure calculations – for example, the electronic structures in metallic lattices, in hydrogen bonded clusters and in radical chemistry can be fairly different. Crudely, the functionals can be classified into two categories depending whether the construction is based on experimental results or theoretical consistency criteria. However, many modern functionals have features from both categories (Jensen, 2007). At times, fitting functionals to empirical data has been greeted with criticism – the opponents argue that the fitting turns DFT into an empirical model. However, during the last decade, likely the most used functional has been the B3LYP functional (Lee et al., 1988; Becke, 1993; Stephens et al., 1994). B3LYP is a so-called *hybrid functional* which combines a fraction of exchage contribution from Hartree-Fock theory and mixes that to semiempirical correlation contributions (Jensen, 2007).

In papers **III** and **IV** all the electronic structure calculations have been performed with the PBE functional, devised by Perdew, Burke and Ernzerhof (Perdew et al., 1996). The PBE functional is a so-called gradient-corrected functional: it depends on the density and on its first derivative (Jensen, 2007). For illustration, the analytical form of the PBE functional is shown in the box below. The parameters on PBE have not been fitted to empirical data, but are based on physical reasoning (Perdew et al., 1996). In this sense, PBE represents DFT in its "pure" *ab initio* form. Although PBE is a fairly old functional, it does perform quite well, especially with hydrogen bonded systems (McGrath et al., 2006; Kuo et al., 2008) – including also atmospheric clusters (Elm et al., 2012; Leverentz et al., 2013). In the paper **IV** PBE is further augmented with a dispersion correction D3 by Grimme and co-workers[4] (Grimme et al., 2010). Typically, proper description of dispersion forces, which originate from the induced or permanent dipole-dipole interactions ("long-range correlations"), have been a weak spot for many density functionals (Jensen, 2007). The D3 correction is computationally fast and seems to yield robust results (Grimme et al., 2010). Also, in paper **II** the final electronic energies were calculated using the wavefunction based RI-MP2 method for

[4]In paper **IV** wrong reference is given in this context; the correct one is Grimme, S., Antony, J., Ehrlich, S., and Krieg, H. (2010). A consistent and accurate ab initio parametrization of density functional dispersion correction (DFT-D) for the 94 elements H-Pu. *J. Chem. Phys.*, 132:154104; http://dx.doi.org/10.1063/1.3382344

To illustrate the complexities involved in the exchange-correlation functionals, this box shows the analytical form of the PBE functional, which was used in papers **III** and **IV**.

Typically the exchange and correlation contributions are separated, $E_{\mathrm{XC}}[\rho] = E_{\mathrm{X}}[\rho] + E_{\mathrm{C}}[\rho]$, and both the contributions are obtained from the exchange/correlation potentials ϵ_i

$$E_{\mathrm{X/C}}[\rho] = \int \epsilon_{\mathrm{X/C}}\, \rho(\vec{r})\, d\vec{r}.$$

The exchange part in PBE is obtained by scaling the exchange potential of a uniform electron gas:

$\epsilon_{\mathrm{X}}^{\mathrm{PBE}} = \epsilon_{\mathrm{X}}^{\mathrm{unif}}\, F(x)$, where $F(x) = 1 + \alpha - \dfrac{\alpha}{1+\beta x^2}$, and α, β are parameters and $x = \dfrac{|\nabla\rho|}{\rho^{4/3}}$.

The correlation part in PBE is also obtained from the uniform electron gas by adding a function $H(t)$ to its correlation potential:

$$\epsilon_{\mathrm{C}}^{\mathrm{PBE}} = \epsilon_{\mathrm{C}}^{\mathrm{unif}} + H(t), \text{ where } H(t) = \gamma f(\zeta) \ln\left[1 + \delta t^2 \left(\frac{1+At^2}{1+At^2+A^2t^4}\right)\right].$$

Here the γ, δ are parameters and $t = \dfrac{x}{2\left(3\pi f(\zeta)\right)^{1/3}}$, and the function $f(\zeta)$ is given as

$f(\zeta) = \left(\dfrac{(1+\zeta)^{2/3} + (1-\zeta)^{2/3}}{2}\right)^3$, where ζ is fractional spin polarization, defined as $\zeta = \dfrac{\rho_\uparrow - \rho_\downarrow}{\rho_\uparrow + \rho_\downarrow}$.

The $\rho_{\uparrow/\downarrow}$ denote the densities of spin up/down electrons.

The factor A in $H(t)$ is given as $A = \dfrac{\delta}{\exp\left[\frac{-\epsilon_{\mathrm{C}}^{\mathrm{unif}}}{\gamma f(\zeta)}\right] - 1}$.

The exchange potential of a uniform electron gas can be calculated exactly: $\epsilon_{\mathrm{X}}^{\mathrm{unif}} = -\dfrac{3}{4}\left(\dfrac{3}{\pi}\right)^{1/3} \rho^{1/3}$.
The same is not true for $\epsilon_{\mathrm{C}}^{\mathrm{unif}}$, and a parameterized potential must be used.

(*Perdew et al., 1996; Jensen, 2007; Tuckerman, 2010*)

the same reason. It should be mentioned that there are also functionals available which address dispersion interactions directly in the exchange-correlation term (see for example Dion et al., 2004; Zhao and Truhlar, 2008).

Basis set expansion Common to both types of electronic structure methods is the need to express the wavefunction or the density in terms of suitable functions. Choosing an explicit form for the functions φ_i in equations (6) and (15) is called the *basis set approximation* (Jensen, 2007). Basically, description of the wavefunction/density of the system (the unknown before the calculation) is expressed with the help of some known functions $f_\nu(\vec{r})$ as

$$\varphi_i(\vec{r}) = \sum_{\nu=1}^{K} C_{\nu i} f_\nu(\vec{r}), \tag{17}$$

where $C_{\nu i}$ are expansion coefficients. Now the unknown part are the coefficients, and indeed, solving the Hartree-Fock or Kohn-Sham equations amounts to finding optimal values for $C_{\nu i}$. Thus it is clear that the better the expansion (17) is able to describe

the true wavefunction/density, the better are the obtained results. Consequently, there is another subdiscipline within the electronic structure methods, similar to the density functional designers, which is devoted in constructing basis sets yielding good results with a minimum CPU cost. Typically, each of the used $f_\nu(\vec{r})$s for a molecular system are a contraction of several Gaussian functions ($\propto e^{-r^2}$) mimicking so-called Slater type functions (or other atomic functions) with an exponential behavior of $\propto e^{-r}$. Reasons for this are practical: even though the Slater functions describe the behavior of electrons more accurately, Gaussian functions are computationally much faster (Szabo and Ostlund, 1996). The faster decay of Gaussian functions is further dealt with by adding additional "diffuse" Gaussian functions with smaller exponents yielding wider spread (Leach, 2001). In molecular systems the electron distribution is seldom spherically symmetric, most often there are some degrees of polarization. To accommodate this, also functions of higher angular momentum are added to basis set. Often the various basis sets are also split between the core and valence electrons, assigning more functions for the valence electrons.

One could easily think that increasing the size of the basis set would always yield better results. Roughly, this is the general trend up to a point, especially in the wavefunction based methods; the more flexible the basis set is, the better it can describe the electronic structure of the system. However, basis sets are just another level of approximation. For example, using larger and larger basis set in DFT will not provide more accurate results in an absolute sense, but only solve the given Kohn-Sham equations with the chosen exchange-correlation functional better – basis sets don't do miracles. Furthermore, the larger the basis set is, the heavier is the computational burden. Thus it would be desirable to use a basis set which is "just large enough", so that adding more basis functions would only have a negligible effect on the quantity of interest. Typically a smaller basis set satisfies this condition in DFT than in the wavefunction based methods.

"Which method to use?" is a question with which most open-minded computational scientists, working with electronic structure calculations, are likely to spend some quality time. The universal answer might be "*Use whatever method which works for your specific problem!*" Unfortunately, this answer has zero information content! A large fraction of the expertise of a computational scientist consists of understanding whether or not a given method works for a given problem, and finding a suitable approach leading to trustworthy results. Often there is no foolproof *a priori* way of

choosing a method for a problem. Testing, guided by experience and literature, is typically a must. Consequently, it is of utmost importance to have a general understanding of the applicability and nature of the computational results. For example, it should be kept in mind that finding the best possible result with a given method is not equivalent to finding "the correct answer" in absolute sense. As argued above, the Schrödinger equation of atmospheric sulfuric acid clusters cannot be solved exactly. From the point-of-view of a practical theoretical physicist, the exact decimals in an approximative solution are irrelevant – only clear, robust results have a physical meaning[5]. Often this means only order of magnitude accuracy.

2.1 The most important quantity: formation free energy

In papers **I** and **II** the machinery of electronic structure methods aims at one goal only: to calculate the formation free energies for the various clusters studied. However, the electronic structure calculations only yield ground state electronic energies at the temperature $T = 0$ K, not free energies at non-zero temperatures. To obtain free energies, one must resort to statistical physics – and to further approximations.

Perhaps the most common way to proceed is to first assume that the different energetic contributions are decoupled. In addition to electronic problem discussed above, molecular systems also have translational, vibrational and rotational degrees of freedom. The electronic contribution is commonly taken to be the ground state energy of the global minimum energy structure. The translational motion of the molecules or clusters is often taken to be that of ideal gas particles. For the remaining contributions the so-called *harmonic oscillator - rigid rotor approximation* is quite typically applied (McQuarrie, 1973; Jensen, 2007). Within this picture, the clusters are treated as equilibrated ideal gas particles and the effect of non-zero temperature is to cause the molecular structures to vibrate harmonically about their equilibrium geometries and to rotate rigidly as a one entity[6]. More technically, with these assumptions it is possible to construct the total partition function Z_{tot} for the system simply as a direct product of the different contributions mentioned above, $Z_{\mathrm{tot}} = Z_{\mathrm{elec}} Z_{\mathrm{trans}} Z_{\mathrm{vib}} Z_{\mathrm{rot}}$ (McQuarrie, 1973). Once the partition function is known, the sought-after free energies can be cal-

[5]In the units used in the work of this thesis, energetic differences of several kcal/mol can be interpreted to be meaningful.

[6]For simplicity, here the zero-point vibrational energy is included in the thermal corrections.

culated using statistical physics. The standard formulae used in papers **I** and **II** are given in the box below.

The total partition function Z_{tot} in the harmonic oscillator - rigid rotor approximation for ideal polyatomic systems is given as:

$$Z_{\text{tot}} = \underbrace{e^{-E_{\text{o}}/k_{\text{B}}T}}_{\equiv Z_{\text{elec}}} \underbrace{\left(\frac{2\pi M k_{\text{B}} T}{h^2}\right)^{3/2} \frac{k_{\text{B}}T}{P}}_{\equiv Z_{\text{trans}}} \underbrace{\left(\prod_{i=1}^{N_{\text{vib}}} \frac{e^{-h\nu_i/2k_{\text{B}}T}}{1-e^{-h\nu_i/k_{\text{B}}T}}\right)}_{\equiv Z_{\text{vib}}} \underbrace{\frac{\pi^{1/2}}{\sigma}\left(\frac{8\pi^2 k_{\text{B}} T}{h^2}\right)^{3/2} (I_1 I_2 I_3)^{1/2}}_{\equiv Z_{\text{rot}}}$$

In the electronic partition function Z_{elec}, only the ground state energy E_{o} is considered and it is assumed to be nondegenerate. In the translational partition function Z_{trans}, the ideal gas volume contribution is expressed in terms of the temperature T and the pressure P. The N_{vib} in the vibrational partition function Z_{vib} is the number of the vibrational modes; for all the molecules/clusters investigated in this work $N_{\text{vib}} = 3 \times$ (number of atomic nuclei) $- 6$. In the rotational partition function Z_{rot}, the σ denotes the number of rotations leaving the system unchanged, and the I_i are the principal moments of inertia.

The connection to the thermodynamics is established via the *Helmholtz free energy* F

$$F = -k_{\text{B}}T \ln\left[Z_{\text{tot}}\right]$$

and all the other thermodynamical quantities can be derived from the F using standard relations.

For example, in the formation of a cluster $(i + j)$ from the monomers/clusters i and j, the *Gibbs formation free energy* $\Delta G(i + j)$ can be calculated as

$$\Delta G(i+j) = \Delta E_{\text{o}}(i+j) - k_{\text{B}}T \ln\left[\frac{Z_{\text{trans}}(i+j) Z_{\text{vib}}(i+j) Z_{\text{rot}}(i+j)}{Z_{\text{trans}}(i) Z_{\text{trans}}(j) Z_{\text{vib}}(i) Z_{\text{vib}}(j) Z_{\text{rot}}(i) Z_{\text{rot}}(j)}\right].$$

Typically the entropy of the system *decreases* in the clustering process (the argument of the logarithm is smaller than one), implying that the change in the electronic energy ΔE_{o} must be negative enough to compensate this for stable clusters.

(*McQuarrie, 1973*)

Anharmonicity By far the most significant contribution to the free energies comes from the ground state electronic energy. The described free energy procedure can be seen as a sort of an extrapolation from the temperature of $T = 0$ K to ambient atmospheric temperatures. In the case of the clusters studied in this thesis, out of the other, "thermal" terms, often the largest contribution comes from the vibrational part. Unfortunately, the harmonic approximation is likely the worst one among all the numerous approximations made along the way from the atomic coordinates to free energies: it is questionable to what extent the vibrational motion of hydrogen bonded clusters is harmonic; in some cases the harmonic approximation is known to break down already for very small cluster sizes (Kathmann et al., 2002, 2007). On the other hand, the harmonic approximation *is* fairly good approximation for some systems, such as for isolated small molecules. However, for the larger systems the approximation is

not made out of ignorance, but rather, out of computational necessity – this applies to all the other approximations described here as well. Several authors have suggested more elaborate ways to treat the vibrations than the harmonic approximation (see for example Chaban et al., 1999; Barone et al., 2004). Perhaps the simplest correction is the scaling of the vibrational frequencies (Scott and Radom, 1996); this approach is also taken in the paper **II**. In this scheme, the obtained frequencies are first scaled by a suitable factor afterwhich they are used in the standard formulae (given in the box above). In paper **II** the calculated DFT frequencies were scaled using higher-level wavefunction based anharmonic frequencies (Kurtén et al., 2007b). The scaling is an *ad hoc* correction, which nevertheless can at times improve the "bare" results. It should be mentioned that typically the simple scaling schemes do not differentiate between the intra- and intermolecular vibrations. For example, in paper **II** the largest anharmonicities arose from the intermolecular vibrations, but the same scaling factor was used for all the vibrations (excluding the zero-point energies). This approach likely overestimated the general anharmonicity, and thus led to slightly too negative formation free energies. Much more sophisticated approach would be to solve the nuclear Schrödinger equation (3) by considering only the relevant areas of the potential energy surface, and thus to concentrate exactly on the known anharmonic vibrational modes (Partanen et al., 2012). Limiting the dimensionality of the potential energy surface makes it possible to solve the vibrational problem completely for the chosen modes, yielding physically rigorous view of the vibration and accurate free energies. Unfortunately, also this approach is much too laborious and computationally costly to be applied for other than the smallest of clusters[7].

In general, obtaining *ab initio* formation free energies beyond the harmonic approximation remains a challenge without universally applicable solutions. Ideally, the method would not only take into account the anharmonicity of the vibrational motion of one particular cluster structure, but also the contributions of *all* the possible cluster structures with a given chemical composition. In practice, this would mean exhaustive sampling of the cluster configuration-space, but unfortunately, this is beyond the cur-

[7]The formation of the sulfuric acid monohydrate has been investigated with the described method. According to preliminary results, the approach yields a Gibbs formation free energy of $\Delta G \approx -2.8$ kcal/mol at $T = 298$ K and $P = 1$ atm. In addition to treating some of the large-amplitude vibrations in the described sophisticated manner, also other molecular configurations than the one corresponding to the global minimum energy have been taken into account (*personal communication with Lauri Partanen, February 2014*). The simple scaling approach in paper **II** produced a slightly more negative formation free energy of $\Delta G = -2.93$ kcal/mol.

rent computational power, especially on *ab initio* level. However, there exists a method which, in principle, is able to describe both the dynamical behavior of the system and sample the relevant configuration-space at feasible computational cost. This method is *molecular dynamics simulation*.

3 First-principles molecular dynamics simulation: *the real computer experiment*

In molecular dynamics simulation, one solves the classical equations of motion of the system in question (Haile, 1997). That is, one basically[8] integrates Newton's second law of motion

$$\mathbf{F}_i(t) = M_i \ddot{\mathbf{R}}_i(t). \tag{18}$$

Here $\mathbf{F}_i(t)$ is the force felt by an entity i (typically an atom or an atomic nuclei) with a mass of M_i at the moment of time t, and $\ddot{\mathbf{R}}_i$ is the second time-derivative of the position vector of the entity. Solving the equations of motion yields the positions and the velocities of the constituents of the system as a function of time – the phase-space trajectory of the system. To put it more bluntly: molecular dynamics simulations show how the system evolves in time. Technically, the phase-space trajectory is a fundamental quantity in molecular dynamics simulations: it establishes a connection between the practical simulations and the more abstract statistical physics (Haile, 1997). This is encapsulated in the *ergodic hypothesis*, which equates the ensemble average of an observable $\langle A(R,P)\rangle$ to its time-average taken over the phase-space trajectory:

$$\langle A(R,P)\rangle = \lim_{t\to\infty} \frac{1}{t} \int_{t_0}^{t_0+t} A\big(R(\tau), P(\tau)\big)\, d\tau. \tag{19}$$

From a practical point-of-view, the simulated system must sample the available phase-space efficiently for equality (19) to hold. It should be noted that a general proof of the ergodic hypothesis is lacking. However, since the first publications on molecular dynamics simulations almost 60 years ago (Alder and Wainwright, 1957, 1959, 1960), an ever-growing mass of scientific work has shown that the time-averages from the simulations can be successfully used to obtain estimates for physical observables. How successfully, depends on the phase-space sampling and on the physical description of the system: essentially, how the forces are calculated in equation (18). In general, most of the molecular dynamics investigations use *pair potentials* to calculate the forces driving the dynamics of the system. Typically these pair potentials are constructed using empirical results, high-level electronic structure calculations and physical reasoning (Leach, 2001). For example, in paper **II** pair potentials were constructed[9] and used

[8] However, in practical simulations, more convenient formulations are typically used.

[9] The potentials were constructed according to the standard OPLS-AA routine (for details, see Jorgensen et al., 1996).

to sample the cluster configuration space prior to the electronic structure calculations (see section 4). The attractive feature of the pair potentials is the relatively light computational burden, especially in comparison to *ab initio* methods. This enables long simulations of large systems, making the physical interpretation of the simulations robust. Pair potentials can also be very accurate when used to study the problem they were designed to describe – the accuracy can be even further increased by considering $\mathcal{N}$-body interactions where $\mathcal{N} > 2$. However, using pair potentials outside their specific scope can lead to nonsensical results. The main drawback of most of the pair potentials is their inability to describe chemical reactions, such as proton transfer. Unfortunately, proton transfer happens to have a very significant role in the life of atmospheric sulfuric acid clusters. To describe the dynamics of these clusters more realistically, one would need a method sophisticated enough to account for the possible changes in the electronic structure of the system on the fly. Essentially, this means using quantum mechanics to calculate the interactions and the resulting forces within the system[10]. In papers **III** and **IV**, this approach was taken in the form of *Born-Oppenheimer first-principles molecular dynamics simulations* (BO-FPMD).

In these simulations the atomic nuclei of the molecules are treated as classical point-like particles (similarly to the pair potential simulations), but the forces between the nuclei are determined from the electronic structure, which is solved using the first-principles methods described in section 2. In the simulations of papers **III** and **IV** the electronic structure of the clusters was solved using density functional theory – in principle it would be possible to use wavefunction methods just as well. As mentioned, solving the electronic structure within the Born-Oppenheimer approximation gives the ground state energy of the system corresponding to the particular spatial nuclear configuration. The forces can then be obtained by the derivative of the energy with respect to the nuclear coordinates (Marx and Hutter, 2009):

$$\mathbf{F}_i(t) = -\nabla_{\mathbf{R}_i} E(R;t) \; . \tag{20}$$

Once the forces are known, the equations of motion can be integrated forward in time. The BO-FPMD scheme proceeds as follows: assume a set of nuclear coordinates and velocities at the instant of time t, say $R(t)$ and $V(t)$, respectively. The nuclear positions

[10]It is possible to construct reactive potentials (see for example van Duin et al., 2001). Also some semiempirical methods, such as the PM3 (see for example Morpurgo et al., 1998), or the so-called density-functional tight-binding method are able to describe the dynamics much better than the simplest pair potentials (see for example Porezag et al., 1995; Ohta et al., 2008).

are known and thus one can evaluate the ground state energy $E(R;t)$. From the energy, one can then obtain the forces at this particular configuration. Knowing the velocities of the atoms in the system and the forces acting on them, integrating the equations of motion yields a new set of coordinates and velocities, $R(t+\Delta t)$ and $V(t+\Delta t)$. Here Δt is the timestep used in the integration – how far in time the system is propagated in one step. Then one solves the electronic structure again at the new nuclear configuration $R(t+\Delta t)$, calculates the forces arising from the new energy, and integrates the system forward in time another Δt. The procedure continues until the dynamical behavior of the system is solved. In papers **III** and **IV** a timestep of $\Delta t = 0.5$ fs was used. One femtosecond (0.000 000 000 000 001 s) is a very short passage of time. However, in first-principles simulations the timestep cannot be much longer, as the used timestep should be clearly shorter than the fastest molecular movement in the system – a timestep 10 to 20 times shorter than the fastest molecular vibration should provide smooth dynamics. On the other hand, it is quite difficult to draw any physical conclusions based only on simulations of some femtoseconds – necessarily picosecond scale should be reached. In paper **III** equilibrium simulations were run for 35 ps for each of the studied clusters. Although this is still very short time in an absolute sense, it is quite a respectable length for first-principles molecular dynamics simulation. Assuming it takes 30 seconds to calculate *one* timestep (realistic estimate for large enough cluster using several processors on a current high-performance supercomputer[11]), the needed 70 000 steps would take roughly 25 *days* of continuous computations! This example demonstrates the main bottleneck in these types of simulations: heavy computational burden. Consequently, the possible system sizes and simulation lengths are considerably smaller and shorter than in pair potential simulations. It should be also noted that in practice this sets limits for the sophistication of the electronic structure calculations: in the first-principles molecular dynamics simulations one is not able to perform as accurate energy calculations as in the static approaches. However, with careful phrasing of research questions the first-principles simulations can shed unique insight into the physical properties of various systems – insight beyond other theoretical tools or experimental methods. Essentially, first-principles molecular simulations are as close as one can get to a "real" computer experiment.

A few comments considering the general molecular dynamics simulation procedure are

[11]For example, in paper **III** the calculation of one timestep for the cluster of two sulfuric acid and two dimethylamine molecules took roughly 40 seconds parallellized on 24 Intel Xeon EP X5660 2.8 GHz processors.

in order – applicable also to the BO-FPMD simulations. In practical simulations, the user must decide how the interactions between the atoms/molecules are handled at large distances. For example, if one wishes to investigate a bulk system, typically *periodic boundary conditions* are used in one or more directions. In such a simulation the primary simulation cell (the box containing the system) is replicated periodically. Thus the closest neighbor for some atom/molecule might be in the periodic image cell, yielding infinite bulklike circumstances (Haile, 1997). On the other hand, simulating isolated systems, as in papers **III** and **IV**, care must be taken to ensure that no artificial "boundary effects" arise. Basically, the electron density should vanish smoothly before the boundary of the simulation cell is reached. In papers **III** and **IV**, a simulation cell of 20 Å × 20 Å × 20 Å was used and the long-range interactions were treated according to the scheme by Martyna and Tuckerman (1999). Also, the integration of the equations of motion is computationally a fairly sophisticated process. In the literature there are several possible schemes of integration. In this thesis the velocity Verlet algorithm (Swope et al., 1982) was used[12]. This algorithm propagates the positions $\mathbf{R}_i$ and the velocities $\mathbf{V}_i$ as follows:

$$\begin{aligned} \mathbf{R}_i(t+\Delta t) =& \mathbf{R}_i(t) + \Delta t \mathbf{V}_i(t) + \frac{\Delta t^2}{2M_i}\mathbf{F}_i(t) \\ \mathbf{V}_i(t+\Delta t) =& \mathbf{V}_i(t) + \frac{\Delta t}{2M_i}\left[\mathbf{F}_i(t) + \mathbf{F}_i(t+\Delta t)\right] \end{aligned} \tag{21}$$

The velocity Verlet algorithm is a relatively simple integrator and it is known to provide robust long-time stability (Tuckerman, 2010).

3.1 The most important feature: molecular movement

As mentioned, the key quantity in molecular dynamics is the phase-space trajectory. More specifically, in the simulations of atmospheric clusters the most interesting feature to observe is the simulated molecular movement under the approximated forces of nature. This is the special asset distinguishing first-principles molecular dynamics from other *ab initio* methods, such as the static electronic structure calculations or Monte Carlo simulations.

[12]Actually, in paper **III** a slightly modified version was used due to the subtleties related to the temperature control.

Microcanonical ensemble The molecular dynamics procedure described so far describes the dynamics of an isolated system. Such a system is characterized by the conservation of three quantities: the number of particles, the volume they are allowed to occupy, and the total energy. The first two requirements are easily fulfilled by specifying the system, and all reasonable integrators conserve the total energy[13]. Here the total energy of the system is the sum of the kinetic energy of the atomic nuclei and the potential energy of the system. The latter is the electronic ground state energy. In other words, the dynamics of an isolated system obeys the simple Hamiltonian $\mathcal{H}(R, P)$:

$$\mathcal{H}(R, P) = \sum_{i=1}^{N_{\text{nuclei}}} \frac{\mathbf{P}_i^2}{2M_i} + E(R). \tag{22}$$

The physics of an isolated system thus corresponds to statistical mechanics in the microcanonical ensemble. From the simulation point-of-view this yields the "purest" kind of dynamics: the molecular movement is governed only by the conservation of the total energy. In paper **IV**, the formation dynamics of small sulfuric acid clusters are investigated using microcanonical simulations (see more in section 4.3).

Canonical ensemble However, the conditions in atmospherically relevant molecular clustering are perhaps never such that the number of particles, the volume where they roam and the total energy are "conserved". On the other hand, macroscopic thermodynamic parameters, such as temperature or pressure are typically known. Thus it would be desirable to run simulations which correspond to these exterior conditions *on a molecular level*. For example, in constant-temperature simulations the average atomic velocity of the system should agree with the desired temperature. It turns out that there are several consistent ways to extend the Hamiltonian of the system to match various external conditions. In paper **III** the dynamics of atmospheric clusters are investigated keeping the temperature constant (in addition to the number of particles and the volume). In this case the Hamiltonian of the system was extended according to the so-called *Nosé-Hoover chain thermostatting* scheme (Martyna et al., 1992; Tobias et al., 1993):

$$\mathcal{H}_{\text{NHC}} = \mathcal{H}(R, P) + \sum_{j=1}^{N_{\text{chain}}} \sum_{k=1}^{N_{\text{dof}}} \frac{p_{\eta_{j,k}}^2}{2W_j} + \frac{3N_{\text{nuclei}}}{N_{\text{dof}}} k_B T \sum_{k=1}^{N_{\text{dof}}} \eta_{1,k} + k_B T \sum_{j=2}^{N_{\text{chain}}} \sum_{k=1}^{N_{\text{dof}}} \eta_{j,k}. \tag{23}$$

[13] *None* of the numerical integrators conserve the total energy perfectly. However, robust integrators, such as the velocity Verlet, can conserve the total energy with a good accuracy.

Here $\mathcal{H}(R, P)$ is the physical Hamiltonian from equation (22), $\eta_{j,k}$ and $p_{\eta_{j,k}}$ are dynamical "thermostatting chain" variables, coupled to each other and to the actual physical variables R and P. W_j are thermostatting parameters defining the strength of the temperature control. N_{chain} sets the length of the chain(s) and N_{dof} specifies whether or not there is one chain for the whole system, one for each atomic nucleus or, most extensively, one for each cartesian degree of freedom. In the paper **III** the last option for N_{dof} was chosen together with a chain length of three. It can be shown that the Hamiltonian $\mathcal{H}_{\text{NHC}}$ produces the correct canonical distributions for all the physical coordinate and momentum variables – and maintains these very robustly (Tuckerman, 2010). Such a simulation samples the canonical ensemble, and accordingly, describes how the clusters behave in thermal equilibrium (see more in section 4.2).

4 Using *ab initio* tools to investigate the first steps of atmospheric new-particle formation

Atmospheric new-particle formation is a particularly interesting example of *a mesoscopic phenomenon*. It is a genuine many-body problem, starting from the realms of quantum mechanics and extending to size ranges where classical physics can be safely applied. In part, it is exactly this cross-over nature of the phenomenon which makes it very challenging to study, both experimentally and theoretically.

On the theoretical side, brute force *ab initio* research is constrained by limitations in system sizes and timescales. Unfortunately, these limitations are met rather fast: first-principles simulation of some tens of picoseconds of a cluster of ten or so molecules is already on the large end of the spectrum. Currently, modelling the entire formation process from individual molecules up to stable particles is out of reach. Although this type of straightforward approach "*put molecules in a box, observe what happens*" is attractive in its directness, it might not be necessary. Large enough particles which behave classically can be treated with more approximative methods. For example, *classical nucleation theory* performs decently well within its area of applicability (Merikanto et al., 2007; Wix et al., 2010). Perhaps a suitable framework to investigate the entire new-particle formation process could be constructed by merging microscopic and macroscopic methods. However, such a grand framework is still to be composed, and until then, the small and large scale results must be combined in an *ad hoc* fashion.

The research presented in this doctoral thesis contributes to the understanding of the small scale processes. The work concentrates on small sulfuric acid clusters – on the properties of these clusters and on the very first steps of their formation. The rest of this section explores how the first-principles tools reviewed in sections 2 and 3 can be used to achieve this.

4.1 Electronic structure calculations indicate trends robustly

As mentioned in section 2.1, the most important quantity to obtain from the electronic structure calculations is the formation free energy of the cluster in question. In the atmospheric context, often *the Gibbs formation free energy* ΔG is used, corresponding to known exterior conditions of pressure, temperature and number of particles (see the

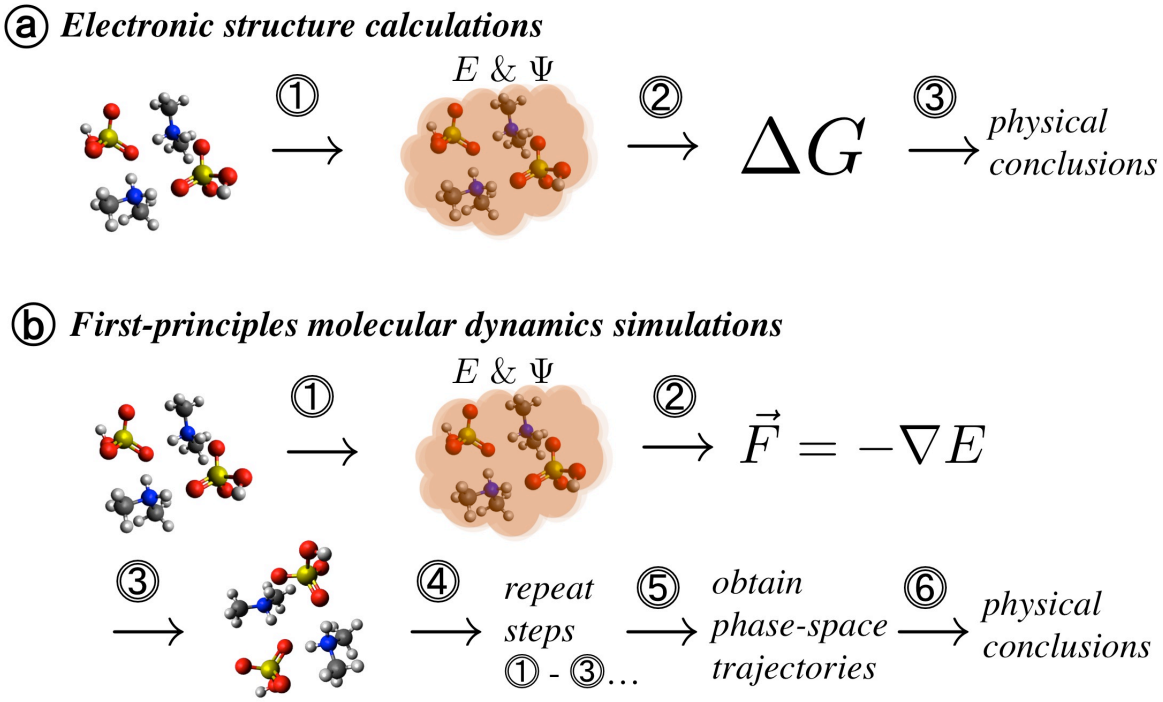

Figure 2: Simplified flowchart showing how the electronic structure calculations and the first-principles molecular dynamics simulations have been used to investigate atmospheric clustering in this thesis. **(a)** In the electronic structure calculations the global minimum energy cluster is searched (1) by solving the Schrödinger equation; (2) formation free energies are calculated based on the properties of the minimum energy clusters; (3) physical conclusions are drawn from the formation free energies. **(b)** Also in the first-principles molecular dynamics simulations the electronic structure of the clusters is obtained (1) by solving the Schrödinger equation; (2) the forces driving the evolution of the system are determined from the electronic structure; (3) the clusters are then propagated forward in time and a new cluster configuration is obtained; (4) the procedure continues for several picoseconds (5) incrementally acquiring the phase-space trajectories; (6) finally, physical conclusions are drawn from the trajectories.

information box in section 2.1). The underlying assumption is that the formation free energy serves as an indicator of the cluster stability. It is further assumed that the most stable cluster for a given molecular configuration is the one "appearing in the atmosphere". In other words, it is assumed that the properties of this cluster are good enough approximations of reality. Basically, this means assuming that the most stable clusters dominate the respective cluster distributions[14].

From nuclear coordinates to free energies With these assumptions, and utilizing the electronic structure methods described in section 2, the physical problem turns into the computational problem of finding the minimum of ΔG. Effectively, this means finding the minimum free energy configurations for all the participating species. Surprisingly, there does not exist a general, infallible and universally applicable method to achieve this. Finding the minimum energy configurations for clusters of few molecules is usually fairly simple task using just bare intuition. For example, in the clustering of two small molecules there are only a handful of possible bonding patterns, and it is an easy job for a person with adequate amounts of physical and chemical intuition to find out which one minimizes the ground state energy of the complex. However, as the system size grows, predicting the most stable cluster becomes difficult. This is due to simple combinatorics: the number of possible and energetically equally good cluster configurations becomes large quite fast.

A typical solution to the problem is to start with a large set of cluster configurations and to narrow the pool of clusters incrementally by finding the best structures with increasingly sophisticated (electronic structure) methods. In paper **II**, pair potential molecular dynamics simulations were used to construct a pool of clusters for sulfuric acid - ammonia/dimethylamine - water systems. This was done by three-step *simulated annealing*. First, all the clusters were simulated at a high temperature of $T = 1500$ K, starting with a random initial configuration. The idea of these high-energy runs was to explore the configuration space as thoroughly as possible. Then, taking the configurations from the $T = 1500$ K simulations, the molecules were cooled down by simulations at a lower temperature of $T = 200$ K in order to form actual bonded clusters. Finally, the clusters were simulated at a temperature of $T = 0.1$ K to reach an energetic minimum. The end-product of the last simulations were then taken as initial guesses

[14]The applicability of this assumption can be tested for example by taking into account several *local* minimum energy structures in addition to the one *global* minimum energy cluster configuration and Boltzmann averaging the energies (Temelso et al., 2012).

for the geometry optimization based on electronic structure methods. As thorough configuration-space sampling using *ab initio* methods is computationally unattainable, the much faster pair potential simulations provide a convenient way to generate initial structures. Although the physics in these simulations is described at a more approximative level, it is likely that the obtained clusters are fairly decent starting guesses for the more sophisticated treatment.

In finding the most stable clusters, the large variety of possible electronic structure methods can cause further complications. Unfortunately, different methods can and do disagree on which configuration of the nuclear coordinates yields the lowest electronic energy. In practice, this means that for example the different density functionals each predict "the best cluster" to be slightly different, typically deviating in bond lengths and angles. Moreover, especially in DFT there is no straightforward way to evaluate which one is the most accurate method. Often the DFT results are benchmarked against high-level wavefunction based methods, which should find the "correct" cluster eventually. Unfortunately, the computational burden of these calculations is typically much too high to be used to optimize atmospheric sulfuric acid clusters. Finally, the computational performance should be evaluated against experimental results when possible. The experimental determination of formation free energies is *extremely* challenging, and for example, for sulfuric acid - amine clusters no direct experimental free energy values are available[15].

It should be stated explicitly that the previous concerns are not disparaging comments, but rather, remarks elucidating that to obtain the one desired number, ΔG, more than "just one calculation" is required. In general, the free energy calculations based on electronic structure methods are on a level of sophistication, where they can offer new physical insight on the first steps of atmospheric new-particle formation. *Clear trends observed in the calculated formation free energies are very likely to convey reliable information about the real world.*

For example, in paper **I** the described free energy scheme was used to investigate the relative stabilities of various (sulfuric acid/bisulfate ion)(amine) clusters in comparison to the (sulfuric acid/bisulfate ion)(ammonia) cluster. Based on the obtained free energies, it could be concluded that amines enhance the clustering clearly more effectively than

[15]Beside the experimental formation free energies, for example cluster structures or vibrational spectra would establish a direct comparison with the experiments. For sulfuric acid - amine clusters studied here, also this data is still to be measured.

the "standard candidate" ammonia. In paper **II**, the work was continued by studying the effect of water on the relative stabilities of (sulfuric acid)(ammonia/dimethylamine) clusters. As sulfuric acid is most probably hydrated in atmospheric conditions (Kurtén et al., 2007b; Temelso et al., 2012), it is important to investigate the role of water in the clustering process. Again, based on calculated formation free energies, it could be concluded that dimethylamine enhances the very first steps of cluster growth better than ammonia also in the presence water.

Evaporation rates Nevertheless, the formation free energies of small clusters *are* conceptually fairly abstract. What would it mean in practice that the cluster A is 4.3 kcal/mol more stable than the cluster B? Perhaps a more intuitive interpretation for the formation free energies can be obtained by using concepts of cluster kinetics. First, assuming that *a detailed balance* holds between the formation and breaking up of a cluster of composition $(i + j)$ from the clusters (or monomers) i and j, and further assuming equilibrium conditions, one can solve the evaporation rate (in units of $^1/_s$) for the reaction in terms of the formation free energies:

$$\gamma_{ij} = \beta_{ij} \frac{c_i c_j}{c_{(i+j)}} = \beta_{ij} c_{\text{ref}} \exp\left[\frac{\Delta G_{(i+j)} - \Delta G_i - \Delta G_j}{k_B T}\right]. \tag{24}$$

Here γ_{ij} is the evaporation/fragmentation rate of a molecule/cluster i from the cluster $(i+j)$, β_{ij} is the collision rate of the entities i and j, c_x are the concentrations and the ΔG_x are the formation free energies of entities x at the temperature T. The reference concentration c_{ref} corresponds to the conditions where the formation free energies are calculated and effectively cancels out the pressure dependence from the expression[16]. Thus, according to the equation (24), other things being equal, the 4.3 kcal/mol more stable cluster A would have more than three orders of magnitude *smaller* evaporation rate than the cluster B at the temperature of $T = 300$ K. Converting the obtained free energies into evaporation rates can indeed give a fresh auxiliary perspective to the energetics of the system (Ortega et al., 2012, 2014).

Kinetic modelling The calculated evaporation rates can be further applied in the kinetic modelling of the cluster concentrations (McGrath et al., 2012). The time-evolution of the concentrations is dictated by a set of coupled differential *birth-death*

[16]The reference concentration c_{ref} is related to the pressure P as $c_{\text{ref}} = P/k_B T$. Only the entropic contribution of the translational motion has pressure dependence in the free energy calculation scheme outlined in section 2.1, and shown in the information box there.

equations

$$\frac{dc_i}{dt} \propto \sum_{jk} \beta_{jk} c_j c_k + \sum_{jk} \gamma_{jk} c_j - \sum_{j} \beta_{ij} c_i c_j - \sum_{j} \gamma_{ij} c_i + (\text{sources}) - (\text{sinks}) \,, \qquad (25)$$

where c_i, the concentration of the cluster i, is increased by the collisions and evaporations leading to this cluster composition (the first two terms, respectively) and is decreased by cluster i colliding with other clusters or fragmenting into smaller sizes (the next two terms, respectively). In addition to these elementary processes, there are usually additional sources and sinks for the monomers and/or clusters as well. For equations (24) and (25) to hold, it must be assumed that equilibrium holds *on a molecular level*. In other words, it is required that the dynamics of the cluster concentrations take place on timescales where the actual molecular level processes have reached an equilibrium. This ensures that the most stable clusters have been found, thus legitimizing the use of evaporation rates obtained from the static free energy calculations. Probably the most appealing feature in the described kinetic modelling approach is the connection it establishes from the *ab initio* formation free energies to the real-world observables, such as the particle formation rate. Importantly, this connection seems to be working. Comparison between numerical modelling (using equations (24) and (25) with hard-spheres collision rates) and a recent state-of-the-art laboratory experiment revealed a very good agreement in estimating the particle formation rate in sulfuric acid - dimethylamine and sulfuric acid - ammonia systems. The modelling captured robustly the qualitative features of the formation rate as a function of the concentrations of the participating species – even the quantitative accuracy was decent (Almeida et al., 2013). Also, the modelled steady-state cluster concentrations compare well with experimental results (Olenius et al., 2013).

The good performance of the modelling suggests that the outlined approach, based on the formation free energies calculated with electronic structure methods, can indeed be used to give (at least) qualitatively reliable results. From the point-of-view of the scientific discovery process, this is a quite pertinent detail. The electronic structure calculations are typically much faster and cheaper, and are generally more convenient to carry out than experimental campaigns. This renders the theoretical tools essential for testing new ideas, predicting trends and providing qualitative explanations.

However, to obtain insight on the dynamics on a molecular level, and to validate and test the various assumptions and approximations, one must resort to molecular dynamics simulations.

4.2 Equilibrium simulations reveal the effect of temperature

In the Earth's atmosphere, the small clusters collide continuously with the air molecules, mainly with N_2 and O_2. On the free energy scheme described above, it is implicitly assumed that these collisions keep the clusters in equilibrium and that the equilibrium properties can then be represented by those of the minimum free energy clusters. In molecular dynamics simulations this assumption could be tested explicitly by modelling the thermalization process by carrier gas collisions (see for example Wedekind et al., 2007). However, in practice the computational burden to perform these kind of simulations using first-principles energy calculations is much too high. Luckily, the extended Hamiltonian approaches, such as the Nosé-Hoover chain method, provide an indirect way to investigate the dynamics under equilibrium conditions. For example, in the constant-temperature simulations in paper **III**, the effect of the carrier gas collisions on the molecular movement of the clusters is approximated by thermostatting the atomic velocities to the desired temperature[17]. At first sight this might seem artificial. However, also in the real atmosphere the thermalization of the clusters by collisions with the inert air molecules happens by exchanging kinetic energy. Depending on the system and how far it is from the dynamical equilibrium, the thermalization by carrier gas collisions might be a very slow process – that is, it might require a huge amount of collisions to reach the equilibrium. On the other hand, under the standard conditions the small clusters collide with the air molecules roughly once in every hundred picoseconds – 10^{10} times in one second. Thus, the Nosé-Hoover chain thermostatting might not be that bad approximation of the dynamical equilibrium after all. However, it must be kept in mind that the thermostatting alters the natural dynamics of the system.

To obtain physically meaningful results from the canonical simulations, first a dynamical equilibrium must be reached. This means that the potential energy of the system should oscillate around a stabilized value. Depending on the system and the starting configuration (the initial phase-space point), this might happen almost immediately or require lengthy simulations. Unfortunately, there is no way to ascertain that a stable equilibrium has been reached. It is part of the simulator expertise to estimate whether

[17]The temperature and the velocities obey the well-known proportionality $T(t) \propto \sum_i V_i(t)^2$. It could be mentioned in passing, that it is fairly simple just to scale the velocities to obtain the desired temperature. However, the simple velocity scaling methods do not typically produce the proper canonical distributions, and consequently, the connection to the thermophysical properties is lost.

or not the equilibrium has been found.

Once the equilibrium has been found, the constant-temperature first-principles molecular dynamics simulations provide a logical continuation to the static free energy calculation scheme outlined in the previous subsection. Among the end-products of the ΔG calculations are the nuclear configurations of the most stable clusters. These serve as excellent starting points for the simulations probing the stability and the dynamics of the clusters: what happens when the thermal motion is turned on?

Dynamical equilibrium properties When the kinetic energy is explicitly considered, the concept of "the most stable cluster" generalizes to a distribution of cluster geometries corresponding to the simulation temperature. No longer are the clusters characterized by the exact minimum energy nuclear coordinates, but by distributions of average distances. Perhaps the first thing to observe in the simulations of atmospheric clusters is how much the dynamical equilibrium structures differ from the static minimum ΔG geometries. If the bonding patterns turned out to be significantly different, this would indicate that the static ΔG cluster configuration is not a good approximation for the particular system at non-zero temperature. For example, in paper **III** stable (sulfuric acid)(ammonia/dimethylamine) clusters were taken from the literature (Ortega et al., 2012) and simulated at the temperature of $T = 300$ K. In the simulations the bonding patterns were observed to be close to those obtained from the static calculations. The clusters exhibited quite pronounced thermal oscillations, and even concerted rotations, but in general, all movement happened about the equilibrium bonding patterns. This is likely due to the nature of the clusters: the proton transfer patterns from sulfuric acid to the base molecules set quite stringent criteria for the possible moderately strong hydrogen bonding patterns, which then "lock" the geometries of the clusters.

However, it is not at all evident that the proton transfer predicted by the static calculations would hold throughout the dynamical simulations. Canonical first-principles molecular dynamics simulations enable the inspection of the *proton control* during the equilibrium (Anderson et al., 2008). Indeed, in paper **IV** in an equilibrium simulation of the (sulfuric acid)$_1$(dimethylamine)$_1$ cluster at $T = 300$ K, the amine controlled the proton 93 % of the time, whereas analysis based on the static calculations would predict a 100 % proton control for the amine. However, by adding just one water molecule to the cluster increased the amine proton control share practically to one hundred percent, even in the dynamical equilibrium simulations.

In addition to the distribution-view, where the time dimension is abstracted away, the simulations naturally offer a time-evolution-view of the properties, showing for example the oscillation period for a certain distance. Importantly, the simulations are able to provide insight into the characteristic molecular level time scales. In the context of the current thesis, the most interesting observables in this category are the molecular vibrations. As the electronic structures are also available from the first-principles simulations, *the electric dipole moment* can be used to investigate the molecular vibrations. The electric dipole moment contains contributions from both the movement of the atomic nuclei and from the electronic structure of the system, and consequently, it is very sensitive to the thermal motion. Thus, the autocorrelation of the dipole moment measures the characteristic vibrational time scales of the cluster – transforming the autocorrelation function into frequency domain then yields a vibrational spectrum. The spectra obtained via this machinery shows the vibrational motion of the clusters *beyond the harmonic approximation*[18]. This is exciting, as the simulated spectra can be directly compared to experimental spectra, and, to the spectra calculated via the static electronic structure methods with the harmonic oscillator - rigid rotor approximations. In paper **III** the latter are compared to the BO-FPMD spectra in the case of various (sulfuric acid)(ammonia/dimethylamine) clusters. The results clearly indicate that the thermal motion of the clusters differs from purely harmonic motion.

The constant-temperature equilibrium simulations sample the canonical ensemble and thus there is a connection between the simulations and thermodynamical quantities. For example, the isochoric heat capacity C_{V} can be obtained with the help of potential energy fluctuations as

$$C_{\mathrm{V}} = \langle (\Delta E)^2 \rangle / k_{\mathrm{B}} T^2, \tag{26}$$

where $\langle (\Delta E)^2 \rangle$ is the variance of the potential energy. The temperature T is proportional to the kinetic energy, and thus the heat capacity C_{V} measures the interplay between the potential and kinetic energies. Paper **III** also compared the heat capacities obtained from the dynamic simulations to those from the static calculations. It was observed that the heat capacities deviated the more the larger the system size was – likely due to the underestimation of C_{V} by the static methods. The main contribution to the static heat capacities comes from the vibrational frequencies, and it is known that the larger the system size is, the worse the harmonic approximation grows, at least

[18]It should be kept in mind, however, that within the BO-FPMD simulations the atomic nuclei are treated classically – in some cases the quantum nature of the nuclei (particularly the quantum tunnelling of protons) can have a crucial role.

for smallest clusters (Kathmann et al., 2007). The heat capacities provide yet another indicator showing that to realistically describe the clusters at non-zero temperatures, more accurate static methods are called for.

Entropic properties The effect of the observed anharmonicity on the most important quantity, ΔG, is very difficult to estimate. This is because the entropic properties cannot be directly evaluated from the simulations as an average over the phase-space trajectory[19]. Nevertheless, the entropic contributions are present in the simulations as the previous examples of the anharmonicity illustrate. Even though the free energies, or other entropic properties, cannot be obtained from single simulations, their derivatives can be. For example, the isochoric heat capacity C_V can be expressed as a derivative of the entropy S

$$C_\mathrm{V} = T \left(\frac{\partial S}{\partial T} \right)_{N,V}, \tag{27}$$

and by combining several simulations performed at different temperatures, it is possible to obtain the change in entropy ΔS by integration

$$\Delta S = \int_{T_0}^{T} \frac{C_\mathrm{V}(T')}{T'} \, dT'. \tag{28}$$

Similar integration schemes can be constructed for other entropic quantities as well. However, as it currently takes roughly a month of continuous computations to obtain *one* data point needed for the integration, it is clear that the first-principles molecular dynamics simulations cannot be the main tool to obtain free energies. In the atmospheric formation free energy context, these simulations could be used to study the general trends and characteristics arising from the more complete phase-space sampling – for small illustrative clusters.

4.3 Collision simulations describe the formation dynamics in detail

It is tempting to contemplate that the first-principles molecular dynamics simulations show us what one would see through an imaginary (and *very* powerful) magnifying glass observing the small atmospheric clusters. In this picture, the canonical simulations

[19]Typically, entropy is proportional to the logarithm of the volume of the entire accessible phase-space.

would represent some sort of a time-lapse movie, showing an average view of the clusters where the air molecules maintaining the equilibrium molecular movement have been abstracted away[20]. However, the *microcanonical simulations* would show us the real thing!

The microcanonical simulations, governed by the Hamiltonian (22), model the dynamics in a most unperturbed fashion. This renders the microcanonical simulations well-suited for investigating the dynamics of atmospheric clustering on a molecular level.

Clustering is a non-equilibrium process In the static ΔG calculations, it is assumed that both the formed cluster and the molecules forming the cluster are perfectly equilibrated in accordance with a given temperature *throughout the process*. Also, in the equilibrium canonical simulations the thermostatting ensures that the nuclear velocities correspond to the given temperature. However, molecular clustering is in fact a rather dynamic non-equilibrium process. By definition, in the clustering the system finds a new, more negative state of potential energy – and the kinetic energy must increase accordingly. Colloquially, the clustering process releases heat. As described earlier, the atmosphere is likely to absorb the released heat but this might take numerous collisions with the air molecules. Even in the case of a relatively fast thermalization, the newly-formed cluster has to cope with the "extra" kinetic energy for several hundreds of picoseconds. What happens to the clusters during this time? In paper **IV**, this was investigated in the case of $(\text{sulfuric acid})_1(\text{water})_{0,1} + (\text{dimethylamine})_1$ clustering by direct collision simulations in the microcanonical ensemble.

According to the simulations, in the clustering of sulfuric acid with dimethylamine, a proton transfer takes place – this is in agreement with static calculations as well. The transfer lowers the potential energy of the complex by several kcal/mol, increasing the kinetic energy by the same amount. The inability to dissipate the released energy leads to a very dynamic cluster configuration after the initial transfer; on average, the dimethylamine controlled the proton only 76 % of the time. Correspondingly, also the

[20]In fact, the botanist Robert Brown must have seen something similar with an actual powerful magnifying glass (optical microscope) while discovering the random, brownian motion of pollen particles in water – and indirectly confirming the existence of molecules. In reality, the imaging of covalent bond structure in single-molecule chemical reactions starts to be possible via atomic force microscopes (de Oteyza et al., 2013). However, with bare human eyes this will not be possible without rather curious future evolution.

structure of the cluster was continuously evolving, and in general, it was different from the static or dynamical equilibrium geometry. The addition of one water molecule, initially bound to the acid, altered the formation dynamics by introducing additional easily accessible degrees of freedom. Based on the simulations, the slightly larger system is better able to accommodate the released energy, leading to a less dynamic structure. In this case the amine controlled the proton for 88 % of the simulation time. However, it should be kept in mind that the released kinetic energy still remains in the cluster. Perhaps this entails that the phase-space is explored more effectively, and that the inevitable collisions with the carrier gas then lead to the dynamical equilibrium in an orderly fashion, somewhat akin to the simulated annealing process described in section 4.1. On the other hand, the "kinetically exited" clusters might be more prone to evaporation/fragmentation upon a collision with a carrier gas molecule with a suitable speed and direction. Based on both the equilibrium and collision simulations, the *spontaneous* evaporation of a sulfuric acid molecule from the small cluster of (sulfuric acid)$_1$(dimethylamine)$_1$ is likely to be a very rare event – free energy change in the evaporation is large and positive. Such an event would raise the potential energy of the system significantly and consequently radically lower the kinetic energy. From the phase-space point-of-view, the evaporation would effectively freeze the molecular movement of the small cluster and correspond to a vanishingly improbable state of the system. It is likely that most of the evaporation events are connected with external kinetic energy change, at least in the case of the small cluster of sulfuric acid and dimethylamine.

Sticking factor & cluster rearrangement Most of the collisions in atmospheric clustering are not likely to be perfectly inelastic. Microcanonical collision simulations provide means to investigate the *sticking factor* in molecular collisions, at least for small systems. In paper **IV**, the sticking factor in (sulfuric acid)$_1$(water)$_{0,1}$ + (dimethylamine)$_1$ *head-on* collisions was observed to be unity. These collision simulations are particularly susceptible for sticking factor investigations: for these systems there are only a handful of primary collision geometries and the proton transfer reaction constitutes a good metric for the sticking by clearly indicating complex formation. Both of these alleviating factors are lost in the subsequent cluster growth. What is more, the *cluster rearrangement* is very likely going to have an even more important role for larger clusters. Especially in the cluster-cluster collisions, or in the cases where sulfuric acid collides with a cluster which is already satisfied with respect to proton transfers, the rearrangement into the global dynamical minimum energy cluster con-

figuration might be very slow – or might not happen at all.

These possibilities and dynamical features serve to remind us on the very complex nature of the clustering process. To deepen our understanding of the clustering on the elementary, molecular level, the described dynamical effects must be fully accounted for. Currently, first-principles molecular dynamics simulation is perhaps the most promising tool to achieve this in practice.

5 Impact of the work and future directions

Theoretical calculations providing experimentally testable predictions are perhaps the most valuable contribution that practical theoretical physics has to offer. The research presented in this doctoral thesis proposed that the amine compounds are likely to have a strongly enhancing role in the first steps of sulfuric acid driven new-particle formation in atmospheric conditions. This prediction, based on electronic structure calculations, was later further quantified in closely related computational work (Ortega et al., 2012; McGrath et al., 2012), and more importantly, also observed in experimental investigations (Berndt et al., 2010; Smith et al., 2010; Zhao et al., 2011; Erupe et al., 2012; Yu et al., 2012; Zollner et al., 2012; Bzdek et al., 2012; Almeida et al., 2013; Berndt et al., 2014).

The amine-enhanced sulfuric acid clustering leading to the formation of stable, measurable aerosol particles, is the first mechanism yielding particle formation rates comparable to the rates typically observed in ambient measurements in pristine locations (Almeida et al., 2013). This does not, however, imply that the mechanism would explain all the ambient observations – or even a significant fraction of the experimental data. Nevertheless, it is very likely that whenever sulfuric acid and amines encounter in the atmosphere, they will cluster rather efficiently and produce aerosol particles. There are some practical implications. In addition to monitoring the sulfuric acid concentrations, or the precursor SO_2 concentrations, it is also important to monitor the ambient amine concentrations and their trends. For example, if the so-called amine scrubbing mechanism (Boot-Handford et al., 2014) becomes more frequently used in carbon capture, the ambient amine concentrations can be expected to rise in the vicinities of fossil-fuel power plants.

The dynamics of small atmospheric clusters are very complex, and the work uncovering the consequences stemming from the molecular level motion has just begun. The presented first-principles molecular dynamics investigations represent steps towards a more elementary understanding of the clustering process – understanding beyond the reach of the current experimental tools. In this research, first-principles simulations were successfully applied to study the dynamics of the clusters both in equilibrium and non-equilibrium conditions. The thermal molecular movement was observed to shape and distort the clusters in an anharmonic fashion and the direct collision simulations revealed very vivid formation dynamics.

The dynamical effects are a manifestation of the entropic features related to all molecular motion, and are likely to have an important contribution to the formation energetics in molecular clustering in general. The results presented in this work suggest that in obtaining a satisfactory understanding of the clustering process, the future first-principles molecular dynamics simulations are likely to have a pivotal role.

Reflections The static electronic structure calculations are likely to remain the main tool in calculating the formation free energies of atmospheric clusters – at least in the foreseeable future. With this respect, it would be most desirable to have a robust machinery for efficient configuration-space sampling. One possibility to generate initial cluster structures for quantum mechanical optimizations might be a combined method of random sampling followed by pair potential molecular dynamics simulations. Also, in addition to finding the global minimum energy cluster for a given composition, it might be interesting to investigate the energetics of clusters which resemble direct collision products of the molecules in question. Perhaps an average over the properties of the different clusters might provide more realistic approximation of the real thing – until the calculation of the free energies is more affordable using first-principles dynamics.

Before actually obtaining all the formation free energies from the first-principles molecular simulations, the simulations could be used to quantify the error introduced into the energetics by the more approximative approaches.

Besides the first-principles simulations with classical nuclei, in the future it might be interesting to study the role of nuclear quantum effects in atmospheric clusters. The results in the present thesis clearly indicate that proton transfer has an important role in the sulfuric acid - amine clusters – it is thus not inconceivable that especially the quantum nature of the proton might be worth a closer look.

Ultimately, physics is an empirical science: the experimental results weigh more than the theoretical considerations. However, an active dialogue between the two approaches is likely the most efficient way to expedite the scientific discovery process. In part, the results presented in this thesis demonstrate that the theoretical approaches can provide valuable insights, and there is no reason to believe that this trend would not continue in the future. Conversely, the electronic structure calculations and the first-principles molecular dynamics simulations have both a lot to offer in unravelling the exact details in atmospheric new-particle formation – from the simulations of electrically neutral and charged clustering to the modelling of the inner workings of measurement devices.

Computational tools: review of used software

Gaussian 03/09 is a multipurpose electronic structure program suite (Gaussian 03, Revision C.02; Gaussian 09, Revision A.1). In this thesis it was used to calculate the anharmonic vibrational frequencies in paper **II**, and in paper **III** to optimize the clusters and to obtain static heat capacities and harmonic vibrational spectra.

TURBOMOLE is a program package for *ab initio* electronic structure calculations (TURBOMOLE, versions 5.8 and 5.91; Ahlrichs et al., 1989; Häser and Ahlrichs, 1989). In this thesis it was used to optimize the cluster structures and to obtain the vibrational frequencies in paper **I**, and to calculate electronic correlation energies in papers **I** and **II**.

SIESTA (*spanish initiative for electronic simulations with thousands of atoms*) is a program to perform electronic structure calculations and *ab initio* molecular dynamics simulations of molecules and solids (version 2.0.1, Soler et al., 2002). In this thesis it was used to perform the structure optimization in paper **II**.

DL_POLY_2 is a parallel molecular dynamics simulation package (version 2.18, Smith et al., 2002). In this thesis it was used to perform the pair potential molecular simulations in paper **II**.

CP2K is a program to perform atomistic and molecular simulations. CP2K is freely available under the GPL license (`www.cp2k.org`). In this thesis it was used to perform all the first-principles molecular dynamics calculations in papers **III** (version 2.2.208) and **IV** (version 2.3). In the simulations, the module QUICKSTEP (VandeVondele et al., 2005) took care of the density functional calculations.

In addition to the actual number crunching, visualization is an important part of the practical scientific discovery process – both in daily hands-on research and in presenting the found results. In papers **I** and **II** the visualization of the molecular clusters was done with *Molekel* (version 4.3, Portmann, 2002), in papers **III** and **IV** with *Avogadro* (version 1.0.3, Hanwell et al., 2012). Also *Spartan'06* (Wavefunction, Inc.) and *Molden* (several versions, Schaftenaar and Noordik, 2000) were both used throughout the work.

In the visualization of the molecular dynamics trajectories, *VMD* (several versions, Humphrey et al., 1996) was extensively used.

Analysis codes were written using `Fortran 95` and `Python`. All the graphs in papers **III** and **IV** were produced with a `Python` plotting library *matplotlib* (Hunter, 2007).

List of symbols

$\hat{X}$	$\cdots$	quantum mechanical operator
∇_i	$\cdots$	gradient operator with respect to i
Ψ	$\cdots$	total wavefunction of the system
$\psi(r)$	$\cdots$	electronic wavefunction – function of the electronic coordinates $r \equiv \vec{r}_1, \vec{r}_2, \ldots, \vec{r}_N$
$\chi(R)$	$\cdots$	nuclear wavefunction – function of the nuclear coordinates $R \equiv \mathbf{R}_1, \mathbf{R}_2, \ldots, \mathbf{R}_{N_{\text{nuclei}}}$
$\varphi_i(\vec{r})$	$\cdots$	1-electron wavefunction (spin orbital)
$f_i(\vec{r})$	$\cdots$	basis set function i
C_{ij}	$\cdots$	basis set expansion coefficient
$\rho(\vec{r})$	$\cdots$	total electron density
E	$\cdots$	energy (possible arguments or sub- and/or superscripts specify it further)
ϵ_i	$\cdots$	energy of an electron described by $\varphi_i(\vec{r})$ in the Hartree-Fock approximation
ϵ_{XC}	$\cdots$	exchange-correlation potential
Q_i	$\cdots$	atomic number of the nucleus i
M_i	$\cdots$	mass of the atomic nucleus i
M	$\cdots$	mass of the whole system
N	$\cdots$	number of electrons in the system
N_{nuclei}	$\cdots$	number of atomic nuclei the system
Z_i	$\cdots$	partition function for the contribution i
ν_i	$\cdots$	vibrational frequency of the vibrational mode i
σ	$\cdots$	number of rotational elements in the point group of the system
I_i	$\cdots$	principal moment of inertia i
T	$\cdots$	temperature
P	$\cdots$	pressure
S	$\cdots$	entropy
F	$\cdots$	Helmholtz free energy
C_{V}	$\cdots$	isochoric heat capacity
ΔG	$\cdots$	Gibbs formation free energy
γ_{ij}	$\cdots$	evaporation/fragmentation rate of an entity i from the cluster $(i+j)$
β_{ij}	$\cdots$	collision rate between entities i and j
c_i	$\cdots$	concentration specified by the subscript i
$\mathbf{F}_i$	$\cdots$	force felt by an entity i
$\mathbf{V}_i$	$\cdots$	velocity of an entity i; $\mathbf{V}_i = \dot{\mathbf{R}}_i$
V	$\cdots$	set of velocities; $V \equiv \mathbf{V}_1, \mathbf{V}_2, \ldots, \mathbf{V}_{N_{\text{nuclei}}}$
$\mathbf{P}_i$	$\cdots$	momentum of an entity i; $\mathbf{P}_i = M_i \mathbf{V}_i$
P	$\cdots$	set of momenta; $P \equiv \mathbf{P}_1, \mathbf{P}_2, \ldots, \mathbf{P}_{N_{\text{nuclei}}}$
Δt	$\cdots$	timestep in molecular dynamics simulations
$\mathcal{H}$	$\cdots$	Hamiltonian of an isolated system – conserved quantity in NVE simulations
$\mathcal{H}_{\text{NHC}}$	$\cdots$	Nosé–Hoover chain Hamiltonian – conserved quantity in Nosé–Hoover chain NVT simulations
$\eta_{i,j}$	$\cdots$	Nosé-Hoover chain thermostatting variable
$p_{\eta_{i,j}}$	$\cdots$	Nosé-Hoover chain thermostatting variable
W_i	$\cdots$	thermostatting parameter
kcal/mol	$\cdots$	unit of energy; 1 kcal/mol $\approx 6.9 \times 10^{-21}$ J
k_B	$\cdots$	Boltzmann constant; $k_B = 1.381 \times 10^{-23}$ J/K
h	$\cdots$	Planck constant; $h = 6.626 \times 10^{-34}$ Js

References

Ahlrichs, R., Bär, M., Häser, M., Horn, H., and Kölmel, C. (1989). Electronic structure calculations on workstation computers: The program system Turbomole. Chem. Phys. Lett., 162: 165–169.

Alder, B. J., and Wainwright, T. E. (1957). Phase Transition for a Hard Sphere System. *J. Chem. Phys.*, 27: 1208–1209.

Alder, B. J., and Wainwright, T. E. (1959). Studies in Molecular Dynamics. I. General Method. *J. Chem. Phys.*, 31: 459–466.

Alder, B. J., and Wainwright, T. E. (1960). Studies in Molecular Dynamics. II. Behavior of a Small Number of Elastic Spheres. *J. Chem. Phys.*, 33: 1439–1451.

Almeida, J., Schobesberger, S., Kürten, A., Ortega, I. K., Kupiainen–Määttä, O., Praplan, A. P., Adamov, A., Amorim, A., Bianchi, F., Breitenlechner, M., David, A., Dommen, J., Donahue, N. M., Downard, A., Dunne, E., Duplissy, J., Ehrhart, S., Flagan, R. C., Franchin, A., Guida, R., Hakala, J., Hansel, A., Heinritzi, M., Henschel, H., Jokinen, T., Junninen, H., Kajos, M., Kangasluoma, J., Keskinen, H., Kupc, A., Kurtén, T., Kvashin, A. N., Laaksonen, A., Lehtipalo, K., Leiminger, M., Leppä, J., Loukonen, V., Makhmutov, V., Mathot, S., McGrath, M. J., Nieminen, T., Olenius, T., Onnela, A., Petäjä, T., Riccobono, F., Riipinen, I., Rissanen, M., Rondo, L., Ruuskanen, T., Santos, F. D., Sarnela, N., Schallhart, S., Schnitzhofer, R., Seinfeld, J. H., Simon, M. Sipilä, M., Stozhkov, Y., Stratmann, F., Tomé, A, Tröstl, J., Tsagkogeorgas, G., Vaattovaara, P, Viisanen, Y., Virtanen, A., Vrtala, A., Wagner, P. E., Weingartner, E., Wex, H., Williamson, C., Wimmer, D., Ye, P., Yli-Juuti, T., Carslaw, K. S., Kulmala, M., Curtius, J, Baltensperger, U., Worsnop, D. R., Vehkamäki, H., and Kirkby, J. (2013). Molecular understanding of sulphuric acid–amine particle nucleation in the atmosphere. *Nature*, 502:359–363.

Anderson, K. E., Siepmann, J. I., McMurry, P. H., and VandeVondele, J. (2008). Importance of the Number of Acid Molecules and the Strength of the Base for Double-Ion Formation in $(H_2SO_4)_m{\cdot}Base{\cdot}(H_2O)_6$ Clusters. *J. Am. Chem. Soc.*, 130: 14144–14147.

Anttila, T., Vehkamäki, H., Napari, I., and Kulmala, M. (2005). Effect of ammonium

bisulphate formation on atmospheric water-sulphuric acid-ammonia nucleation. *Boreal Env. Res.*, 10: 511–523.

Ball, S. M., Hanson, D. R., Eisele, F. L., and McMurry, P. H. (1999). Laboratory studies of particle nucleation: Initial results for H_2SO_4, H_2O, and NH_3 vapors. *J. Geophys. Res.*, 104: 23709–23718.

Barone, V. (2004). Vibrational zero-point energies and thermodynamic functions beyond the harmonic approximation. *J. Chem. Phys.*, 120: 3059–3065.

Becke, A. D. (1993) Density-functional thermochemistry. III. The role of exact exchange. *J. Chem. Phys.*, 98: 5648–5652.

Berndt, T., Stratmann, F., Sipilä, M., Vanhanen, J., Petäjä, T., Mikkilä, J., Grüner, A., Spindler, G., Lee Mauldin III, R., Curtius, J., Kulmala, M., and Heintzenberg, J. (2010). Laboratory study on new particle formation from the reaction OH + SO_2: influence of experimental conditions, H_2O vapour, NH_3 and the amine tert-butylamine on the overall process. *Atmos. Chem. Phys.*, 10: 7101–7116.

Berndt, T., Sipilä, M., Stratmann, F., Petäjä, T., Vanhanen, J., Mikkilä, J., Patokoski, J., Taipale, R., Mauldin III, R. L., and Kulmala, M. (2014). Enhancement of atmospheric H_2SO_4/H_2O nucleation: organic oxidation products versus amines. *Atmos. Chem. Phys.*, 14: 751–764.

Boot-Handford, M. E., Abanades, J. C., Anthony, E. J., Blunt, M. J., Brandani, S., Mac Dowell, N., Fernández, J. R., Ferrari, M.-C., Gross, R., Hallett, J. P., Haszeldine, R. S., Heptonstall, P., Lyngfelt, A., Makuch, Z., Mangano, E., Porter, R. T. J., Pourkashanian, M., Rochelle, G. T., Shah, N., Yaoa, J. G., and Fennell, P. S. (2014). Carbon capture and storage update. *Energy Environ. Sci.*, 7: 130–189.

Bzdek, B. R., Ridge, D. P., and Johnston, M. V. (2012). Size-Dependent Reactions of Ammonium Bisulfate Clusters with Dimethylamine. *J. Phys. Chem. A*, 114: 11638–11644.

Chaban, G. M., Jung, J. O., and Gerber, R. B. (1999). *Ab initio* calculation of anharmonic vibrational states of polyatomic systems: Electronic structure combined with vibrational self-consistent field. *J. Chem. Phys.*, 111: 1823–1829.

Chen, M., Titcombe, M., Jiang, J., Jen, C., Kuang, C., Fischer, M. L., Eisele, F. L., Siepmann, J. I., Hanson, D. R., Zhao, J., and McMurry, P. H. (2012). Acid-base

chemical reaction model for nucleation rates in the polluted atmospheric boundary layer. *Proceedings of the National Academy of Sciences of the United States of America*, 109: 18713–18718.

Coffman, D. J., and Hegg, D. A. (1995). A Preliminary study of the effect of ammonia on particle nucleation in the marine boundary layer. *J. Geophys. Res.*, 100: 7147–7160.

de Oteyza, D. G., Gorman, P., Chen, Y.-C., Wickenburg, S., Riss, A., Mowbray, D. J., Etkin, G., Pedramrazi, Z., Tsai, H.-Z., Rubio, A., Crommie, M. F., Fischer, F. R. (2013). Direct Imaging of Covalent Bond Structure in Single-Molecule Chemical Reactions. *Science*, 340: 1434–1437.

Dion, M., Rydberg, H., Schröder, E., Langreth, D. C., and Lundqvist, B. I. (2004). Van der Waals Density Functional for General Geometries. *Phys. Rev. Lett.*, 92: 246401.

Ehn, M., Thornton, J. A., Kleist, E., Sipilä, M., Junninen, H., Pullinen, I., Springer, M., Rubach, F., Tillmann, R., Lee, B., Lopez-Hilfiker, F., Andres, St., Acir, I.-H., Rissanen, M., Jokinen, T., Schobesberger, S., Kangasluoma, J., Kontkanen, J., Nieminen, T., Kurtén, T., Nielsen, L. B., Jørgensen, S., Kjaergaard, H. G., Canagaratna, M., Dal Maso, M., Berndt, T., Petäjä, T., Wahner, A., Kerminen, V.-M., Kulmala, M., Worsnop, D. R., Wildt, J., and Mentel, T. F. (2014). A large source of low-volatility secondary organic aerosol. *Nature*, 506: 476–479.

Elm, J., Bilde, M., and Mikkelsen, K. V. (2012). Assessment of Density Functional Theory in Predicting Structures and Free Energies of Reaction of Atmospheric Prenucleation Clusters. *J. Chem. Theory Comput.*, 8: 2071–2077.

Erupe, M. E., Viggiano, A. A., and Lee, S.-H. (2012). The effect of trimethylamine on atmospheric nucleation involving H_2SO_4. *Atmos. Chem. Phys.*, 11: 4767–4775.

Gaussian 03, Revision C.02, Frisch, M. J., Trucks, G. W., Schlegel, H. B., Scuseria, G. E., Robb, M. A., Cheeseman, J. R., Montgomery, Jr., J. A., Vreven, T., Kudin, K. N., Burant, J. C., Millam, J. M., Iyengar, S. S., Tomasi, J., Barone, V., Mennucci, B., Cossi, M., Scalmani, G., Rega, N., Petersson, G. A., Nakatsuji, H., Hada, M., Ehara, M., Toyota, K., Fukuda, R., Hasegawa, J., Ishida, M., Nakajima, T., Honda, Y., Kitao, O., Nakai, H., Klene, M., Li, X., Knox, J. E., Hratchian, H. P., Cross, J. B., Bakken, V., Adamo, C., Jaramillo, J., Gomperts, R., Stratmann, R.

E., Yazyev, O., Austin, A. J., Cammi, R., Pomelli, C., Ochterski, J. W., Ayala, P. Y., Morokuma, K., Voth, G. A., Salvador, P., Dannenberg, J. J., Zakrzewski, V. G., Dapprich, S., Daniels, A. D., Strain, M. C., Farkas, O., Malick, D. K., Rabuck, A. D., Raghavachari, K., Foresman, J. B., Ortiz, J. V., Cui, Q., Baboul, A. G., Clifford, S., Cioslowski, J., Stefanov, B. B., Liu, G., Liashenko, A., Piskorz, P., Komaromi, I., Martin, R. L., Fox, D. J., Keith, T., Al-Laham, M. A., Peng, C. Y., Nanayakkara, A., Challacombe, M., Gill, P. M. W., Johnson, B., Chen, W., Wong, M. W., Gonzalez, C., and Pople, J. A., Gaussian, Inc., Wallingford CT, 2004.

Gaussian 09, Revision A.1, M. J. Frisch, G. W. Trucks, H. B. Schlegel, G. E. Scuseria, M. A. Robb, J. R. Cheeseman, G. Scalmani, V. Barone, B. Mennucci, G. A. Petersson, H. Nakatsuji, M. Caricato, X. Li, H. P. Hratchian, A. F. Izmaylov, J. Bloino, G. Zheng, J. L. Sonnenberg, M. Hada, M. Ehara, K. Toyota, R. Fukuda, J. Hasegawa, M. Ishida, T. Nakajima, Y. Honda, O. Kitao, H. Nakai, T. Vreven, J. A. Montgomery, Jr., J. E. Peralta, F. Ogliaro, M. Bearpark, J. J. Heyd, E. Brothers, K. N. Kudin, V. N. Staroverov, R. Kobayashi, J. Normand, K. Raghavachari, A. Rendell, J. C. Burant, S. S. Iyengar, J. Tomasi, M. Cossi, N. Rega, J. M. Millam, M. Klene, J. E. Knox, J. B. Cross, V. Bakken, C. Adamo, J. Jaramillo, R. Gomperts, R. E. Stratmann, O. Yazyev, A. J. Austin, R. Cammi, C. Pomelli, J. W. Ochterski, R. L. Martin, K. Morokuma, V. G. Zakrzewski, G. A. Voth, P. Salvador, J. J. Dannenberg, S. Dapprich, A. D. Daniels, Ö. Farkas, J. B. Foresman, J. V. Ortiz, J. Cioslowski,

Ge, X., Wexler, A. S., and Clegg, S. L. (2011). Atmospheric amines-Part I. A review. *Atmos. Environ.*, 45: 524–546.

Grimme, S., Antony, J., Ehrlich, S., and Krieg, H. (2010). A consistent and accurate ab initio parametrization of density functional dispersion correction (DFT-D) for the 94 elements H-Pu. *J. Chem. Phys.*, 132: 154104.

Häser, M. and Ahlrichs, R. (1989). Improvements on the direct SCF method. *J. Comput. Chem.*, 10: 104–111.

Hättig, C., and Weigend, F. (2000). CC2 excitation energy calculations on large molecules using the resolution of the identity approximation. *J. Chem. Phys.*, 113: 5154–5161.

Haile, J. M. (1997). Molecular Dynamics Simulation. Elementary Methods. Wiley Professional Paperback Edition. John Wiley & Sons. Inc., New York.

Hanson, D. R., McMurry, P. H., Jiang, J., Tanner, D., and Huey, L. G. (2011). Ambient pressure proton transfer mass spectrometry: detection of amines and ammonia. *Environ. Sci. Technol.*, 45: 8881–8888.

Hanwell, M. D., Curtis, D. E., Lonie, D. C., Vandermeersch, T., Zurek, E., and Hutchison, G. R. (2012). Avogadro: an advanced semantic chemical editor, visualization, and analysis platform. *Journal of Cheminformatics*, 4: 17.

Hinds, W. C. (1999). Aerosol Technology: Properties, Behavior, and Measurement of Airborne Particles, 2nd edition. John Wiley & Sons, Inc., New York, NY, USA.

Hohenberg, P., and Kohn, W. (1964). Inhomogeneous Electron Gas. *Phys. Rev.*, 136: B864–B871.

Humphrey, W., Dalke, A., and Schulten, K. (1996). VMD – Visual Molecular Dynamics. *J. Molec. Graphics*, 14: 33–38.

Hunter, E. P., and Lias, S. G. (1998). Evaluated Gas Phase Basicities and Proton Affinities of Molecules: An Update. *J. Phys. Chem. Ref. Data*, 27: 413–656.

Hunter, J. D. (2007). Matplotlib: A 2D graphics environment. *Computing In Science & Engineering*, 9: 90–95.

Ianni, J. C., and Bandy, A. R. (1999). A Density Functional Theory Study of the Hydrates of $NH_3{\cdot}H_2SO_4$ and Its Implications for the Formation of New Atmospheric Particles. *J. Phys. Chem. A*, 103: 2801–2811.

Iida, K, Stolzenburg, M., McMurry, P., Dunn, M. J., Smith, J. N., Eisele, F, and Keady, P. (2006). Contribution of ion-induced nucleation to new particle formation: Methodology and its application to atmospheric observations in Boulder, Colorado *J. Geophys. Res.*, 111: D23201.

Jensen, F. (2007). Introduction to Computational Chemistry, second edition. John Wiley & Sons Ltd, West Sussex, England.

Jorgensen, W. L., Maxwell, D. S., and Tirado-Rives, J. (1996). Development and Testing of the OPLS All-Atom Force Field on Conformational Energetics and Properties of Organic Liquids. *J. Am. Chem. Soc.*, 118: 11225–11236.

Jung, J., Fountoukis, C., Adams, P. J., and Pandis, S. N. (2009) Simulation of in-situ ultrafine particle formation in the Eastern United States using PMCAMx-UF. *Proceedings of the 18th International Conference on Nucleation and Atmospheric Aerosols, Prague, Czech Republic, 10–14 August 2009*, 338–342.

Kathmann, S. M., Schenter, G. K., and Garrett, B. C. (2002). Understanding the sensitivity of nucleation kinetics: A case study on water. *J. Chem. Phys.*, 116: 5046–5057.

Kathmann, S., Schenter, G., and Garrett, B. (2007). The Critical Role of Anharmonicity in Aqueous Ionic Clusters Relevant to Nucleation. *J. Phys. Chem. C*, 111: 4977–4983.

Kazil, J., Lovejoy, E. R., Barth, M. C., and O'Brien, K. (2006). Aerosol nucleation over oceans and the role of galactic cosmic rays. *Atmos. Chem. Phys.*, 6: 4905–4924.

Kerminen, V.-M., Petäjä, T., Manninen, H. E., Paasonen, P., Nieminen, T., Sipilä, M., Junninen, H., Ehn, M., Gagné, S., Laakso, L., Riipinen, I., Vehkamäki, H., Kurten, T., Ortega, I. K., Dal Maso, M., Brus, D., Hyvärinen, A., Lihavainen, H., Leppä, J., Lehtinen, K. E. J., Mirme, A., Mirme, S., Hõrrak, U., Berndt, T., Stratmann, F., Birmili, W., Wiedensohler, A., Metzger, A., Dommen, J., Baltensperger, U., Kiendler-Scharr, A., Mentel, T. F., Wildt, J., Winkler, P. M., Wagner, P. E., Petzold, A., Minikin, A., Plass-Dülmer, C., Pöschl, U., Laaksonen, A., and Kulmala, M. (2010). Atmospheric nucleation: highlights of the EUCAARI project and future directions. *Atmos. Chem. Phys.*, 10:10829–10848.

Kirkby, J., Curtius, J., Almeida, J., Dunne, E., Duplissy, J., Ehrhart, S., Franchin, A., Gagné, S., Ickes, L., Kürten, A., Kupc, A., Metzger, A., Riccobono, F., Rondo, L., Schobesberger, S., Tsagkogeorgas, G., Wimmer, D., Amorim, A. Bianchi, F., Breitenlechner, M., David, A., Dommen, J., Downard, A., Ehn, M., Flagan, R. C., Haider, S., Hansel, A., Hauser, D., Jud, W., Junninen, H., Kreissl, F., Kvashin, A., Laaksonen, A., Lehtipalo, K., Lima, J., Lovejoy, E. R., Makhmutov, V., Mathot, S., Mikkilä, J., Minginette, P., Mogo, S., Nieminen, T., Onnela, A., Pereira, P., Petäjä, T., Schnitzhofer, R., Seinfeld, J. H., Sipilä, M., Stozhkov, Y., Stratmann, F., Tomé, A., Vanhanen, J., Viisanen, Y., Vrtala, A., Wagner, P. E., Walther, H., Weingartner, E., Wex, H., Winkler, P. M., Carslaw, K. S., Worsnop, D. R., Baltensperger, U., and Kulmala, M. (2011). Role of sulphuric acid, ammonia and galactic cosmic rays in atmospheric aerosol nucleation. *Nature*, 476, 429–433.

Korhonen, P., Kulmala, M., Laaksonen, A., Viisanen, Y., McGraw, R., and Seinfeld, J. H. (1999). Ternary nucleation of H_2SO_4, NH_3, and H_2O in the atmosphere. *J. Geophys. Res.*, 104: 26349–26353.

Kuang, C., McMurry, P. H., McCormick, A. V., and Eisele, F. L. (2008). Dependence of nucleation rates on sulfuric acid vapor concentration in diverse atmospheric locations. *J. Geophys. Res.*, 113: D10209.

Kulmala, M., Vehkamäki, H., Petäjä, T., Dal Maso, M., Lauri, A., Kerminen, V.-M., Birmili, W., and McMurry, P.H. (2004). Formation and growth rates of ultrafine atmospheric particles: a review of observations. *Aerosol Science*, 35, 143–176.

Kulmala, M., Riipinen, I., Nieminen, T., Hulkkonen, M., Sogacheva, L., Manninen, H. E., Paasonen, P., Petäjä, T., Dal Maso, M., Aalto, P. P., Viljanen, A., Usoskin, I., Vainio, R., Mirme, S., Mirme, A., Minikin, A., Petzold, A., Hõrrak, U., Plaß-Dülmer, C., Birmili, W., and Kerminen, V.-M. (2010). Atmospheric data over a solar cycle: no connection between galactic cosmic rays and new particle formation *Atmos. Chem. Phys.*, 10: 1885–1898.

Kuo, I.-F. W., Mundy, C. J., McGrath, M. J., and Siepmann, J. I. (2008). Structure of the Methanol Liquid-Vapor Interface: A Comprehensive Particle-Based Simulation Study. *J. Phys. Chem. C*, 112: 15412–15418.

Kurtén, T., Torpo, L., Ding, C.-G., Vehkamäki, H., Sundberg, M. R., Laasonen, K., and Kulmala, M. (2007a). A density functional study on water-sulfuric acid-ammonia clusters and implications for atmospheric cluster formation. *J. Geophys. Res.*, 112: D04210.

Kurtén, T., Noppel, M., Vehkamäki, H., Salonen, M., and Kulmala, M. (2007b). Quantum chemical studies of hydrate formation of H_2SO_4 and HSO_4^-. *Boreal Env. Res.*, 12: 431–453.

Larson, L. J., Largent, A., and Tao, F.-M. (1999). Structure of the Sulfuric Acid-Ammonia System and the Effect of Water Molecules in the Gas Phase. *J. Phys. Chem. A*, 103: 6786–6792.

Leach, A. R. (2001). Molecular Modelling. Principles and Applications. 2nd Edition. Pearson Education Limited, Harlow, England.

Lee, C., Yang, W., and Parr, R. G. (1988). Development of the Colic-Salvetti correlation-energy formula into a functional of the electron density. *Phys. Rev. B.*, 37: 785–789.

Leverentz, H. R., Siepmann, J. I., Truhlar, D. G., Loukonen, V., and Vehkamäki, H. (2013). Energetics of Atmospherically Implicated Clusters Made of Sulfuric Acid, Ammonia, and Dimethyl Amine. *J. Phys. Chem. A*, 117: 3819–3825.

Lim, S. S., Vos, T., Flaxman, A. D., Danaei, G., Shibuya, K., Adair-Rohani, H., Amann, M., Anderson, H. R., Andrews, K. G., Aryee, M., Atkinson, C., Bacchus, L. J., Bahalim, A. N., Balakrishnan, K., Balmes, J., Barker-Collo, S., Baxter, A., Bell, M. L., Blore, J. D., Blyth, F., Bonner, C., Borges, G., Bourne, R., Boussinesq, M., Brauer, M., Brooks, P., Bruce, N. G., Brunekreef, B., Bryan-Hancock, C., Bucello, C., Buchbinder, R., Bull, F., Burnett, R. T., Byers, T. E., Calabria, B., Carapetis, J., Carnahan, E., Chafe, Z., Charlson, F., Chen, H. L., Chen, J. S., Cheng, A. T. A., Child, J. C., Cohen, A., Colson, K. E., Cowie, B. C., Darby, S., Darling, S., Davis, A., Degenhardt, L., Dentener, F., Des Jarlais, D. C., Devries, K., Dherani, M., Ding, E. L., Dorsey, E. R., Driscoll, T., Edmond, K., Ali, S. E., Engell, R. E., Erwin, P. J., Fahimi, S., Falder, G., Farzadfar, F., Ferrari, A., Finucane, M. M., Flaxman, S., Fowkes, F. G. R., Freedman, G., Freeman, M. K., Gakidou, E., Ghosh, S., Giovannucci, E., Gmel, G., Graham, K., Grainger, R., Grant, B., Gunnell, D., Gutierrez, H. R., Hall, W., Hoek, H. W., Hogan, A., Hosgood, H. D., Hoy, D., Hu, H., Hubbell, B. J., Hutchings, S. J., Ibeanusi, S. E., Jacklyn, G. L., Jasrasaria, R., Jonas, J. B., Kan, H. D., Kanis, J. A., Kassebaum, N., Kawakami, N., Khang, Y. H., Khatibzadeh, S., Khoo, J. P., Kok, C., Laden, F., Lalloo, R., Lan, Q., Lathlean, T., Leasher, J., L., Leigh, J., Li, Y., Lin, J. K., Lipshultz, S. E., London, S., Lozano, R., Lu, Y., Mak, J., Malekzadeh, R., Mallinger, L., Marcenes, W., March, L., Marks, R., Martin, R., McGale, P., McGrath, J., Mehta, S., Mensah, G. A., Merriman, T. R., Micha, R., Michaud, C., Mishra, V., Hanafiah, K. M., Mokdad, A. A., Morawska, L., Mozaffarian, D., Murphy, T., Naghavi, M., Neal, B., Nelson, P. K., Nolla, J. M., Norman, R., Olives, C., Omer, S. B., Orchard, J., Osborne, R., Ostro, B., Page, A., Pandey, K. D., Parry, C. D. H., Passmore, E., Patra, J., Pearce, N., Pelizzari, P. M., Petzold, M., Phillips, M. R., Pope, D., Pope, C. A., Powles, J., Rao, M., Razavi, H., Rehfuess, E. A., Rehm, J. T., Ritz, B., Rivara, F. P., Roberts, T., Robinson, C., Rodriguez-Portales, J. A., Romieu, I., Room, R., Rosenfeld, L. C., Roy, A., Rushton, L., Salomon, J. A., Sampson, U., Sanchez-Riera, L., Sanman, E., Sapkota, A., Seedat, S., Shi, P. L., Shield, K., Shivakoti, R., Singh, G. M., Sleet,

D. A., Smith, E., Smith, K. R., Stapelberg, N. J. C., Steenland, K., Stockl, H., Stovner, L. J., Straif, K., Straney, L., Thurston, G. D., Tran, J. H., Van Dingenen, R., van Donkelaar, A., Veerman, J. L., Vijayakumar, L., Weintraub, R., Weissman, M. M., White, R. A., Whiteford, H., Wiersma, S. T., Wilkinson, J. D., Williams, H. C., Williams, W., Wilson, N., Woolf, A. D., Yip, P., Zielinski, J. M., Lopez, A. D., Murray, C. J. L., and Ezzati, M. (2012). A comparative risk assessment of burden of disease and injury attributable to 67 risk factors and risk factor clusters in 21 regions, 1990-2010: a systematic analysis for the Global Burden of Disease Study 2010. *Lancet*, 380, 2224 – 2260.

Lovejoy, E. R., Curtius, J., and Froyd, K. D. (2004). Atmospheric ion-induced nucleation of sulfuric acid and water. *J. Geophys. Res.*, 109: D08204.

Mäkelä, J. M., Yli-Koivisto, S., Hiltunen, V., Seidl, W., Swietlicki, E., Teinilä, K., Sillanpää, M., Koponen, I. K., Paatero, J., Rosman, K., and Hämeri, K. (2001). Chemical composition of aerosol during particle formation events in boreal forest. *Tellus*, 53B:380–393.

Manninen, H. E., Nieminen, T., Riipinen, I., Yli-Juuti, T., Gagné, S., Asmi, E., Aalto, P. P., Petäjä, T., Kerminen, V.-M., and Kulmala, M. (2009). Charged and total particle formation and growth rates during EUCAARI 2007 campaign in Hyytiälä. Atmos. Chem. Phys., 9: 4077–4089.

Martyna, G. J., Klein, M. L., and Tuckerman, M. E. (1992). Nosé-Hoover chains: The canonical ensemble via continuous dynamics. *J. Chem. Phys.*, 97: 2635–2643.

Martyna, G. J., and Tuckerman, M. E. (1999). A reciprocal space based method for treating long range interactions in ab initio and force-field-based calculations in clusters. *J. Chem. Phys.*, 110: 2810–2821.

Marx, D., and Hutter, J. (2009). *Ab Initio* Molecular Dynamics: Basic Theory and Advanced Methods. Cambridge University Press, Cambridge, UK.

McGrath, M. J., Siepmann, J. I., Kuo, I.-F. W., and C. J. Mundy (2006). Vapor-liquid equilibria of water from first principles: comparison of density functionals and basis sets. *Mol. Phys.*, 104: 3619–3626.

McGrath, M. J., Olenius, T., Ortega, I. K., Loukonen, V., Paasonen, P., Kurtén, T., Kulmala, M., and Vehkamäki, H. (2012). Atmospheric Cluster Dynamics Code: a

flexible method for solution of the birth-death equations. *Atmos. Chem. Phys.*, 12: 2345–2355.

McQuarrie, D. A. (1973). Statistical Thermodynamics. Harper & Row, Publishers, Inc., New York, NY., USA.

Merikanto, J., Zapadinsky, E., Lauri, A., and Vehkamäki, H. (2007). Origin of the failure of classical nucleation theory: incorrect description of the smallest clusters. *Phys. Rev. Lett.*, 98: 145702.

Merikanto, J., Spracklen, D. V., Mann, G. W., Pickering, S. J., and Carslaw, K. S. (2009). Impact of nucleation on global CCN. *Atmos. Chem. Phys.*, 9: 8601–8616.

Morpurgo, S., Bossa, M. Morpurgo, G. O. (1998). Critical test of PM3-calculated proton transfer activation energies: a comparison with ab initio and AM1 calculations. *J. Mol. Struct.: THEOCHEM*, 429: 71–80.

Nadykto, A.B., and Yu, F. (2007). Strong hydrogen bonding between atmospheric nucleation precursors and common organics. *Chem. Phys. Lett.*, 435: 14-–18.

O'Dowd, C. D., Jimenez, J. L., Bahreini, R., Flagan, R. C., Seinfeld, J. H., Hämeri, K., Pirjola, L., Kulmala, M., Jennings, S. G., and Hoffmann, T. (2002). Marine aerosol formation from biogenic iodine emissions. *Nature*, 417: 632–636.

Ohta, Y., Okamoto, Y., Irle, S., and Morokuma, K. (2008). Rapid Growth of a Single-Walled Carbon Nanotube on an Iron Cluster: Density-Functional Tight-Binding Molecular Dynamics Simulations. *ACS Nano*, 2: 1437–1444.

Olenius, T., Schobesberger, S., Kupiainen-Määttä, O., Franchin, A., Junninen, H., Ortega, I. K., Kurtén, T., Loukonen, V., Worsnop, D. R., Kulmala, M., and Vehkamäki, H. (2012). Comparing simulated and experimental molecular cluster distributions. Faraday Discuss., 165: 75–89.

Ortega, I. K., Kupiainen, O., Kurtén, T., Olenius, T., Wilkman, O., McGrath, M. J., Loukonen, V., and Vehkamäki, H. (2012). From quantum chemical formation free energies to evaporation rates. *Atmos. Chem. Phys.*, 12: 225–235.

Ortega, I. K., Olenius, T., Kupiainen-Määttä, O., Loukonen, V., Kurtén, T., and Vehkamäki, H. (2014). Electrical charging changes the composition of sulfuric acid-ammonia/dimethylamine clusters. *Atmos. Chem. Phys. Discuss.*, 14: 1317–1348.

Parr, R. G., and Yang, W. (1989) Density-functional theory of atoms and molecules. Oxford University Press, New York, NY., USA.

Partanen, L., Hänninen, V., and Halonen, L. (2012) Ab Initio Structural and Vibrational Investigation of Sulfuric Acid Monohydrate. *J. Phys. Chem. A*, 116: 2867–2879.

Perdew, J. P., Burke, K., and Ernzerhof, M. (1996). Generalized Gradient Approximation Made Simple. *Phys. Rev. Lett.*, 77: 3865–3868.

Pople, J. A., HeadGordon, M., and Raghavachari, K. (1987). Quadratic configuration interaction. A general technique for determining electron correlation energies. *J. Chem. Phys.*, 87: 5968–5975.

Porezag, D., Frauenheim, T., K´ohler, T., Seifert, G., and Kaschner, R. (1995). Construction of tight-binding-like potentials on the basis of density-functional theory: Application to carbon. *Phys. Rev. B.*, 51: 12947–12957.

Portmann, S. (2002). MOLEKEL, Version 4.3.win32. Swiss Center for Scientific Computing (CSCS)/ETHZ, Switzerland.

Raes, F., Janssens, A., and Van Dingenen, R. (1986). The role of ion-induced aerosol formation in the lower atmosphere. *J. Aerosol Sci.*, 17: 466–470.

Ruusuvuori, K., Kurtén, T., Ortega, I. K., Faust, J., and Vehkamäki, H. (2013). Proton affinities of candidates for positively charged ambient ions in boreal forests. *Atmos. Chem. Phys.*, 13: 10397–10404.

Schaftenaar, G., and Noordik, J. H. (2000). Molden: a pre- and post-processing program for molecular and electronic structures. *J. Comput.-Aided Mol. Design*, 14: 123–134.

Schobesberger, S., Junninen, H., Bianchi, F., Lönn, G., Ehn, M., Lehtipalo, K., Dommen, J., Ehrhart, S., Ortega, I. K., Franchin, A., Nieminen, T., Riccobono, F., Hutterli, M., Duplissy, J., Almeida, J., Amorim, A., Breitenlechner, M., Downard, A. J., Dunne, E. M., Flagan, R. C., Kajos, M., Keskinen, H., Kirkby, J., Kupc, A., Kürten, A., Kurtén, T., Laaksonen, A., Mathot, S., Onnela, A., Praplan, A. P., Rondo, L., Santos, F. D., Schallhart, S., Schnitzhofer, R., Sipilä, M., Tomé, A., Tsagkogeorgas, G., Vehkamäki,H., Wimmer, D., Baltensperger, U., Carslaw, K. S., Curtius, J., Hansel, A., Petäjä, T., Kulmala, M., Donahue, N. M., Worsnop, D. R.

(2013). Molecular understanding of atmospheric particle formation from sulfuric acid and large oxidized organic molecules. *Proc. Natl. Acad. Sci. USA*, 110: 17223–17228 (2013).

Scott, A. P., and Radom, L. (1996). Harmonic Vibrational Frequencies: An Evaluation of Hartree-Fock, Møller-Plesset, Quadratic Configuration Interaction, Density Functional Theory, and Semiempirical Scale Factors. *J. Chem. Phys.*, 100: 16502–16513.

Seinfeld, J.H., and Pandis, S.N. (2006). Atmospheric Chemistry and Physics: From Air Pollution to Climate Change. John Wiley & Sons, Inc., New York, NY., USA.

Shah, A. S. V., Langrish, J. P., Nair, H., McAllister, D. A., Hunter, A. L., Donaldson, K., Newby, D. E., and Mills, N. L. (2013). Global association of air pollution and heart failure: a systematic review and meta-analysis. *Lancet*, 382: 1039–1048.

Smith, J. N., Barsanti, K. C., Friedli, H. R., Ehn, M., Kulmala, M., Collins, D. R., Scheckman, J. H., Williams, B. J., and McMurry, P. H. (2010). Observations of aminium salts in atmospheric nanoparticles and possible climatic implications. *Proc. Natl. Acad. Sci. USA*, 107: 6634–6639.

Smith, W., Yong, C. W., and Rodger, P. M. (2002). DL_POLY: Application to molecular simulation. *Molec. Simulat.*, 28: 385–471.

Soler, J. M., Artacho, E., Gale, J. D., Garcia, A., Junquera, J., Ordejon, P., and Sanchez-Portal, D. (2002). The SIESTA method for ab initio order-N materials simulation. *J. Phys.:Condens. Mat.*, 14: 2745–2779.

Sorokin, A., and Arnold, F. (2007). Laboratory study of cluster ions formation in H_2SO_4-H_2O system: implications for threshold concentration of gaseous H2SO4 and ion-induced nucleation kinetics. *Atmos. Environ.*, 41: 3740–3747.

Stephens, P. J., Devlin, F. J., Chabalowski, C. F., and Frisch, M. J. (1994). Ab Initio Calculation of Vibrational Absorption and Circular Dichroism Spectra Using Density Functional Force Fields. *J. Phys. Chem.*, 98: 11623–11627.

Swope, W. C., Andersen, H. C., and Berens, P. H., and Wilson, K. R. (1982). A computer simulation method for the calculation of equilibrium constants for the formation of physical clusters of molecules: Application to small water clusters. *J. Chem. Phys.*, 76: 637–649.

Szabo, A., and Ostlund, N. S. (1996). Modern Quantum Chemistry. Introduction to Advanced Electronic Structure Theory. Dover Publications, Inc., Mineola, NY, USA. *Unabridged and unaltered republication of the "First Edition, Revised," originally published by the McGraw-Hill Publishing Company, New York, 1989. The original edition was published by the Macmillan Publishing Company, New York, 1982.*

Temelso, B., Morrell, T. E., Shields, R. M., Allodi, M. A., Wood, E. K., Kirschner, K. N., Castonguay, T. C., Archer, K. A., and Shields, G. C. (2012). Quantum Mechanical Study of Sulfuric Acid Hydration: Atmospheric Implications. *J. Phys. Chem. A*, 116: 2209–2224.

Tobias, D. J., Martyna, G. J., and Klein, M. L. (1993). Molecular Dynamics Simulations of a Protein in the Canonical Ensemble. *J. Phys. Chem.*, 97: 12959–12966.

Torpo, L., Kurtén, T., Vehkamäki, H., Sundberg, M.R., Laasonen, K., and Kulmala, M. (2007). The significant role of ammonia in atmospheric nanoclusters. *J. Phys. Chem. A*, 111: 10671—10674.

Tuckerman, M. E. (2010). Statistical Mechanics: Theory and Molecular Simulation. Oxford University Press, Oxford, UK.

TURBOMOLE V5.8 2005 and V5.91 2007, a development of University of Karlsruhe and Forschungszentrum Karlsruhe GmbH, 1989-2007, TURBOMOLE GmbH, since 2007; available from `http://www.turbomole.com`.

Turco, R. P., Zhao, J.-X., and Yu, F. (1998). A new source of tropospheric aerosols: Ion–ion recombination. *Geophys. Res. Lett.*, 25: 635–638.

VandeVondele, J., Krack, M., Mohamed, F., Parrinello, M., Chassaing, T., and Hutter, J. (2005). QUICKSTEP: Fast and accurate density functional calculations using a mixed Gaussian and plane waves approach. *Comput. Phys. Commun.*, 167: 103–128.

van Duin, A. C. T., Dasgupta, S., Lorant, F., and Goddard III, W. A. (2001). ReaxFF: A Reactive Force Field for Hydrocarbons. *J. Phys. Chem. A*, 105: 9396–9409.

Wavefunction, Inc. (2006). Spartan '06, Windows version. Irvine, CA, US.

Wedekind, J., Reguera, D., and Strey, R. (2007). Influence of thermostats and carrier gas on simulations of nucleation. *J. Chem. Phys.*, 127: 064501.

Weigend, F, and Hšer, M. (1997). RI-MP2: First derivatives and global consistency. *Theor. Chem. Acc.*, 97:331–340.

Wix, A., Brachert, L., Sinanis, S., and Schaber, K. (2010). A simulation tool for aerosol formation during sulphuric acid absorption in a gas cleaning process. *Journal of Aerosol Science*, 41: 1066–1079.

Yli-Juuti, T. (2013). On the growth of atmospheric nanoparticles by organic vapors. Academic dissertation. Report Series in Physics, HU-P-D208, University of Helsinki.

Yu, H., and Lee, S.-H. (2012). Chemical ionisation mass spectrometry for the measurement of atmospheric amines. *Environ. Chem.*, 9: 190–201.

Yu, H., McGraw, R., Lee, S.-H. (2012). Effects of amines on formation of sub-3 nm particles and their subsequent growth. *Geophys. Res. Lett.*, 39: L02807.

Zhao, Y., and Truhlar, D. G. (2008). The M06 suite of density functionals for main group thermochemistry, thermochemical kinetics, noncovalent interactions, excited states, and transition elements: two new functionals and systematic testing of four M06-class functionals and 12 other functionals. *Theor. Chem. Accounts*, 120: 215–241.

Zhao, J., Smith, J. N., Eisele, F. L., Chen, M., Kuang, C., and McMurry, P. H. (2011). Observation of neutral sulphuric acid-amine containing clusters in laboratory and ambient measurements. *Atmos. Chem. Phys.*, 11: 10823–10836.

Zollner, J. H., Glasoe, W. A., Panta, B., Carlson, K. K., McMurry, P. H., and Hanson, D. R. (2012). Sulfuric acid nucleation: power dependencies, variation with relative humidity, and effect of bases. *Atmos. Chem. Phys.*, 12: 4399–4411.

Paper I

Atmos. Chem. Phys., 8, 4095–4103, 2008
www.atmos-chem-phys.net/8/4095/2008/

Atmospheric Chemistry and Physics

Amines are likely to enhance neutral and ion-induced sulfuric acid-water nucleation in the atmosphere more effectively than ammonia

T. Kurtén, V. Loukonen, H. Vehkamäki, and M. Kulmala

Division of Atmospheric Sciences and Geophysics, Dept. of Physics, P.O.Box 64, 00014 University of Helsinki, Finland

Received: 12 February 2008 – Published in Atmos. Chem. Phys. Discuss.: 16 April 2008
Revised: 17 June 2008 – Accepted: 17 June 2008 – Published: 30 July 2008

Abstract. We have studied the structure and formation thermodynamics of dimer clusters containing H_2SO_4 or HSO_4^- together with ammonia and seven different amines possibly present in the atmosphere, using the high-level ab initio methods RI-MP2 and RI-CC2. As expected from e.g. proton affinity data, the binding of all studied amine-H_2SO_4 complexes is significantly stronger than that of $NH_3 \bullet H_2SO_4$, while most amine-HSO_4^- complexes are only somewhat more strongly bound than $NH_3 \bullet HSO_4^-$. Further calculations on larger cluster structures containing dimethylamine or ammonia together with two H_2SO_4 molecules or one H_2SO_4 molecule and one HSO_4^- ion demonstrate that amines, unlike ammonia, significantly assist the growth of not only neutral but also ionic clusters along the H_2SO_4 co-ordinate. A sensitivity analysis indicates that the difference in complexation free energies for amine- and ammonia-containing clusters is large enough to overcome the mass-balance effect caused by the fact that the concentration of amines in the atmosphere is probably 2 or 3 orders of magnitude lower than that of ammonia. This implies that amines might be more important than ammonia in enhancing neutral and especially ion-induced sulfuric acid-water nucleation in the atmosphere.

1 Introduction

Based on experimental and modeling results, particle formation by nucleation in the lower atmosphere is thought to involve water and sulfuric acid, with possible contributions from ions, ammonia or various organic molecules (Korhonen et al., 1999; Kulmala et al., 2000; Anttila et al., 2005). Recent experimental results (Kulmala et al., 2007) indicate that neutral mechanisms are likely to dominate nucleation at least in boreal forest areas, with ion-induced nucleation playing only a small role. The effect of ammonia in the sulfuric acid-water nucleation process has been studied extensively. Experimental results (Ball et al., 1999) suggest that ammonia enhances nucleation by 1–2 orders of magnitude, whereas theoretical studies have previously given varying predictions. Recent quantum chemical calculations demonstrate that when appropriate methods are applied to sufficiently large cluster structures (containing two or more sulfuric acid molecules), also molecular-level simulations reproduce the experimentally observed nucleation-enhancing effect (Kurtén et al., 2007a; Torpo et al., 2007; Nadykto and Yu, 2007). Experiments (Ball et al., 1999), updated and corrected classical nucleation theory simulations (Anttila et al., 2005) and quantum chemical calculations are now all in qualitative agreement, and indicate a modest enhancement of sulfuric acid-water nucleation by ammonia in most atmospheric conditions.

Based on both experimental and theoretical results (Kulmala et al., 2004a), neutral binary sulfuric acid-water nucleation alone can not explain most of the new-particle formation events observed in the atmosphere. Also, in a recent study, Laakso et al. (2007) measured boundary layer particle formation using a hot-air balloon, and came to the conclusion that ion-induced nucleation of water-sulfuric acid clusters can not explain the observed formation of charged nanoparticles. In numerical simulations based on the thermodynamic data of Lovejoy et al. (2004), they found that that binary ion-induced nucleation could not explain most of the observed nucleation even if sulfuric acid concentrations twice as large as those estimated from the measured SO_2 concentrations were used. This would suggest that some other

Correspondence to: T. Kurtén
(theo.kurten@helsinki.fi)

compounds are involved in stabilizing the clusters. Kurtén et al. (2007b) recently computed formation energies for small neutral and ionic sulfuric acid-water and sulfuric acid-water-ammonia clusters, and found that the HSO_4^- ion is very weakly bound to ammonia. This result was confirmed by Ortega et al. (2008), who also computed formation energies of charged clusters containing HSO_4^-, NH_3 and up to three H_2SO_4 molecules, and found that ammonia does not enhance ion-induced sulfuric acid-water nucleation. Some other compound or family of compounds are thus needed to explain the experimental observations of Laakso et al. (2007).

Like ammonia, amines are able to form e.g. nitrate or sulfate salts in atmospheric conditions. Indeed, chemical intuition and proton affinity data (Hunter and Lias, 1998) indicates that proton transfer should occur more easily for amine-acid clusters than for ammonia-acid clusters, leading to stronger binding. Based on laboratory chamber experiments and quantum chemical calculations on crystal structures, Murphy et al. (2007) recently reported that for nucleation processes involving nitric acid, amines such as diethylamine may be more effective than ammonia in forming new particles. Based on a combination of smog chamber experiments and field measurements, Angelino et al. (2001) suggested that amine chemistry "may play a significant role in particle formation in regions with high amine concentrations" due to both acid-base and oxidation reactions. Also, in an experimental study by Mäkelä et al. (2001) dimethylammonium, the ionic form of dimethylamine, was found to be present in aerosol particles during particle formation events and/or the immediately following particle growth processes in Hyytiälä, Southern Finland. The relative difference between event and non-event dimethylamine concentrations in the aerosol phase were approximately 50-fold, indicating that dimethylamine is involved in particle formation. In view of these results, it is possible that amines, instead of ammonia, are the primary enhancers of sulfuric acid-water nucleation, or may at least significantly contribute to particle formation in the atmosphere.

As a first step in the investigation of the atmospheric relevance of sulfuric acid-amine clusters, we have calculated the structure and binding energies of clusters comprising one sulfuric acid and either ammonia, methylamine, dimethylamine, trimethylamine, ethylamine, diethylamine, triethylamine or ethylmethylamine, using high-level ab initio methods. The same calculations were then performed with the hydrogensulfate ion instead of sulfuric acid. Based on the results of these calculations, as well as the results of Mäkelä et al. (2001), further calculations were then carried out on clusters containing dimethylamine or ammonia together with either two sulfuric acid molecules or one sulfuric acid molecule and one hydrogensulfate ion. Qualitative estimates for the formation enthalpies, entropies and Gibbs free energies were then computed for all clusters using the harmonic oscillator and rigid rotor approximations.

2 Computational details

All calculations were performed using the Turbomole v.5.8. program suite (Ahlrichs et al., 1989; Häser and Ahlrichs, 1989). For structure optimizations and vibrational frequency calculations, we used the RI-MP2 method (Weigend and Häser, 1997; Weigend et al., 1998) with the frozen-core approximation and the aug-cc-pV(D+d)Z basis set (Dunning et al., 2001), though some test optimizations were also performed using the larger aug-cc-pV(T+d)Z basis set (Dunning et al., 2001) (see the supporting information for details). The auxiliary basis sets needed for the RI expansion are given by Weigend et al. (2002). Final electronic energies were computed using the RI-MP2 and RI-CC2 methods (Christiansen et al., 1995) and the aug-cc-pV(T+d)Z basis set. Though the correlation energy computed by the RI-CC2 method is more accurate than that given by RI-MP2, the RI-CC2 method is primarily designed to compute molecular properties rather than energies, and it should therefore be noted that the results are thus not as accurate as those computed using, for example, the more demanding coupled cluster methods CCSD or CCSD(T). In a recent high-level study on small neutral and charged sulfuric acid - water clusters (Kurtén et al., 2007b), we have shown that at the RI-MP2 level, increasing the basis set size beyond aug-cc-pV(T+d)Z has only a small effect on the intermolecular binding (complexation) energies. The commonly used counterpoise (CP) correction seems to significantly exaggerate basis-set related errors for large basis sets containing multiple diffuse basis functions (Kurtén et al., 2007b; Feller, 1992), and is therefore not computed here. The convergence with respect to the electronic energy in the self-consistent field (SCF) step was 10^{-7} a.u. (atomic units), and the convergence with respect to the gradient was 10^{-4} a.u. For the numerical frequency calculations, a step-size of 0.01 a.u. and a SCF convergence limit of 10^{-8} a.u. were used, based on test calculations carried out as part of an earlier study on sulfuric acid-ammonia clusters (Kurtén et al., 2007c). As the emphasis of this study is on comparing complex formation free energies of amine- and ammonia-containing clusters rather than on computing accurate absolute free energies, no scaling factors were used to account for vibrational anharmonicity. For details on the effect of anharmonicity on this type of cluster structures, and on the difficulties in constructing reliable scaling factor approaches for free energy calculations, see Kurtén et al. (2007b).

3 Results and discussion

The structures of the studied dimer clusters are shown in Figs.1–2. Figure 1 contains the neutral H_2SO_4-amine dimer complexes, while Fig. 2 contains the ionic HSO_4^--amine dimer complexes. The structures are drawn using the MOLEKEL 4.3 visualization package (Portmann, 2002). The corresponding electronic energies,

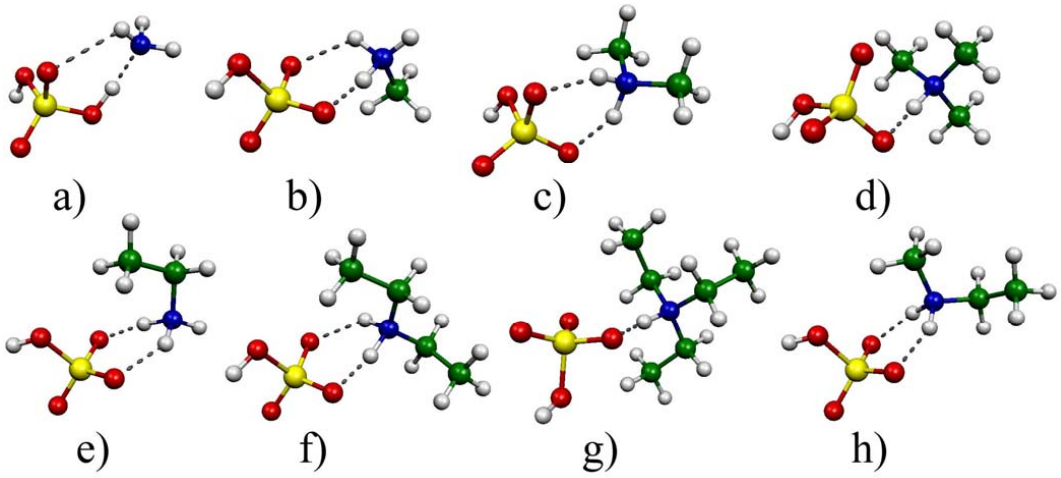

Fig. 1. The structures of dimer clusters containing sulfuric acid and ammonia or various amines: **a)** $H_2SO_4 \bullet NH_3$, **b)** $H_2SO_4 \bullet CH_3NH_2$, **c)** $H_2SO_4 \bullet (CH_3)_2NH$, **d)** $H_2SO_4 \bullet (CH_3)_3N$, **e)** $H_2SO_4 \bullet CH_3CH_2NH_2$, **f)** $H_2SO_4 \bullet (CH_3CH_2)_2NH$, **g)** $H_2SO_4 \bullet (CH_3CH_2)_3N$, **h)** $H_2SO_4 \bullet (CH_3CH_2)NH(CH_3)$. Hydrogen bonds are indicated by dashed lines. Color coding: yellow = sulfur, red = oxygen, blue = nitrogen, green = carbon and white = hydrogen.

Table 1. Electronic energies computed for the dimer formation reactions at different levels of theory. DZ and TZ correspond to aug-cc-pV(D+d)Z and aug-cc-pV(T+d)Z, respectively. All values correspond to geometries optimized at the RI-MP2/aug-cc-pV(D+d)Z level.

Reaction	ΔE_0, RI-MP2/DZ kcal/mol	ΔE_0, RI-MP2/TZ kcal/mol	ΔE_0, RI-CC2/TZ kcal/mol
$H_2SO_4 + NH_3 \leftrightarrow H_2SO_4 \bullet NH_3$	−16.99	−17.08	−17.37
$H_2SO_4 + CH_3NH_2 \leftrightarrow H_2SO_4 \bullet CH_3NH_2$	−21.91	−21.90	−22.84
$H_2SO_4 + CH_3CH_2NH_2 \leftrightarrow H_2SO_4 \bullet CH_3CH_2NH_2$	−23.78	−23.40	−24.53
$H_2SO_4 + (CH_3)_2NH \leftrightarrow H_2SO_4 \bullet (CH_3)_2NH$	−26.73	−26.06	−27.22
$H_2SO_4 + (CH_3CH_2)_2NH \leftrightarrow H_2SO_4 \bullet (CH_3CH_2)_2NH$	−30.05	−29.09	−30.19
$H_2SO_4 + (CH_3)_3N \leftrightarrow H_2SO_4 \bullet (CH_3)_3N$	−28.71	−27.51	−28.47
$H_2SO_4 + (CH_3CH_2)_3N \leftrightarrow H_2SO_4 \bullet (CH_3CH_2)_3N$	−33.09	−31.05	−32.16
$H_2SO_4 + (CH_3CH_2)NH(CH_3) \leftrightarrow H_2SO_4 \bullet (CH_3CH_2)NH(CH_3)$	−28.14	−27.34	−28.48
$HSO_4^- + NH_3 \leftrightarrow HSO_4^- \bullet NH_3$	−10.79	−10.60	−10.85
$HSO_4^- + CH_3NH_2 \leftrightarrow HSO_4^- \bullet CH_3NH_2$	−10.66	−9.79	−10.12
$HSO_4^- + CH_3CH_2NH_2 \leftrightarrow HSO_4^- \bullet CH_3CH_2NH_2$	−12.07	−10.92	−11.36
$HSO_4^- + (CH_3)_2NH \leftrightarrow HSO_4^- \bullet (CH_3)_2NH$	−14.06	−13.65	−14.25
$HSO_4^- + (CH_3CH_2)_2NH \leftrightarrow HSO_4^- \bullet (CH_3CH_2)_2NH$	−15.47	−14.56	−15.33
$HSO_4^- + (CH_3)_3N \leftrightarrow HSO_4^- \bullet (CH_3)_3N$	−13.12	−12.09	−12.80
$HSO_4^- + (CH_3CH_2)_3N \leftrightarrow HSO_4^- \bullet (CH_3CH_2)_3N$	−15.61	−13.81	−14.78
$HSO_4^- + (CH_3CH_2)NH(CH_3) \leftrightarrow HSO_4^- \bullet (CH_3CH_2)NH(CH_3)$	−15.03	−14.31	−15.03

enthalpies and entropies are presented in the supporting information along with the coordinates for all studied cluster structures (http://www.atmos-chem-phys.net/8/4095/2008/acp-8-4095-2008-supplement.pdf).

The electronic energies for the formation of the various dimer clusters from their constituent molecules are shown in Table 1. The values have been computed at three levels of theory: RI-MP2/aug-cc-pV(D+d)Z, RI-MP2/aug-cc-pV(T+d)Z, and RI-CC2/aug-cc-pV(T+d)Z. Table 2 lists the corresponding enthalpies, entropies and Gibbs free energies for complex formation at 298 K and 1 atm reference pressure, computed using the RI-MP2/aug-cc-pV(D+d)Z harmonic vibrational frequencies with the RI-CC2/aug-cc-pV(T+d)Z electronic energies. The use of harmonic vibrational frequencies for the HSO_4^- ion causes moderately large errors in the absolute values of the complexation free energy for the ionic

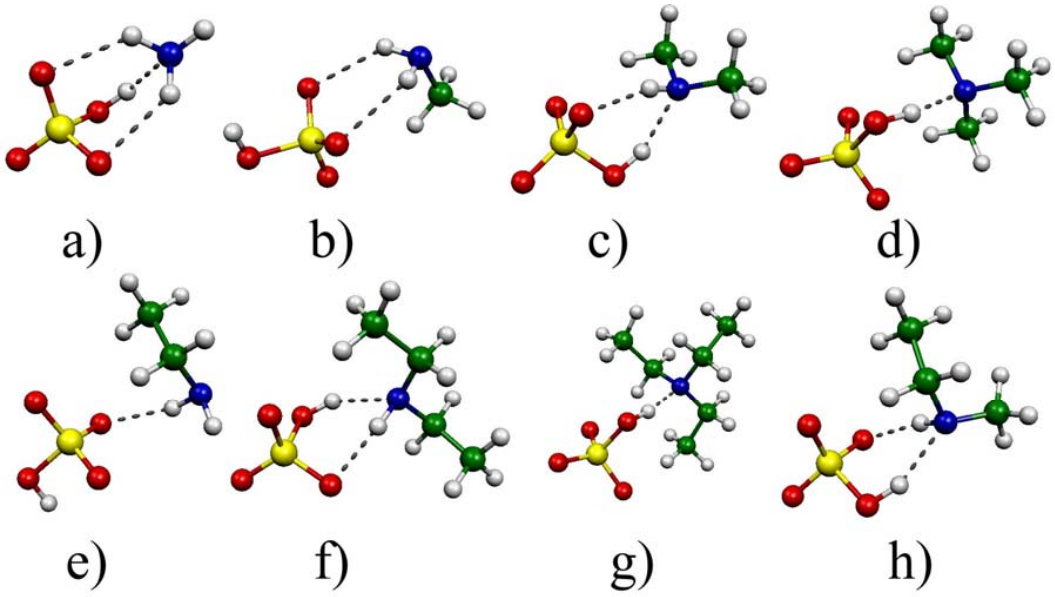

Fig. 2. The structures of ionic dimer clusters containing a hydrogensulfate ion and ammonia or various amines: **a)** $HSO_4^-\bullet NH_3$, **b)** $HSO_4^-\bullet CH_3NH_2$, **c)** $HSO_4^-\bullet(CH_3)_2NH$, **d)** $HSO_4^-\bullet(CH_3)_3N$, **e)** $HSO_4^-\bullet CH_3CH_2NH_2$, **f)** $HSO_4^-\bullet(CH_3CH_2)_2NH$, **g)** $HSO_4^-\bullet(CH_3CH_2)_3N$, **h)** $HSO_4^-\bullet(CH_3CH_2)NH(CH_3)$. Hydrogen bonds are indicated by dashed lines. Color coding as in Fig. 1.

Table 2. Enthalpies, entropies and Gibbs free energies computed for the dimer formation reactions at 298 K and 1 atm reference pressure for all reactants. All values correspond to RI-MP2/aug-cc-pV(D+d)Z geometries and harmonic vibrational frequencies and RI-CC2/aug-cc-pV(T+d)Z electronic energies.

Reaction	ΔH (298 K) kcal/mol	ΔS (298 K) cal/Kmol	ΔG(298 K) kcal/mol
$H_2SO_4 + NH_3 \leftrightarrow H_2SO_4\bullet NH_3$	−16.06	−31.60	−6.64
$H_2SO_4 + CH_3NH_2 \leftrightarrow H_2SO_4\bullet CH_3NH_2$	−20.87	−36.62	−9.95
$H_2SO_4 + CH_3CH_2NH_2 \leftrightarrow H_2SO_4\bullet CH_3CH_2NH_2$	−22.45	−38.22	−11.06
$H_2SO_4 + (CH_3)_2NH \leftrightarrow H_2SO_4\bullet(CH_3)_2NH$	−24.73	−37.14	−13.66
$H_2SO_4 + (CH_3CH_2)_2NH \leftrightarrow H_2SO_4\bullet(CH_3CH_2)_2NH$	−27.73	−37.65	−16.53
$H_2SO_4 + (CH_3)_3N \leftrightarrow H_2SO_4\bullet(CH_3)_3N$	−26.01	−36.08	−15.26
$H_2SO_4 + (CH_3CH_2)_3N \leftrightarrow H_2SO_4\bullet(CH_3CH_2)_3N$	−29.54	−41.04	−17.30
$H_2SO_4 + (CH_3CH_2)NH(CH_3) \leftrightarrow H_2SO_4\bullet(CH_3CH_2)NH(CH_3)$	−25.94	−36.78	−14.97
$HSO_4^- + NH_3 \leftrightarrow HSO_4^-\bullet NH_3$	−9.07	−40.57	1.75
$HSO_4^- + CH_3NH_2 \leftrightarrow HSO_4^-\bullet CH_3NH_2$	−8.68	−33.14	1.20
$HSO_4^- + CH_3CH_2NH_2 \leftrightarrow HSO_4^-\bullet CH_3CH_2NH_2$	−10.00	−33.82	0.09
$HSO_4^- + (CH_3)_2NH \leftrightarrow HSO_4^-\bullet(CH_3)_2NH$	−12.73	−40.15	−0.76
$HSO_4^- + (CH_3CH_2)_2NH \leftrightarrow HSO_4^-\bullet(CH_3CH_2)_2NH$	−14.37	−43.76	−0.94
$HSO_4^- + (CH_3)_3N \leftrightarrow HSO_4^-\bullet(CH_3)_3N$	−11.27	−39.46	0.50
$HSO_4^- + (CH_3CH_2)_3N \leftrightarrow HSO_4^-\bullet(CH_3CH_2)_3N$	−13.35	−44.80	0.01
$HSO_4^- + (CH_3CH_2)NH(CH_3) \leftrightarrow HSO_4^-\bullet(CH_3CH_2)NH(CH_3)$	−13.49	−38.20	−1.71

clusters, as the free ion is likely to possess an internal rotation degree of freedom (Kurtén et al., 2007b). However, the contribution of this error source is essentially constant, so the relative energetics (e.g. differences in formation free energies between HSO_4^--ammonia and HSO_4^--amine complexes) are still relatively reliable.

It can be seen from Tables 1 and 2 that the complexes of sulfuric acid and the hydrogensulfate ion with the various amines studied are almost always stronger bound than the corresponding complexes with ammonia. (The sole exception is $HSO_4^-\bullet CH_3NH_2$, which is slightly less stable than $HSO_4^-\bullet NH_3$ with respect to the electronic energy, though

not the free energy.) For the neutral dimers, the stabilization effect associated with the substitution of one or more hydrogens of ammonia with alkyl groups is very large, on the order of 5–15 kcal/mol. The magnitude of this effect systematically increases both with the number and size of the alkyl substituents. As expected, the ordering of the complexation free energies for the neutral dimers follows that of the proton affinites reported by Hunter and Lias (1998). However, for the charged dimers, this is not the case. Overall, the stabilization effect is much smaller for the charged clusters, on the order of 0–3 kcal/mol, and while increasing the substituent size still systematically increases the stability of the complex, the dimers containing disubstituted amines are more stable than the dimers containing mono- or trisubstituted amines.

For the neutral complexes, the main reason for the large effect on the formation energies is apparent from Fig. 1: the alkyl groups on the amines are better able to stabilize the positive charge associated with proton transfer from an SOH group to the nitrogen atom, which leads to the formation of a strongly bound ion pair. For H_2SO_4-NH_3 clusters, in contrast, the presence of two sulfuric acids are required for proton transfer to occur (Kurtén et al., 2007a; Nadykto and Yu, 2007). This also explains, on a microscopic level, the growth in stability (and increase in proton affinity) as a function of substituent size and number: larger and more numerous substituents are able to stabilize the positive charge better.

In the case of the HSO_4^- ion, there is no weakly bound proton to transfer, and the change in stability is correspondingly smaller, as it involves only the strengthening of existing hydrogen bonds instead of the formation of new ion pairs. The decrease in stability in going from di- to trisubstituted amines is probably explained by the fact that while the disubstituted amines can form two hydrogen bonds with HSO_4^-, the trisubstituted amines can form only one, as they lack the additional hydrogen atom needed for the bond (see Fig. 2). For the neutral complexes, the increased ion pair stabilization in going from di- to trisubstituted amines seems to outweigh the absence of the second, weaker hydrogen bond. However, the difference in stability between dimers containing di- and trisubstituted amines is much smaller than the difference between dimers containing mono- and disubstitude amines, especially in the case of the neutral complexes. While it is very unlikely that the addition of water molecules will change the central conclusion that amines are much more strongly bound to sulfuric acid than ammonia is, hydration may change the bonding patterns seen in Figs. 1–3, and affect the relative stability of different amine-acid clusters. For example, the more highly substituted amines are less hydrophilic than ammonia or the less substituted amines. Thus, accounting for hydration of the clusters is likely to somewhat decrease the differences in stability observed in Tables 1 and 2.

In order to assess the importance of amines for sulfuric acid-related nucleation processes, it is not enough to know how strongly they are bound to a single sulfuric acid molecule (or hydrogensulfate ion). Information on the ability of the amines to promote the addition of further sulfuric acid molecules to the cluster, and thus lower the nucleation barrier, is also required. Toward this end, we have computed reaction free energies for the addition of a sulfuric acid molecule to a cluster containing one sulfuric acid molecule or hydrogensulfate ion together with either ammonia or dimethylamine. Data for the dimer clusters containing only H_2SO_4 and HSO_4^- is provided for reference. Dimethylamine was chosen as a representative amine both due to computational considerations - it is considerably smaller than e.g. triethylamine – and based on the results of Mäkelä et al. (2001) which indicate that it is present in the atmosphere in boreal forest conditions. The results are presented in Tables 3 and 4, while the corresponding lowest-energy cluster structures are shown in Fig. 3. A comparison of Fig. 3 with Tables 3 and 4 shows that even though the structure and binding patterns of the ammonia- and dimethylamine-containing clusters are similar, dimethylamine enhances the addition of sulfuric acid to the clusters considerably more

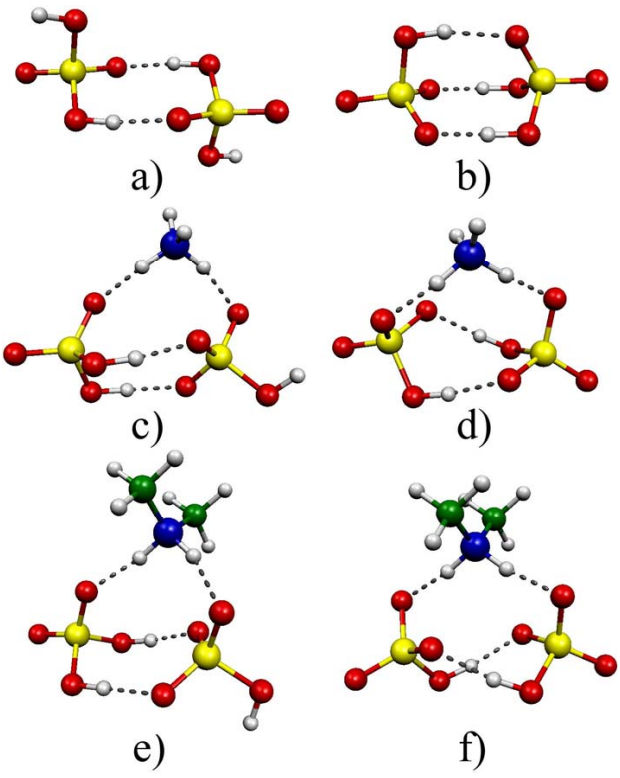

Fig. 3. The structures of most stable cluster structures containing two sulfuric acid molecules or one sulfuric acid and one hydrogensulfate ion: **a)** $(H_2SO_4)_2$, **b)** $H_2SO_4 \bullet HSO_4^-$, **c)** $(H_2SO_4)_2 \bullet NH_3$, **d)** $H_2SO_4 \bullet HSO_4^- \bullet NH_3$, **e)** $(H_2SO_4)_2 \bullet (CH_3)_2NH$, **f)** $H_2SO_4 \bullet HSO_4^- \bullet (CH_3)_2NH$. Hydrogen bonds are indicated by dashed lines. Color coding as in Fig. 1.

Table 3. Electronic energies computed for the addition of sulfuric acid to various clusters, at different levels of theory. DZ and TZ correspond to aug-cc-pV(D+d)Z and aug-cc-pV(T+d)Z, respectively. All values correspond to geometries optimized at the RI-MP2/aug-cc-pV(D+d)Z level.

Reaction	ΔE_0, RI-MP2/DZ kcal/mol	ΔE_0, RI-MP2/TZ kcal/mol	ΔE_0, RI-CC2/TZ kcal/mol
$H_2SO_4 + H_2SO_4 \leftrightarrow (H_2SO_4)_2$	−17.99	−18.97	−19.04
$H_2SO_4 \bullet NH_3 + H_2SO_4 \leftrightarrow (H_2SO_4)_2 \bullet NH_3$	−29.51	−30.53	−31.21
$H_2SO_4 \bullet (CH_3)_2NH + H_2SO_4 \leftrightarrow (H_2SO_4)_2 \bullet (CH_3)_2NH$	−33.66	−34.38	−34.41
$HSO_4^- + H_2SO_4 \leftrightarrow HSO_4^- \bullet H_2SO_4$	−47.11	−48.87	−49.05
$HSO_4^- \bullet NH_3 + H_2SO_4 \leftrightarrow HSO_4^- \bullet H_2SO_4 \bullet NH_3$	−49.68	−50.27	−51.23
$HSO_4^- \bullet (CH_3)_2NH + H_2SO_4 \leftrightarrow HSO_4^- \bullet H_2SO_4 \bullet (CH_3)_2NH$	−59.01	−58.39	−59.40

Table 4. Enthalpies, entropies and Gibbs free energies computed for the addition of sulfuric acid to various ammonia or dimethylamine-containing clusters, at 298 K and 1 atm reference pressure for all reactants. All values correspond to RI-MP2/aug-cc-pV(D+d)Z geometries and harmonic vibrational frequencies and RI-CC2/aug-cc-pV(T+d)Z electronic energies.

Reaction	ΔH (298 K) kcal/mol	ΔS (298 K) cal/Kmol	ΔG(298 K) kcal/mol
$H_2SO_4 + H_2SO_4 \leftrightarrow (H_2SO_4)_2$	−17.81	−36.51	−6.93
$H_2SO_4 \bullet NH_3 + H_2SO_4 \leftrightarrow (H_2SO_4)_2 \bullet NH_3$	−28.74	−48.00	−14.43
$H_2SO_4 \bullet (CH_3)_2NH + H_2SO_4 \leftrightarrow (H_2SO_4)_2 \bullet (CH_3)_2NH$	−32.70	−44.97	−19.29
$HSO_4^- + H_2SO_4 \leftrightarrow HSO_4^- \bullet H_2SO_4$	−48.20	−47.29	−34.10
$HSO_4^- \bullet NH_3 + H_2SO_4 \leftrightarrow HSO_4^- \bullet H_2SO_4 \bullet NH_3$	−49.57	−45.39	−34.75
$HSO_4^- \bullet (CH_3)_2NH + H_2SO_4 \leftrightarrow HSO_4^- \bullet H_2SO_4 \bullet (CH_3)_2NH$	−56.94	−49.93	−42.05

effectively than ammonia, with the difference in reaction free energies being approximately 5 kcal/mol for the neutral clusters and 7 kcal/mol for the charged clusters. Especially the latter results is significant, as it implies that, despite the low attraction between the various amines and the HSO_4^- ion, amines, unlike ammonia, might still enhance ion-induced sulfuric acid nucleation. This is especially relevant given the suggestion by Laakso et al. (2007) that some third compound besides sulfuric acid and water is needed to explain the observed ion-induced contribution to nucleation events in the boreal forest.

Beside thermodynamic data at standard conditions, information on the concentrations of the reactant species is also required to determine the atmospheric role of sulfuric acid-amine cluster formation. From the law of mass balance, the ratio of the concentrations of e.g. dimethylamine - containing clusters to ammonia - containing clusters can be expressed as:

$$\frac{[X \bullet (CH_3)_2NH]}{[X \bullet NH_3]} = \frac{[(CH_3)_2NH]}{[NH_3]} e^{\frac{-\Delta\Delta G_0}{RT}} \quad (1)$$

where X indicates some cluster composition (e.g. $H_2SO_4 \bullet H_2SO_4$ or $H_2SO_4 \bullet HSO_4^-$), T is the temperature in Kelvin, R is the molar gas constant and $\Delta\Delta G_0$ is the difference in the standard free energies of formation for the $X \bullet (CH_3)_2NH$ and $X \bullet NH_3$ clusters. Thus, if the gas-phase concentration of dimethylamine is e.g. 100–1000 times smaller than the concentration of ammonia, the formation free energies for the dimethylamine-containing clusters must be more than 3–4 kcal/mol lower than that of the ammonia-containing clusters for their concentrations to be equal.

Unfortunately, there is very little data on the atmospheric concentrations of any amine species. According to Schade and Crutzen (1995), the combined global emissions of methylamine, dimethylamine and trimethylamine in 1988 were 150±60 TgN, about 3/4 of which consisted of trimethylamine. This corresponds to about 1/150 of the global ammonia emissions, implying that, on average, amine concentrations are at least two orders of magnitude lower than those of ammonia. As ammonia concentrations in continental air are typically in the 0.1–10 ppb range (Seinfeld and Pandis, 1998), this would indicate that amine concentrations are on the order of 1–100 ppt. Because amines are more rapidly oxidized by OH than ammonia, this should probably be considered an upper limit, and far from the emission sources the amine- to ammonia-concentration ratio may be

Table 5. Ratio of the concentrations of dimethylamine-containing to ammonia-containing neutral and ionic trimer clusters, as a function of the gas-phase concentration ratio of dimethylamine to ammonia in a hypothetical steady-state situation, based on the free energies of complex formation given in Tables 2 and 4.

$[(CH_3)_2NH]/[NH_3]$ ratio	$[(H_2SO_4)_2\bullet(CH_3)_2NH]/[(H_2SO_4)_2\bullet NH_3]$ ratio	$[HSO_4^-\bullet H_2SO_4\bullet(CH_3)_2NH]/[HSO_4^-\bullet H_2SO_4\bullet NH_3]$ ratio
1:10	5.2×10^7:1	1.5×10^6:1
1:100	5.2×10^6:1	1.5×10^5:1
1:1000	5.2×10^5:1	1.5×10^4:1
1:10000	5.2×10^4:1	1.5×10^3:1

even smaller. However, at a boreal forest site in Hyytiälä, Finland, trimethylamine concentrations during a spring measurement campaign (Sellegri et al., 2005) varied between 34 and 80 ppt, indicating that the order-of-magnitude estimate above may be roughly correct. Close to amine emission sources, concentrations may be much higher, e.g. diethylamine and butylamine concentrations of over 100 ppb have been reported in the vicinity of a dairy farm in California (Rabaud et al., 2003).

These measurements and estimates show that the number concentration of amine molecules may well be equal to or greater than that of sulfuric acid, which typically has concentrations of 10^7 molecules cm^{-3} (corresponding to 0.4 ppt at 298 K) or less in non-polluted areas (Spracklen et al., 2006). Even for amine concentrations as low as 1 ppt, the collision rate of amine and sulfuric acid molecules would thus still be on the order of 10^4–10^5 collisions $cm^{-3}\,s^{-1}$, indicating that the formation of atmospherically significant amounts of amine-sulfuric acid clusters is at least not ruled out by collision kinetics. Still, in these conditions each sulfuric acid molecule or small cluster collides with an amine molecule only every 100 s or so, implying that while amines are likely to play a significant role in the initial steps of nucleation, their role in subsequent particle growth is likely to be minor. This is in line with atmospheric observations which indicate that the vapors responsible for the formation of 1 nm – scale particles are not the same as those responsible for the growth of particles (Kulmala et al., 2007).

Using the Eq. (1) together with free energies for complexation given in Tables 2 and 4, we have computed the ratio of the concentrations of $(H_2SO_4)_2\bullet(CH_3)_2NH$ to $(H_2SO_4)_2\bullet NH_3$ and $HSO_4^-\bullet H_2SO_4\bullet(CH_3)_2NH$ to $HSO_4^-\bullet H_2SO_4\bullet NH_3$ clusters as a function of the ratio of ammonia and dimethylamine concentrations. As the concentration ratios do not depend strongly on the temperature, results are shown only for 298 K. The results are presented in Table 5. It can be seen from Table 5 that even if the concentration of gas-phase dimethylamine is only one thousandth of the ammonia concentration, amine-containing clusters are still likely to dominate the cluster distribution. However, the application of Eq. (1) presumes a pseudo-steady-state situation, where the formation of complexes does not significantly deplete the gas-phase reservoir of reactant molecules. For very low absolute amine concentrations, this is almost certainly not the case: the formation of sulfuric acid-amine clusters will then quickly deplete the amine reservoir, and steady-state conditions will not apply. The results presented here should therefore be considered as qualitative order-of-magnitude assessments. A quantitatively reliable determination of the relative atmospheric importance of amine- and ammonia-containing clusters would require both much more reliable concentration data as well as fully kinetic nucleation simulations, which are beyond the scope of this study.

Previously, it has been thought that vegetation influences new-particle formation mainly via the emission of various types of terpenes, which are oxidized in the atmosphere to form condensable vapors (Kulmala et al., 2004b). These vapors may then participate in nucleation (O'Dowd et al., 2002), e.g. via reacting or clustering with sulfuric acid molecules. As vegetation is a also source of amines, a nucleation mechanism involving enhancement of sulfuric acid-water nucleation by biogenic amines would provide another link between biogenic vapor emissions from forests and particle formation. The results presented here indicate that the stable pool of 1.5–1.8 nm neutral clusters observed by Kulmala et al. (2007) in boreal forest conditions are likely to contain contributions from amine-sulfuric acid clustering rather than ammonia-sulfuric acid clustering reactions.

4 Conclusions

The dimer clusters of ammonia and seven different amine species with H_2SO_4 and HSO_4^- were studied using the RI-MP2 and RI-CC2 methods. Further calculations were performed on trimer clusters containing ammonia or dimethylamine together with two H_2SO_4 molecules or one H_2SO_4 molecule and one HSO_4^- ion. The computed free energies for complex formation show that amines are considerably

more effective than ammonia in enhancing the addition of sulfuric acid molecules to both neutral and ionic sulfuric acid clusters. This is especially relevant for the ionic clusters, as previous experimental and theoretical studies indicate that in addition to sulfuric acid and water, the participation of some third compound, other than ammonia, is needed to explain the ion-induced contribution to observed nucleation rates. Our results indicate that both neutral and ion-induced nucleation mechanisms involving sulfuric acid are likely to be enhanced much more effectively by amines than by ammonia, even after the differences in their atmospheric concentrations are accounted for. Quantitative determination of the effect of amines on sulfuric acid-water nucleation, and especially the relative effect of different amines, will require the explicit modeling of amine-sulfuric acid cluster hydration, which is beyond the scope of the present paper.

Acknowledgements. We acknowledge the Scientific Computing Center (CSC) in Espoo, Finland for computing time and the Academy of Finland for financial support. Furthermore, we wish to thank Martta Salonen for useful assistance.

Edited by: A. Wiedensohler

References

Ahlrichs, R., Bär, M., Häser, M., Horn, H., and Kölmel, C.: Electronic structure calculations on workstation computers: The program system Turbomole, Chem. Phys. Lett., 162, 165–169, 1989.

Angelino, A., Suess, D. T., and Prather, K.: Formation of Aerosol Particles from Reactions of Secondary and Tertiary Alkylamines: Characterization by Aerosol Time-of-Flight Mass Spectrometry, Environ. Sci. Technol. 35, 3130–3138, 2001.

Anttila, T., Vehkamäki, H., Napari, I., and Kulmala, M.: Effect of ammonium bisulphate formation on atmospheric water-sulphuric acid-ammonia nucleation, Boreal Env. Res., 10, 511–523, 2005.

Ball, S. M., Hanson, D. R., Eisele, F. L. ,and McMurry, P. H.: Laboratory studies of particle nucleation: Initial results for H_2SO_4, H_2O, and NH_3 vapors, J. Geophys. Res. D, 104, 23 709–23 718, 1999.

Christiansen, O., Koch, H., and Jørgensen, P.: The second-order approximate coupled cluster singles and doubles model CC2, Chem. Phys. Lett., 243, 409–418, 1995.

Dunning Jr., T. H., Peterson, K. A., and Wilson, A. K.: Gaussian basis sets for use in correlated molecular calculations. X. The atoms aluminum through argon revisited, J. Chem. Phys., 114, 9244–9253, 2001.

Feller, A. D.: Application of systematic sequences of wave functions to the water dimer, J. Chem. Phys., 96, 6104–6114, 1992.

Hunter, E. P. and Lias, S. G.: Evaluated Gas Phase Basicities and Proton Affinities of Molecules: An Update, J. Phys. Chem. Ref. Data, 27, 413–656 (data available online via the NIST Chemistry WebBook), 1998.

Häser, M. and Ahlrichs, R: Improvements on the direct SCF method, J. Comput. Chem., 10, 104–111, 1989.

Korhonen, P., Kulmala, M., Laaksonen, A., Viisanen, Y., McGraw, R., and Seinfeld, J. H.: Ternary nucleation of H_2SO_4, NH_3, and H_2O in the atmosphere, J. Geophys. Res., 104, 26 349–26 353, 1999.

Kulmala, M., Pirjola, L., and Mäkelä, J. M.: Stable sulphate clusters as a source of new atmospheric particles, Nature, 404, 66–69, 2000.

Kulmala, M., Vehkamäki, H., Petäjä, T., Dal Maso, M., Lauri, A., Kerminen, V.-M., Birmili, W., and McMurry, P. H.: Formation and growth rates of ultrafine atmospheric particles: a review of observations, J. Aerosol Sci., 35, 143–176, 2004a.

Kulmala, M., Suni, T., Lehtinen, K. E. J., Dal Maso, M., Boy, M., Reissell, A., Rannik, Ü., Aalto, P., Keronen, P., Hakola, H., Bäck, J., Hoffmann, T., Vesala, T., and Hari, P.: A new feedback mechanism linking forests, aerosols, and climate, Atmos. Chem. Phys., 4, 557–562, 2004b, http://www.atmos-chem-phys.net/4/557/2004/.

Kulmala, M., Riipinen, I., Sipilä, M., Manninen, H. E., Petäjä, T., Junninen, H., Dal Maso, M., Mordas, G., Mirme, A., Vana, M., Hirsikko, A., Laakso, L., Harrison, R. M., Hanson, I., Leung, C., Lehtinen, K. E. J., and Kerminen, V.-M.: Towards Direct Measurement of Atmospheric Nucleation, Science, 318, 89–92, 2007.

Kurtén, T., Torpo, L., Ding, C.-G., Vehkamäki, H., Sundberg, M. R., Laasonen, K., and Kulmala, M.: A density functional study on water-sulfuric acid-ammonia clusters and implications for atmospheric cluster formation, Geophys. Res., 112, D04210, doi:10.1029/2006JD007391, 2007a.

Kurtén, T., Noppel, M., Vehkamäki, H., Salonen, M., and Kulmala, M.: Quantum chemical studies of hydrate formation of H_2SO_4 and HSO_4^-, Boreal Env. Res., 12, 431–453, 2007b.

Kurtén, T., Torpo, L., Sundberg, M. R., Vehkamäki, H., and Kulmala, M: Estimation of the NH_3:H_2SO_4 ratio of nucleating clusters in atmospheric conditions using quantum chemical methods, Atmos. Chem. Phys., 7, 2765–2773, 2007c, http://www.atmos-chem-phys.net/7/2765/2007/.

Laakso, L., Grönholm, T., Kulmala, L., Haapanala, S., Hirsikko, A., Lovejoy, E. R., Kazil, J., Kurtén, T., Boy, M., Nilsson, E. D., Sogachev, A., Riipinen, I., Strattman, F., and Kulmala, M.: Hot-air balloon measurements of vertical variation of boundary layer new particle formation, Boreal Env. Res., 12, 279–294, 2007.

Lovejoy, E. R., Curtius, J., and Froyd, K. D.: Atmospheric ion-induced nucleation of sulfuric acid and water, J. Geophys. Res., 109, D08204, doi:10.1029/2003JD004460, 2004.

Mäkelä, J. M., Yli-Koivisto, S., Hiltunen, V., Seidl, W., Swietlicki, E., Teinilä, K., Sillanpää, M., Koponen, I. K., Paatero, J., Rosman, K., and Hämeri, K.: Chemical composition of aerosol during particle formation events in boreal forest, Tellus, 53B, 380–393, 2001.

Murphy, S. M., Sorooshian, A., Kroll, J. H., Ng, N. L., Chhabra, P., Tong, C., Surratt, J. D., Knipping, E., Flagan, R. C., and Seinfeld, J. H: Secondary aerosol formation from atmospheric reactions of aliphatic amines, Atmos. Chem. Phys., 7, 2313–2337, 2007, http://www.atmos-chem-phys.net/7/2313/2007/.

Nadykto, A. B. and Yu, F.: Strong hydrogen bonding between atmospheric nucleation precursors and common organics, Chem. Phys. Lett., 435, 14–18, 2007.

O'Dowd, C. D., Aalto, P., Hämeri, K., Kulmala, M., and Hoffmann, T.: Atmospheric particles from organic vapours, Nature, 416, 497–498, 2002.

Ortega, I. K., Kurtén, T., Vehkamäki, H., and Kulmala, M: The Role

of Ammonia in Sulfuric Acid Ion-Induced Nucleation, Atmos. Chem. Phys., 8, 2859–2867, 2008, http://www.atmos-chem-phys.net/8/2859/2008/.

Portmann, S.: MOLEKEL, Version 4.3.win32. Swiss Center for Scientific Computing (CSCS)/ETHZ, Switzerland, 2002.

Rabaud, N. E., Ebeler, S. E., Ashbaugh, L. L., and Flocchini, R. G.: Characterization and quantification of odorous and non-odorous volatile organic compounds near a commercial dairy in California, Atmos. Environ., 37, 933–940, 2003.

Schade, G. W. and Crutzen, P. J.: Emission of aliphatic amines from animal husbandry and their reactions: Potential source of N_2O and HCN, J. Atmos. Chem. 22, 319–346, 1995.

Seinfeld, J. H. and Pandis, S. N.: Atmospheric Chemistry and Physics: From Air Pollution to Climate Change, Wiley & Sons, New York, USA, 1998.

Sellegri, K., Hankel, M, Umann, B., Arnold, F., and Kulmala, M.: Measurements of organic gases during aerosol formation events in the boreal forest atmosphere during QUEST, Atmos. Chem. Phys., 5, 373–384, 2005, http://www.atmos-chem-phys.net/5/373/2005/.

Spracklen, D. V., Carslaw, K. S., Kulmala, M., Kerminen, V.-M., Mann, G. W., and Sihto, S.-L.: The contribution of boundary layer nucleation events to total particle concentrations on regional and global scales, Atmos. Chem. Phys., 6, 5631–5648, 2006, http://www.atmos-chem-phys.net/6/5631/2006/.

Torpo, L., Kurtén, T., Vehkamäki, H., Sundberg, M. R., Laasonen, K., and Kulmala, M.: The significant role of ammonia in atmospheric nanoclusters, J. Phys. Chem. A, 111, 10 671–10 674, 2007.

Weigend, F. and Häser, M: RI-MP2: first derivatives and global consistency, Theor. Chem. Acc., 97, 331–340, 1997.

Weigend, F., Häser, M., Patzelt, H., and Ahlrichs, R.: RI-MP2: Optimized auxiliary basis sets and demonstration of efficiency, Chem. Phys. Lett., 294, 143–152, 1998.

Weigend, F., Köhn, A., and Hättig, C.: Efficient use of the correlation consistent basis sets in resolution of the identity MP2 calculations, J. Chem. Phys., 116, 3175–3183, 2002.

Paper II

Atmos. Chem. Phys., 10, 4961–4974, 2010
www.atmos-chem-phys.net/10/4961/2010/
doi:10.5194/acp-10-4961-2010

Atmospheric Chemistry and Physics

Enhancing effect of dimethylamine in sulfuric acid nucleation in the presence of water – a computational study

V. Loukonen[1], T. Kurtén[1], I. K. Ortega[1], H. Vehkamäki[1], A. A. H. Pádua[2], K. Sellegri[3], and M. Kulmala[1]

[1]Division of Atmospheric Sciences, Department of Physics, P. O. Box 64, 00014 University of Helsinki, Finland
[2]Laboratoire Thermodynamique et Interactions Moléculaires, Université Blaise Pascal, Clermont-Ferrand and CNRS, 63177 Aubière, France
[3]Laboratoire de Météorologie Physique, OPGC/CNRS, Université Blaise Pascal, 24 avenue des Landais, 63170 Aubière, France

Received: 19 January 2010 – Published in Atmos. Chem. Phys. Discuss.: 1 February 2010
Revised: 3 May 2010 – Accepted: 21 May 2010 – Published: 28 May 2010

Abstract. We have studied the hydration of sulfuric acid – ammonia and sulfuric acid – dimethylamine clusters using quantum chemistry. We calculated the formation energies and thermodynamics for clusters of one ammonia or one dimethylamine molecule together with 1–2 sulfuric acid and 0–5 water molecules. The results indicate that dimethylamine enhances the addition of sulfuric acid to the clusters much more efficiently than ammonia when the number of water molecules in the cluster is either zero, or greater than two. Further hydrate distribution calculations reveal that practically all dimethylamine-containing two-acid clusters will remain unhydrated in tropospherically relevant circumstances, thus strongly suggesting that dimethylamine assists atmospheric sulfuric acid nucleation much more effectively than ammonia.

1 Introduction

The fourth assessment report of the Intergovernmental Panel on Climate Change concludes that aerosols remain the dominant uncertainty in predicting radiative forcing and climate change (Intergovermental Panel for Climate Change, 2007; for a recent supplementary to the fourth IPCC report see e.g. The Copenhagen Diagnosis, 2009). Furthermore, modeling studies indicate that over the continents, around 30% of the total aerosol particle budget forms in the atmosphere (Spracklen et al., 2006). However, despite its importance, the comprehension of the very first steps of aerosol particle formation, i.e. the microscopic understanding of nucleation, is still vague.

Currently, it is thought that the key ingredients in new-particle formation in the troposphere are sulfuric acid and water. Sulfuric acid concentrations have been observed to correlate with new-particle formation rates in a large variety of conditions (e.g., Weber et al., 1996, 1997; Kulmala et al., 2006; Sihto et al., 2006; Riipinen et al., 2007) and the ubiquitous water is most likely involved (Kulmala et al., 2004). It is also known, based on both experimental and theoretical results, that most of the observed new-particle formation events can not be explained by electrically neutral binary sulfuric acid-water nucleation alone. Therefore, atmospheric nucleation mechanisms have been proposed to involve contributions from ions, ammonia or various organic compounds (Korhonen et al., 1999; Kavouras et al., 1999; Kulmala et al., 2000; Yu and Turco, 2000).

Recently, the role of ions in atmospheric nucleation processes has been in the focus of intensive debate. There has been some controversy over the percentage contribution of ion-induced nucleation, with a few studies claiming that ion-induced nucleation dominates (e.g., Kazil et al., 2006; Yu and Turco, 2008) and others finding contributions of 1–10% (e.g., Iida et al., 2006; Manninen et al., 2009). Recent observational studies (Kulmala et al., 2010) demonstrate a non-existent correlation between cosmic rays – the primary source of ions in the atmosphere – and nucleation rates or particle formation event frequencies, strongly suggesting that ion-induced nucleation pathways play only a minor role.

Correspondence to: V. Loukonen
(ville.loukonen@helsinki.fi)

Published by Copernicus Publications on behalf of the European Geosciences Union.

The role of ammonia in atmospheric nucleation has also been extensively discussed lately. At the moment, experiments and theoretical calculations are in qualitative agreement, stating that ammonia has a modest enhancing effect on sulfuric acid-water nucleation (Anttila et al., 2005; Kurtén et al., 2007b; Torpo et al., 2007; Nadykto et al., 2007; Ball et al., 2007). However, this effect is too small to explain the observed particle formation rates in the atmosphere. Clearly, there is a need for some other compounds to explain atmospheric observations. These compounds should also stabilize the sulfuric acid solution in the way that the saturation vapour pressure of sulfuric acid over the freshly formed particles is very small.

One such prominent possibility are the amines. Besides ammonia, amines are one of the few basic compounds present in the atmosphere, and as such can be expected to bind strongly to sulfuric acid.

Recent field (Mäkelä et al., 2001; Smith et al., 2008, 2010), laboratory (Murphy et al., 2007; Bzdek et al., 2010; Wang et al., 2010) and modelling (Barsanti et al., 2009) studies indicate that various amines might have a significant role in the formation and subsequent growth of new aerosol particles. Indeed, some amines may even be more effective than ammonia in enhancing the particle formation. In addition, in a recent quantum chemical study involving several amines possibly present in the vapor phase in the atmosphere, it was found that all of them formed significantly more strongly bound structures with sulfuric acid than ammonia (Kurtén et al., 2008). Although this was expected from e.g. proton affinity data, it was also demonstrated that dimethylamine assists the growth of both neutral and ionic clusters in the H_2SO_4 coordinate more effectively than ammonia, implying that amines are more likely to enhance sulfuric acid-water nucleation (Kurtén et al., 2008).

In this study we have explicitly investigated the hydration of dimethylamine – containing sulfuric acid clusters using quantum chemical methods, and compared their structures and properties to those of equally hydrated sulfuric acid-ammonia clusters. This study will give new insight especially on the role of dimethylamine in sulfuric acid driven nucleation in the presence of water, but it also adds new knowledge to the previous research on H_2SO_4-H_2O (e.g., Bandy and Ianni, 1998; Re et al., 1999; Ding et al., 2003; Al Natsheh et al., 2004; Kurtén et al., 2007a) and H_2SO_4-NH_3-H_2O (e.g., Ianni and Bandy, 1999; Larson et al., 1999; Kurtén et al., 2007b;) clusters. Focusing particularly on dimethylamine is a choice guided partly by previous results. For instance, in one study dimethlyammonium ($(CH_3)_2NH_2^+$) concentrations in accumulation mode aerosol particles during nucleation event days in boreal forest conditions was measured to be 50 times higher than during non-event days, thus strongly indicating that dimethylamine was involved in particle formation (Mäkelä et al., 2001). Furthermore, as a disubstituted amine dimethylamine may be regarded as a sort of "average amine" with respect to the basicity and the number of hydrogen bonds it can form. The choice was also partly guided by practical limitations: inclusion of e.g. all the other alkylamines in this study would be computationally unfeasible.

2 Computational details

The calculations were carried out applying a systematic multi-step procedure for quantum chemistry (Ortega et al., 2008) with additional molecular dynamics (MD) simulations. Part of the initial structures were taken from previous studies when available, and created using chemical intuition when not. However, as the size of the cluster grows, the number of possible bonding patterns increases rapidly, and so the task of finding the most stable conformer for a large cluster becomes nontrivial. To overcome this inevitable problem of all quantum chemistry cluster studies, we used MD simulations to generate additional initial guesses for all the structures, thus covering the configuration-space more thoroughly. This was done with the DL_POLY_2 program (Smith et al., 2002) and custom-built force fields. We used a simple three-step simulated annealing optimization method, with the temperatures 1500 K, 200 K and 0.1 K, taking the relaxed structures after the last step as a guess structure for the conformer in question. The force-fields used were non-reactive, so e.g. proton transfer reactions could not be modeled dynamically and therefore the different stages of deprotonation had to be taken into account manually by performing simulations of different protonation states for the structures. Force-field parameters and additional MD simulation details are given in the supplementary material, see http://www.atmos-chem-phys.net/10/4961/2010/acp-10-4961-2010-supplement.zip.

Once a fair set of initial guesses (min. 10) for every structure was collected, we optimized the clusters with the SIESTA program (Soler et al., 2002), using the BLYP (Mielhich et al., 1989) functional and the DZP basis set with tight convergence criteria (0.01 eV/Ang force tolerance with a step size of 0.02 Bohr for geometry optimization and a step size of 0.01 Bohr for frequencies). The BLYP/DZP-combination for the geometry optimization is based on performance studies for molecular clusters optimization using the SIESTA program. This particular choice was found to be the best between accuracy and computational effort (Ortega et al., 2008). For each stoichiometry, several of the most promising (lowest-energy) clusters were then chosen for single-point energy calculations with the TURBOMOLE program (Ahlrichs et al., 1989), using the RI-MP2 (Bernholdt et al., 1996; Møller and Plesset, 1934) method with the aug-cc-pV(T+d)Z (Dunning et al., 2001) basis set. Although DFT-methods in general have problems describing weak interactions arising from dispersion forces, the geometries and vibrational frequencies should be qualitatively reliable. The dispersion contribution to the final electronic energies is then taken into account more faithfully by the

RI-MP2 calculations. Previously performed basis set extrapolation calculations (Kurtén et al., 2007a, b) showed that for the RI-MP2 method the basis set effects beyond the aug-cc-pV(T+d)Z level are relatively small, so the chosen basis set should be accurate enough for our present purposes. Furthermore, as we are primarily interested in relative binding energies, inaccuraries such as basis set superposition error have an even smaller effect on our energetics.

Thermal contributions to the Gibbs free energies were estimated using the standard harmonic oscillator and rigid rotor approximations, with reference conditions of 298.15 K and 1 atm. However, in nature the molecular clusters are far from rigid or harmonic. We took these physical anharmonicities into account by scaling the calculated vibrational frequencies, since the explicit calculation of anharmonic vibrational frequencies for even a medium size cluster is practically impossible due to the extremely high computational cost.

For some of the smaller clusters under study (free water, free sulfuric acid, mono- and dihydrates of sulfuric acid) the scaling factors were obtained by comparison with high-level (MP2/aug-cc-pV(D+d)Z level) anharmonic literature values (Kurtén et al., 2007a). To obtain scaling factors for free ammonia and dimethylamine, the corresponding anharmonic frequencies were explicitly calculated using the GAUSSIAN 03 program suite (Gaussian 03, Revision C.02, 2004) at the MP2/aug-cc-pVDZ level of theory.

For all the individual vibrational frequencies (3N-6 for molecules/clusters with N atoms) of the abovementioned free molecules and small clusters, we computed the ratios of the high-level anharmonic values to the harmonic frequencies calculated with SIESTA. This yielded an estimate for the deviation from the real (anharmonic) vibrations caused by the harmonic approximation. The scaling factor corresponding to the structure in question was then constructed by taking an average of the ratios. Of course, this procedure does not differentiate between the differences originating from the harmonic approximation and those inherent to the methods and basis sets used for the electronic structure calculation. It is an inescapable fact that some fraction of the real physical anharmonicity is always beyond the reach of even the best imaginable computational approach. Since the purpose of this study is not to investigate the nature of the vibrational anharmonicity per se, but to use applied quantum mechanics to assess the nucleation enhancing roles of dimethylamine and ammonia, the use of the scaling procedure described is well justified, as it provides predictive, qualitative accuracy.

In this study we did not take into account the fact that the enthaply and entropy are relatively more sensitive to the low-frequency vibrations, but used the abovementioned scaling factors as such for the entropies and for the thermal parts of enthalpies. However, for the zero-point vibrational energy contribution of the enthalpies, the scaling factor s was modified to s_{ZPE}:

$$s_{\mathrm{ZPE}} = 0.5(1+s). \quad (1)$$

Table 1. The individual scaling factors used in this study; s for the entropies and thermal parts of enthalpies, and s_{ZPE} for the zero-point vibrational energy contribution of enthalpy. Here "monohydrate" refers to the monohydrate of sulfuric acid and "dihydrate" to the dihydrate of sulfuric acid. The lower part of the table shows a comparison between the averages of the individual scaling factors used in this study and other scaling factors for some common exchange and correlation functionals (Merrick et al., 2007). However, the values are not directly comparable as they are obtained using different procedures.

complex	scaling factor s	scaling factor s_{ZPE}
water	0.99079	0.99540
ammonia	0.98543	0.99271
dimethylamine	1.00964	1.00482
sulfuric acid	0.99732	0.99866
monohydrate	0.90305	0.95152
dihydrate	0.84271	0.92136
average	*0.95482*	*0.97741*
method	scaling factor s	scaling factor s_{ZPE}
this study	0.9548	0.9774
B-LYP/6-31G(d)	0.9940	1.0135
B-LYP/6-311+G(2df,p)	0.9994	1.0186
B1-LYP/6-31G(d)	0.9561	0.9760
B1-LYP/6-311+G(2df,p)	0.9639	0.9840
B3-LYP/6-31G(d)	0.9613	0.9813
B3-LYP/6-311+G(2df,p)	0.9686	0.9889
O3-LYP/6-31G(d)	0.9617	0.9826
O3-LYP/6-311+G(2df,p)	0.9701	0.9918

This approach seems to capture the qualitative behavior of the scaling factors generally used for thermal contributions and zero-point vibrational energies (see for example Grev et al. (1991), Scott and Radom (1996) and Merrick et al. (2007) for more discussion on the scaling factors).

The individual scaling factors used in this study are collected in Table 1. Table 1 shows also the averages of the individual scaling factors used in this study in comparison with other scaling factors (taken from Merrick et al., 2007) for the same exchange or correlation functionals as used here. It should be noted that the scaling factors used in this study and the literature scaling factors are not directly comparable, as they are obtained by different procedures. However, it can be seen that most often the scaling factors used for zero-point energy contribution are closer to unity than the ones used for other contributions.

By this, we obtained the scaling factors needed for the calculations of thermal contributions to the formation energies for free water, sulfuric acid, ammonia, dimethylamine, mono- and dihydrates of sulfuric acid. For the other dimer structures ($(H_2SO_4)_2$, $H_2SO_4{\cdot}NH_3$, $H_2SO_4{\cdot}(CH_3)_2NH$) we

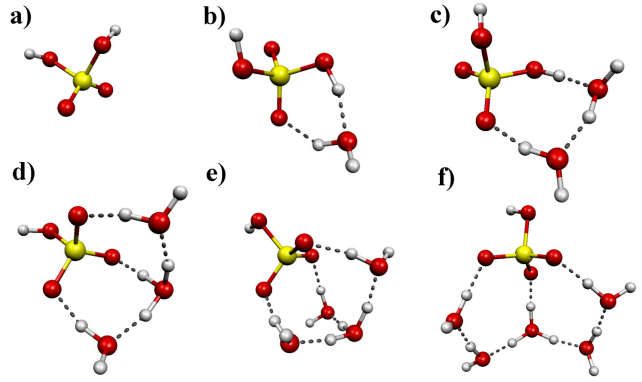

Fig. 1. The most stable structures with respect to the formation free energy ΔG (at T=298.15 K and P=1 atm) for clusters consisting of one sulfuric acid and 0–5 water molecules: **(a)** H_2SO_4, **(b)** $H_2SO_4{\cdot}H_2O$, **(c)** $H_2SO_4{\cdot}(H_2O)_2$, **(d)** $H_2SO_4{\cdot}(H_2O)_3$, **(e)** $H_2SO_4{\cdot}(H_2O)_4$, **(f)** $H_2SO_4{\cdot}(H_2O)_5$.

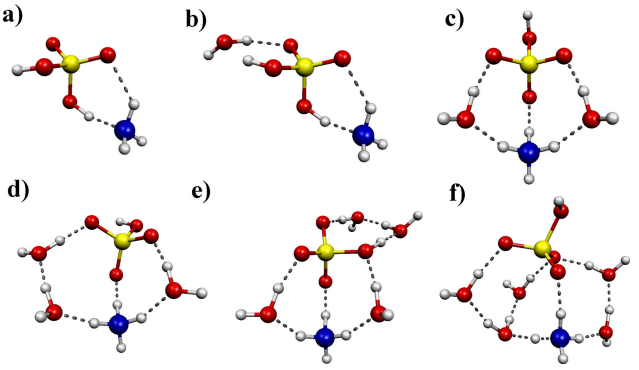

Fig. 2. The most stable structures with respect to the formation free energy ΔG (at T=298.15 K and P=1 atm) for clusters consisting of one sulfuric acid with ammonia and 0–5 water molecules: **(a)** $H_2SO_4{\cdot}NH_3$, **(b)** $H_2SO_4{\cdot}NH_3{\cdot}H_2O$, **(c)** $H_2SO_4{\cdot}NH_3{\cdot}(H_2O)_2$, **(d)** $H_2SO_4{\cdot}NH_3{\cdot}(H_2O)_3$, **(e)** $H_2SO_4{\cdot}NH_3{\cdot}(H_2O)_4$, **(f)** $H_2SO_4{\cdot}NH_3{\cdot}(H_2O)_5$.

used the scaling factors of the monohydrate. For other structures with more than two molecules, we used the scaling factors of the dihydrate. This will introduce some extra inaccuracy to the scheme, but as it is probable that the relative differences in scaling factors get smaller as the size of the clusters grows, the effect for qualitative accuracy is considered to be negligible. In general, the uncertainty in the absolute formation free energies obtained as described above can be several kilocalories per mole. However, in this study we are mainly interested in the the relative formation free energies, and the uncertainty related to those values is most likely on the order of 1–2 kcal/mol (see e.g. Kurtén and Vehkamäki, 2008).

The harmonic and anharmonic frequencies, and the derivation of the scaling factors are given as a supplementary material, see http://www.atmos-chem-phys.net/10/4961/2010/acp-10-4961-2010-supplement.zip.

3 Results and discussion

The electronic energies ΔE_{elec} (at the RI-MP2/aug-cc-pV(T+d)Z level of theory) and the corresponding thermodynamical quantities enthalpy ΔH, entropy ΔS and the Gibbs free energy ΔG (at T=298.15 K and P=1 atm) for the formation of all the complexes under study from individual constituent molecules are presented in Table 2. The most stable clusters with respect to the Gibbs free energy ΔG at T=298.15 K and P=1 atm are shown in Figs. 1–6. In all the Figs. 1–6, the a)-structures are the non-hydrated ones, the b)-structures the monohydrates, the c)-structures the dihydrates, and so on. The sulfur atoms are depicted in yellow, oxygen atoms in red, nitrogen atoms in blue, carbon atoms in green and the hydrogen atoms in white. The hydrogen bonds are indicated with dotted lines.

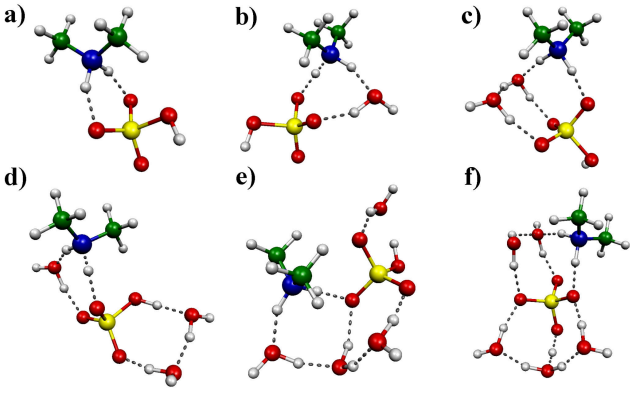

Fig. 3. The most stable structures with respect to the formation free energy ΔG (at T=298.15 K and P=1 atm) for clusters consisting of one sulfuric acid with dimethylamine and 0–5 water molecules: **(a)** $H_2SO_4{\cdot}(CH_3)_2NH$, **(b)** $H_2SO_4{\cdot}(CH_3)_2NH{\cdot}H_2O$, **(c)** $H_2SO_4{\cdot}(CH_3)_2NH{\cdot}(H_2O)_2$, **(d)** $H_2SO_4{\cdot}(CH_3)_2NH{\cdot}(H_2O)_3$, **(e)** $H_2SO_4{\cdot}(CH_3)_2NH{\cdot}(H_2O)_4$, **(f)** $H_2SO_4{\cdot}(CH_3)_2NH{\cdot}(H_2O)_5$.

3.1 Acid addition

In order to compare the enhancing (nucleation barrier-lowering) effects of dimethylamine and ammonia in sulfuric acid-water nucleation, we have calculated the Gibbs free energies of the addition of one H_2SO_4 molecule to clusters consisting of one sulfuric acid, ammonia or dimethylamine and 0–5 water molecules. These values are also compared to the corresponding free energies for clusters with only sulfuric acid and water. The results, obtained from the values given in Table 2 as (ΔG of acid addition) $= \Delta G(n_{\mathrm{acids}}) - \Delta G(n_{\mathrm{acids}}-1)$, where $\Delta G(n_{\mathrm{acids}})$ is the formation free energy for a complex with n_{acids} sulfuric acid molecules, are shown in Fig. 7.

Table 2. The electronic binding energies ΔE_{elec} (at the RI-MP2/aug-cc-pV(T+d)Z level of theory) and the thermochemical parameters enthalpy ΔH, entropy ΔS and the Gibbs free energy ΔG (at T=298.15 K and P=1 atm) for the formation of molecular clusters under study.

Reaction	ΔE_{elec} (kcal/mol)	ΔH (kcal/mol)	ΔS (cal/(mol K))	ΔG (kcal/mol)
$H_2SO_4+H_2O \rightarrow H_2SO_4 \cdot H_2O$	−12.04	−11.98	−30.37	−2.93
$H_2SO_4+2H_2O \rightarrow H_2SO_4 \cdot (H_2O)_2$	−24.20	−24.97	−62.74	−6.26
$H_2SO_4+3H_2O \rightarrow H_2SO_4 \cdot (H_2O)_3$	−35.89	−36.66	−99.12	−7.11
$H_2SO_4+4H_2O \rightarrow H_2SO_4 \cdot (H_2O)_4$	−49.79	−49.30	−138.14	−8.11
$H_2SO_4+5H_2O \rightarrow H_2SO_4 \cdot (H_2O)_5$	−58.59	−57.70	−159.92	−10.01
$H_2SO_4+NH_3 \rightarrow H_2SO_4 \cdot NH_3$	−16.57	−17.87	−29.06	−9.21
$H_2SO_4+NH_3+H_2O \rightarrow H_2SO_4 \cdot NH_3 \cdot H_2O$	−28.05	−29.22	−63.57	−10.26
$H_2SO_4+NH_3+2H_2O \rightarrow H_2SO_4 \cdot NH_3 \cdot (H_2O)_2$	−44.30	−43.78	−99.94	−13.98
$H_2SO_4+NH_3+3H_2O \rightarrow H_2SO_4 \cdot NH_3 \cdot (H_2O)_3$	−55.30	−54.41	−128.30	−16.16
$H_2SO_4+NH_3+4H_2O \rightarrow H_2SO_4 \cdot NH_3 \cdot (H_2O)_4$	−66.30	−64.95	−163.93	−16.07
$H_2SO_4+NH_3+5H_2O \rightarrow H_2SO_4 \cdot NH_3 \cdot (H_2O)_5$	−78.74	−76.05	−193.03	−18.49
$H_2SO_4+(CH_3)_2NH \rightarrow H_2SO_4 \cdot (CH_3)_2NH$	−24.42	−26.41	−36.36	−15.57
$H_2SO_4+(CH_3)_2NH+H_2O \rightarrow H_2SO_4 \cdot (CH_3)_2NH \cdot H_2O$	−40.07	−43.11	−67.16	−23.09
$H_2SO_4+(CH_3)_2NH+2H_2O \rightarrow H_2SO_4 \cdot (CH_3)_2NH \cdot (H_2O)_2$	−52.19	−54.01	−103.84	−23.05
$H_2SO_4+(CH_3)_2NH+3H_2O \rightarrow H_2SO_4 \cdot (CH_3)_2NH \cdot (H_2O)_3$	−62.30	−63.74	−135.73	−23.28
$H_2SO_4+(CH_3)_2NH+4H_2O \rightarrow H_2SO_4 \cdot (CH_3)_2NH \cdot (H_2O)_4$	−75.48	−75.03	−172.53	−23.59
$H_2SO_4+(CH_3)_2NH+5H_2O \rightarrow H_2SO_4 \cdot (CH_3)_2NH \cdot (H_2O)_5$	−84.49	−84.72	−208.54	−22.55
$2H_2SO_4 \rightarrow (H_2SO_4)_2$	−18.92	−20.53	−32.69	−10.78
$2H_2SO_4+H_2O \rightarrow (H_2SO_4)_2 \cdot H_2O$	−32.86	−35.01	−68.50	−14.59
$2H_2SO_4+2H_2O \rightarrow (H_2SO_4)_2 \cdot (H_2O)_2$	−48.35	−49.65	−106.34	−17.95
$2H_2SO_4+3H_2O \rightarrow (H_2SO_4)_2 \cdot (H_2O)_3$	−59.94	−60.31	−138.18	−19.11
$2H_2SO_4+4H_2O \rightarrow (H_2SO_4)_2 \cdot (H_2O)_4$	−72.56	−72.12	−173.66	−20.34
$2H_2SO_4+5H_2O \rightarrow (H_2SO_4)_2 \cdot (H_2O)_5$	−88.35	−86.81	−216.29	−22.32
$2H_2SO_4+NH_3 \rightarrow (H_2SO_4)_2 \cdot NH_3$	−46.20	−47.54	−75.16	−25.13
$2H_2SO_4+NH_3+H_2O \rightarrow (H_2SO_4)_2 \cdot NH_3 \cdot H_2O$	−59.81	−60.26	−105.94	−28.68
$2H_2SO_4+NH_3+2H_2O \rightarrow (H_2SO_4)_2 \cdot NH_3 \cdot (H_2O)_2$	−68.54	−68.24	−139.90	−26.53
$2H_2SO_4+NH_3+3H_2O \rightarrow (H_2SO_4)_2 \cdot NH_3 \cdot (H_2O)_3$	−86.95	−85.86	−183.01	−31.29
$2H_2SO_4+NH_3+4H_2O \rightarrow (H_2SO_4)_2 \cdot NH_3 \cdot (H_2O)_4$	−95.83	−93.66	−215.91	−29.28
$2H_2SO_4+NH_3+5H_2O \rightarrow (H_2SO_4)_2 \cdot NH_3 \cdot (H_2O)_5$	−109.44	−107.26	−250.69	−32.51
$2H_2SO_4+(CH_3)_2NH \rightarrow (H_2SO_4)_2 \cdot (CH_3)_2NH$	−59.09	−62.78	−76.61	−39.94
$2H_2SO_4+(CH_3)_2NH+H_2O \rightarrow (H_2SO_4)_2 \cdot (CH_3)_2NH \cdot H_2O$	−70.88	−73.88	−111.48	−40.64
$2H_2SO_4+(CH_3)_2NH+2H_2O \rightarrow (H_2SO_4)_2 \cdot (CH_3)_2NH \cdot (H_2O)_2$	−80.68	−81.12	−146.83	−37.35
$2H_2SO_4+(CH_3)_2NH+3H_2O \rightarrow (H_2SO_4)_2 \cdot (CH_3)_2NH \cdot (H_2O)_3$	−97.56	−99.36	−183.84	−44.55
$2H_2SO_4+(CH_3)_2NH+4H_2O \rightarrow (H_2SO_4)_2 \cdot (CH_3)_2NH \cdot (H_2O)_4$	−110.90	−111.20	−218.66	−46.00
$2H_2SO_4+(CH_3)_2NH+5H_2O \rightarrow (H_2SO_4)_2 \cdot (CH_3)_2NH \cdot (H_2O)_5$	−120.15	−118.74	−253.70	−43.10

As expected from previous studies (Kurtén et al., 2008), in the absence of water molecules, dimethylamine enhances the addition of another sulfuric acid to the cluster much more effectively than ammonia. Adding water molecules complicates the picture, as the number of possible bonding patterns in the clusters increases.

At first sight, the relative order of the free energy changes ΔG for the clusters with one water molecules might seem surprising, since the acid addition energies of dimethylamine- and ammonia-containing clusters are predicted to be very similar. The qualitative shape of the curves can, however, be explained by structural factors. The addition of another acid to the cluster containing one sulfuric acid, one ammonia and one water is predicted to promote a proton transfer reaction from one of the acids to ammonia, leading to a much stronger bonding and thus a strongly negative free energy change ΔG value. For the cluster containing one sulfuric acid, one water and one dimethylamine, a corresponding increase in bonding strength can not take place, as our calculations predict proton transfer to have occurred already for the one-acid case. In addition, since the dimethylammonium ion can only form two hydrogen bonds (whereas the ammonium ion can in principle form four, though in practice usually only three), adding another acid to

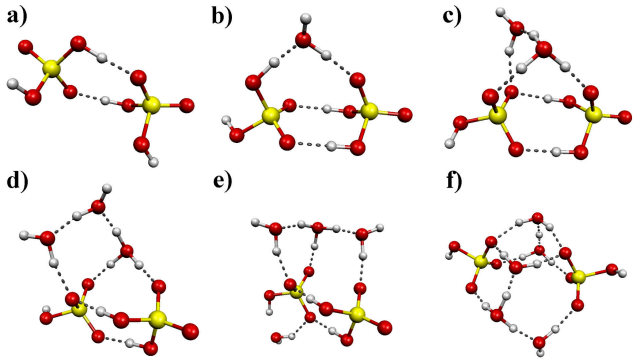

Fig. 4. The most stable structures with respect to the formation free energy ΔG (at T=298.15 K and P=1 atm) for clusters consisting of two sulfuric acids and 0–5 water molecules: **(a)** $(H_2SO_4)_2$, **(b)** $(H_2SO_4)_2{\cdot}H_2O$, **(c)** $(H_2SO_4)_2{\cdot}(H_2O)_2$, **(d)** $(H_2SO_4)_2{\cdot}(H_2O)_3$, **(e)** $(H_2SO_4)_2{\cdot}(H_2O)_4$, **(f)** $(H_2SO_4)_2{\cdot}(H_2O)_5$.

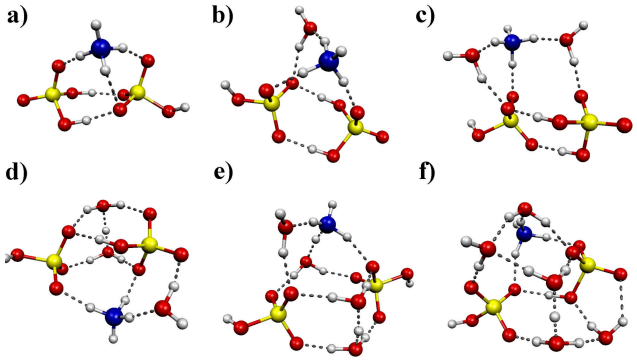

Fig. 5. The most stable structures with respect to the formation free energy ΔG (at T=298.15 K and P=1 atm) for clusters consisting of two sulfuric acids with ammonia and 0–5 water molecules: **(a)** $(H_2SO_4)_2{\cdot}NH_3$, **(b)** $(H_2SO_4)_2{\cdot}NH_3{\cdot}H_2O$, **(c)** $(H_2SO_4)_2{\cdot}NH_3{\cdot}(H_2O)_2$, **(d)** $(H_2SO_4)_2{\cdot}NH_3{\cdot}(H_2O)_3$, **(e)** $(H_2SO_4)_2{\cdot}NH_3{\cdot}(H_2O)_4$, **(f)** $(H_2SO_4)_2{\cdot}NH_3{\cdot}(H_2O)_5$.

the dimethylamine-acid-water cluster requires breaking one of the existing amine-water bonds (compare the b)-structures in Figs. 1 and 4, 2 and 5, and in 3 and 6).

In the clusters containing two water molecules, proton transfer already occurs with one sulfuric acid in the presence of both ammonia and dimethylamine, and our calculations predict that addition of another acid does not lead to a second proton transfer, i.e. one of the acids does not dissociate at this hydration level (see the c)-structures in Figs. 2 and 5, and in 3 and 6). In contrast, for the two-water clusters without any base molecules, the addition of the second acid causes the first proton transfer reaction (see the structure c) in Fig. 4), leading to a slight increase in stability for the plain sulfuric acid-water clusters, as can be seen from Fig. 7. Similarly to the case of sulfuric acid, dimethylamine and one water, acid addition to the dimethylamine-containing two-water cluster is made relatively less favorable by the need to break one of the existing amine-water hydrogen bonds. Thus, all three free energy values for acid addition to the two-water clusters are relatively similar.

Addition of an acid to the three-water clusters leads to a second proton transfer for the ammonia- and amine-containing structures, again increasing the difference between base-containing and plain sulfuric acid clusters (see the d)-structures in Figs. 4–6). Furthermore, for clusters containing three or more water molecules, the relative advantage (with respect to acid addition) of ammonia-containing clusters due to the greater number of H-bonds formed by NH_4^+ compared to $(CH_3)_2NH_2^+$ has disappeared, as both molecules are fully "saturated" by H-bonds already in the one-acid clusters. Thus, the greater basicity of dimethylamine (which leads to a greater stabilization of the formed ion pairs) is able to dominate the formation energetics, and for extensively hydrated clusters, dimethylamine enhances sulfuric acid addition much more effectively than ammonia.

As an interesting detail, our calculations predict that in the cluster of one acid and one dimethylamine with five waters, also the other proton of the acid is at least partly transferred, thus leading to the formation of a sulfate double-ion SO_4^{2-} (cf. structure f) in Fig. 3). This behavior is not observed in other clusters. This might be due to the fact that the cluster in question is relatively the most basic and extensively hydrated one. This implies that one might expect sulfate formation in extensively hydrated clusters of two acids and two amines. Also, the addition of the second acid to the structure of one acid, amine and five waters causes rearrangements in the bonding patterns, leading to a somewhat less negative formation energy.

In a recent first-principles molecular dynamics (FPMD) study (Anderson et al., 2008) involving 1–2 sulfuric acids with 6 water molecules and a collection of bases (including ammonia and methylamine), it was concluded that in the clusters containing two sulfuric acids, proton transfer will always take place, whereas in the clusters containing only a single sulfuric acid, the transfer will not happen, even in the presence of ammonia (though proton transfer was predicted to happen in the presence of methylamine or pyrimidine). The first conclusion regarding the two-acid clusters is in accord with our results presented here, but the latter is contradictory: our calculations predict deprotonation in the plain single-acid clusters already with three waters, and in the clusters of single acid and ammonia with two waters or more (cf. Figs. 1–2).

In Anderson et al. (2008), the difference between FPMD results and previous quantum chemistry studies (where minimum-energy geometries were used, as here) was attributed to dynamic effects. Test calculations on $H_2SO_4{\cdot}(H_2O)_5$ clusters at the BLYP/TZVPP level (corresponding to the method used in the FPMD study) tentatively support this conclusion, as the minimum-energy geometry

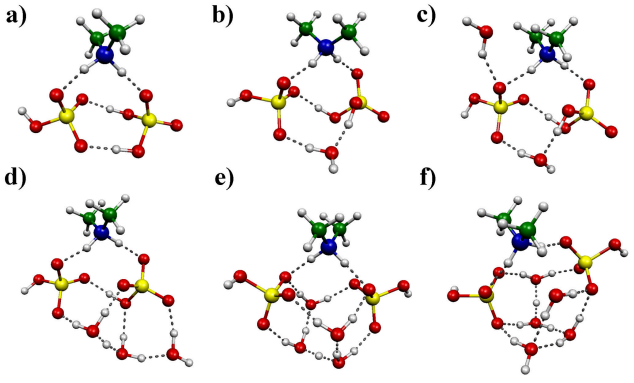

Fig. 6. The most stable structures with respect to the formation free energy ΔG (at T=298.15 K and P=1 atm) for clusters consisting of two sulfuric acids with dimethylamine and 0–5 water molecules: **(a)** $(H_2SO_4)_2 \cdot (CH_3)_2NH$, **(b)** $(H_2SO_4)_2 \cdot (CH_3)_2NH \cdot H_2O$, **(c)** $(H_2SO_4)_2 \cdot (CH_3)_2NH \cdot (H_2O)_2$, **(d)** $(H_2SO_4)_2 \cdot (CH_3)_2NH \cdot (H_2O)_3$, **(e)** $(H_2SO_4)_2 \cdot (CH_3)_2NH \cdot (H_2O)_4$, **(f)** $(H_2SO_4)_2 \cdot (CH_3)_2NH \cdot (H_2O)_5$.

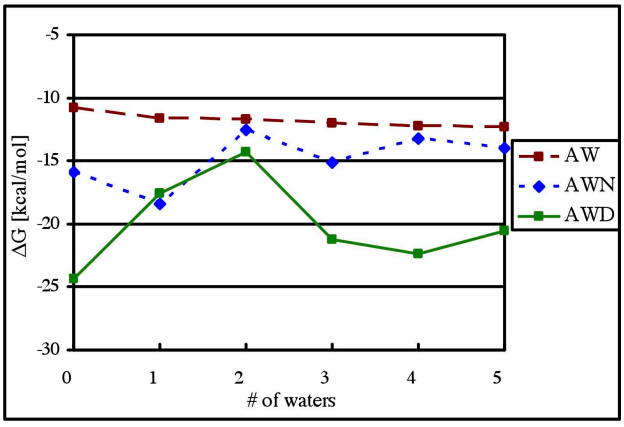

Fig. 7. The free energy change ΔG of addition of one H_2SO_4 molecule to the clusters containing one sulfuric acid and 0–5 water molecules. AW: clusters with only sulfuric acid and water; AWN: clusters containing one sulfuric acid and an ammonia molecule; AWD: clusters containing one sulfuric acid and a dimethylamine molecule.

at this level is found to contain an ion pair, whereas the FPMD simulations at the same level predict no proton transfer even for the $H_2SO_4 \cdot (H_2O)_6$ cluster. However, it should be noted that previous quantum chemistry studies (Kurtén et al., 2007b; Nadykto et al., 2007) predict an earlier onset of proton transfer than e.g. the method used here, and that the difference between different quantum chemical energy models is likely of the same order of magnitude as the difference between static and dynamic simulations. Furthermore, in our geometry optimizations on clusters without base molecules, the protonation state of the sulfuric acid molecules (or corresponding hydrogensulfate ions) typically did not change, but remained the same as in the initial guess geometry. Thus, intact molecules remained intact, and ion pairs remained as ion pairs, regardless of the global minimum-energy geometry of the stoichiometry in question. This implies that the phase-space sampling of the FPMD simulation may not be complete (as cautioned in Anderson et al., 2008), and that simulations starting from ion-pair geometries might have led to different conclusions.

Nevertheless, the possibility that dynamic effects act to diminish the extent of proton transfer in small clusters is intriguing, and should be kept in mind during the analysis of our results. In terms of the acid addition energetics presented above, the lack of proton transfer in all $H_2SO_4 \cdot NH_3 \cdot (H_2O)_x$ ($x<7$) clusters suggested in Anderson et al. (2008) would serve to make the addition of acid molecules to ammonia-containing clusters somewhat more favorable than predicted here for $x \geq 2$. On the other hand, the lack of a second proton transfer (from acid to water) in all two-acid clusters (as predicted in Anderson et al., 2008) would correspondingly make the addition of acid molecules to both ammonia and dimethylamine-containing clusters somewhat less favorable for most clusters with $x \geq 3$. For the dimethylamine-containing five-water cluster, acid addition might again be somewhat more favorable than predicted here, since the partial formation of SO_4^{2-} could be cancelled out by dynamic effects. For the dry clusters (i.e. those containing no water), the possible role of dynamic effects will not change the conclusions, as both methods (the static calculations presented here and FPDM in Anderson et al., 2008) are in agreement concerning the degree of proton transfer. As discussed in the next section, the atmospheric relevance of our results is primarily related to these clusters.

3.2 Hydration

The pattern of acid addition energetics seen in Fig. 7 is likely to have interesting implications for the relative enhancement of nucleation by amines compared to ammonia as a function of relative humidity. To draw further conclusions, we need to know how the number of water molecules in the clusters is affected by the relative humidity. Towards this end, we have calculated the equilibrium hydrate distributions, i.e. the equilibrium fractions of the cluster "cores" (the non-aqueous part of the clusters consisting of sulfuric acid and base molecules) having a different number of water molecules attached to them.

The number concentration of a hydrate, e.g. one H_2SO_4 with n water molecules can be given as (Noppel et al., 2002)

$$\rho(1,n) = K_1 K_2 \cdots K_n \left(\frac{\rho_{\text{water}}^{\text{free}}}{\rho} \right)^n \rho_{H_2SO_4}^{\text{free}}, \quad (2)$$

where K_m are the equilibrium constants

$$K_m = e^{-\frac{\Delta G_m}{RT}} \quad (3)$$

with ΔG_m the formation free energy of an m-hydrate formed from one water molecule and $(m-1)$-hydrate, T the temperature and R the molar gas constant, all in SI units. The free monomer concentration of water is approximately given by

$$\rho_{\text{water}}^{\text{free}} = \frac{S}{k_{\text{B}}T} P_{\text{water}}^{\text{eq}}, \quad (4)$$

where S is the saturation ratio (here S is defined as a ratio of the proper partial pressure of the water vapor to the saturation vapor pressure and thus the relative humidity is defined as RH=100%$\times S$), k_{B} the Boltzmann constant in SI units, T the temperature in Kelvins and $P_{\text{water}}^{\text{eq}}$ the saturation vapor pressure of water (Seinfeld and Pandis, 1998) in Pascals. This is a valid approximation, since the hydration of the small clusters does not significantly affect the amount of free water molecules available, as there are always several orders of magnitude more water molecules in the atmosphere than any other condensing species.

The reference concentration ρ can be given in terms of some reference pressure P (here P=1 atm), the Boltzmann constant k_{B} and the temperature T as

$$\rho = \frac{P}{k_{\text{B}}T}. \quad (5)$$

As we are interested in the relative fractions of the different hydrates of the cluster cores, the absolute concentrations of the nonhydrated core clusters are not needed. For example, in the particular case of hydration of one sulfuric acid molecule, the concentration of free sulfuric acid $\rho_{\text{H}_2\text{SO}_4}^{\text{free}}$ is eventually cancelled out from the final expressions. Thus, the relative concentration of some m-hydrate in this case is then given as

$$\frac{\rho(1,m)}{\rho_{\text{H}_2\text{SO}_4}^{\text{total}}} = \frac{\rho(1,m)}{\rho(1,0)+\rho(1,1)+\cdots+\rho(1,n)} = \frac{K_1K_2\cdots\left(S\frac{P_{\text{water}}^{\text{eq}}}{P}\right)^m}{1+K_1S\frac{P_{\text{water}}^{\text{eq}}}{P}+\cdots+K_1K_2\cdots K_n\left(S\frac{P_{\text{water}}^{\text{eq}}}{P}\right)^n}, \quad (6)$$

where the hydration level m can take values between 1 and n, n being the amount of water molecules in the most extensively hydrated case.

In all hydrate distribution calculations, we assume equilibrium conditions, and furthermore that all the sulfuric acid is contained in the specific hydrates whose distribution is under study. For instance, while calculating hydrate distributions for clusters of one sulfuric acid molecule and no base molecules, we ignore all the other sulfuric acid-containing clusters. Since the purpose of this calculation is to estimate the hydration of different cluster "cores", this approach is justifiable.

To assess the extent of hydration in different circumstances, we calculated the hydrate distributions for the plain sulfuric acid clusters (one and two acids) and for the clusters containing either one or two acids together with one ammonia or dimethylamine molecule, at different relative humidities (RH) and temperatures. Assuming that the enthalpy and entropy of cluster formation are fairly constant with respect to the temperature, one can approximate the Gibbs formation free energies at different temperatures based on the values calculated at 298.15 K (and given in Table 2) as $\Delta G(T) = \Delta H(298.15K) - T\Delta S(298.15K)$. The temperature sensitivity of the hydrate distributions with constant relative humidity was observed to be weak. This is most likely due to the opposed temperature-behaviour of the formation free energy and the absolute water concentration. For instance, lowering the temperature shifts the Gibbs free energies into more negative direction, and as such implies more hydration. However, decreasing temperature also diminishes the absolute water concentration, and to a large extent these two competing effects cancel out, thus leaving the hydrate distributions reasonably temperature-independent.

The sensitivity of the hydrate distributions to the relative humidity is more noticeable and thus worth a more detailed analysis. The general trend in all cases is more extensive hydration with the growing RH, as expected, although all the clusters do pose a different characteristics of hydration. The hydrate distributions for all the studied core clusters are presented in Figs. 8–10 for three values of the relative humidity (20%, 50% and 80%) with a constant temperature of 298.15 K. This temperature does not represent the conditions of the whole troposphere, but as mentioned, the hydrate distribution at constant RH does not significantly change upon temperature changes of a few tens of degrees.

The plain sulfuric acid clusters – both the one- and two-acid clusters – were most extensively hydrated, as can be seen in Fig. 8. At most tropospherically reasonable conditions (relative humidity and temperature), the total concentration of sulfuric acid in these clusters was dispersed mainly in the mono- and dihydrates. With increasing RH, the peak of the distribution moves from unhydrated clusters to dihydrates in such a manner that unhydrated clusters dominate only when the relative humidity is less that ten per cent. The hydrate distributions for sulfuric acid calculated here are fairly consistent with earlier high-level quantum chemistry studies (Kurtén et al., 2007a) as well with experimental measurements (Hanson and Eisele, 2000). However, it might be possible that the methods used in this study underestimate the extent of hydration slightly, at least in comparison with Kurtén et al. (2007a) and Hanson and Eisele (2000).

The hydration patterns of clusters containing one sulfuric acid with ammonia and one sulfuric acid with dimethylamine are more interesting, as Fig. 9 reveals. The dimer complex of sulfuric acid and ammonia hydrates quite effectively at higher RH. More than 50% of the clusters are hydrated already with the relative humidities greater than 45%. As the RH grows, the peak of the distribution shifts through dihydrate to trihydrate (RH>80%), bypassing almost completely the monohydrate. This behavior can probably be explained by considering the structure of the $H_2SO_4{\cdot}NH_3{\cdot}H_2O$ cluster: here the acid is still intact, as opposed to the two- and three-water cases where the acid has dissociated, leading to

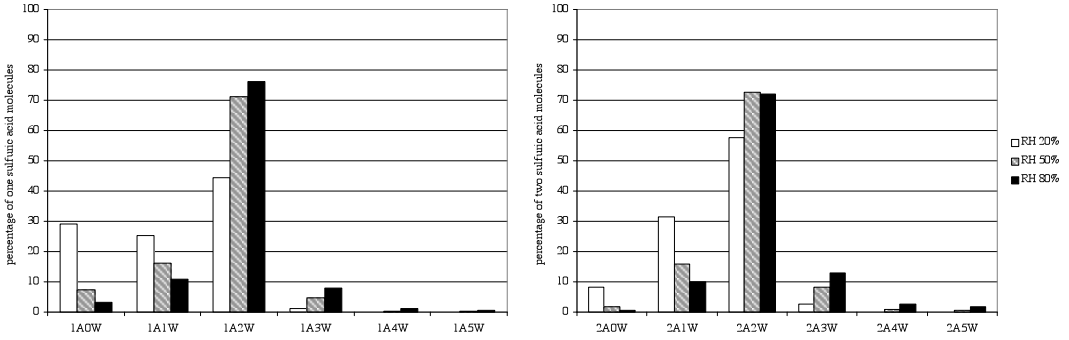

Fig. 8. Hydrate distributions of clusters with one sulfuric acid molecule (left) and clusters with two sulfuric acid molecules (right) at three different relative humidities. 1AxW≡ $H_2SO_4 \cdot (H_2O)_x$ and 2AxW≡$(H_2SO_4)_2 \cdot (H_2O)_x$. In all cases T=298.15 K.

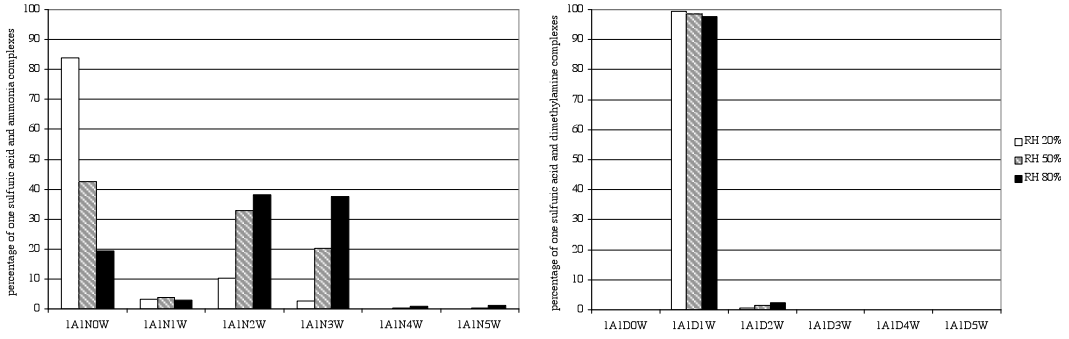

Fig. 9. Hydrate distributions of clusters with one sulfuric acid and ammonia (left) and clusters with one sulfuric acid and dimethylamine (right) at three different relative humidities. 1A1NxW≡$H_2SO_4 \cdot NH_3 \cdot (H_2O)_x$ and 1A1DxW≡$H_2SO_4 \cdot (CH_3)_2NH \cdot (H_2O)_x$. In all cases T=298.15 K.

stronger bonding (cf. the acid addition discussion above). On the other hand, the hydrate distribution of the sulfuric acid and dimethylamine complex is virtually static with respect to the changes in relative humidity and temperature. The peak of the cluster distribution is in this case the monohydrate with a share of practically 100 per cent (cf. right panel of the Fig. 9). This would suggest that the clusters consisting of one sulfuric acid and dimethylamine will always bond with just one water molecule regardless of how much water actually is available. This also implies that at lower values of relative humidity (RH<45%), a single sulfuric acid molecule bound to dimethylamine binds water slightly better than a single sulfuric acid molecule bound to ammonia. One reason for this might be the attractive dipole-dipole interaction between the acid-amine cluster ($(CH_3)_2NH_2^+ \cdot HSO_4^-$) and the water molecule, and the subsequent strong hydrogen bonding (cf. the acid addition discussion above and the structure b) in Fig. 3). In the case of sulfuric acid and ammonia, there is no strong dipole-dipole interaction between the cluster and water, and as mentioned, the portion of acid-ammonia monohydrate of the total acid concentration is negligible.

The hydrate distributions of the two-acid clusters with ammonia and dimethylamine have yet different characteristics, as is evident from the Fig. 10. The ammonia-containing distribution peaks at the monohydrate, whereas dimethylamine-containing clusters stay almost completely dry. The behavior of the former is in accordance with the acid addition discussion: the complex of two sulfuric acids, ammonia and one water molecule is the most strongly bound of all the two acid-ammonia clusters considered in this study. In addition to the first proton transfer reaction occurring at this hydration level, this particular structure has a convenient symmetry with respect to the possible hydrogen bonds ammonia can form to stabilize the cluster, i.e. ammonia is able to bind the two acids and water strongly together (cf. structure b) in Fig. 5). Similar reasoning explains also the two-acid distribution with dimethylamine since the most energetically stable cluster is the unhydrated one. Structural reasons for this are compelling: dimethylamine can bind two acids together due to its ability to a form maximum of two hydrogen bonds (cf. structure a) in Fig. 6). Including water molecules to this complex means breaking some of the existing, "strong" hydrogen bonds, and it seems that the new bonding patterns compensate this loss of binding energy only after the second

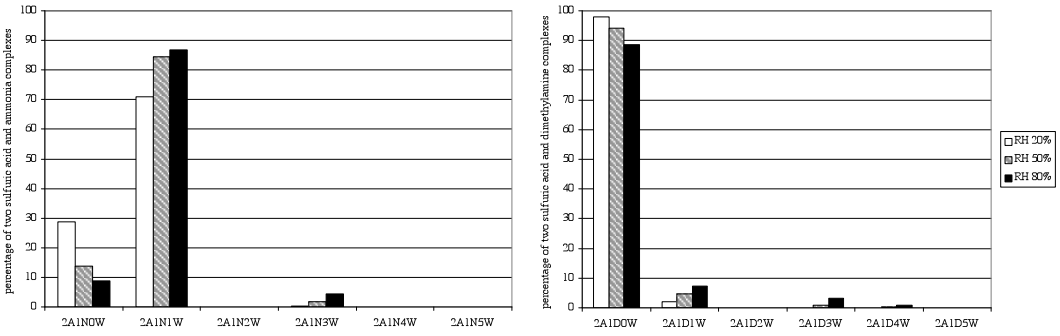

Fig. 10. Hydrate distributions of clusters with two sulfuric acid and ammonia (left) and clusters with two sulfuric acid and dimethylamine (right) at three different relative humidities. 2A1NxW≡$(H_2SO_4)_2\cdot NH_3\cdot(H_2O)_x$ and 2A1DxW≡$(H_2SO_4)_2\cdot(CH_3)_2NH\cdot(H_2O)_x$. In all cases T=298.15 K.

proton transfer happens. For the second proton transfer to take place, according to our calculations, there must be three or more water molecules in the cluster (cf. the acid addition discussion). Consequently, this requires very high supersaturations. In order to have the fraction of the hydrated clusters compatible to the unhydrated one, a relative humidity on the order of 250% is required. This very strongly suggests that the two-acid clusters with dimethylamine will remain unhydrated in all tropospherically relevant conditions.

It should be mentioned that the details of the hydrate distributions are quite sensitive to the vibrational frequencies and thus to the particular scaling used, since the inaccuracies in thermochemistry affect the hydrate distribution cumulatively. However, perhaps the most important result here, the reluctance of the amine-containing two-acid cluster to hydrate, did not quantitatively change with different vibrational scaling approaches.

3.3 Atmospheric relevance

Of course, the formation energetics do not solely govern the cluster distributions in the atmosphere. Often the absolute and relative concentrations of the species in question have a large and more decisive role. The effect of concentration on the cluster distributions can be estimated with the law of mass balance (as done above for the case of water concentrations, see Eq. 6). For example, for the most probable two-acid clusters with different bases, i.e. two sulfuric acids with dimethylamine and no waters and two acids with ammonia and one water molecule (at T=298.15 K and RH=50%, cf. discussion above and Fig. 10), the ratio of concentrations can be given as:

$$\frac{[(H_2SO_4)_2\cdot(CH_3)_2NH]}{[(H_2SO_4)_2\cdot NH_3\cdot H_2O]} = \frac{[(CH_3)_2NH]}{[NH_3]}\frac{e^{-\frac{\Delta\Delta G}{RT}}}{[H_2O]}, \quad (7)$$

where $\Delta\Delta G$ is the difference in the formation free energies of the two clusters, that is,

$$\Delta\Delta G \equiv \Delta G((H_2SO_4)_2\cdot(CH_3)_2NH) - \Delta G(\,(H_2SO_4)_2 \cdot NH_3\cdot H_2O\,), \quad (8)$$

ΔG(X) being the formation free energy of the complex X, R is the molar gas constant and T the temperature in Kelvins. An expression for the concentration of water can be obtained from Eqs. (4) and (5) as

$$[H_2O] = \frac{P^{eq}_{water}}{P}S, \quad (9)$$

where P^{eq}_{water} is the saturation vapor pressure of water, P reference pressure and S the saturation ratio.

There is typically more ammonia in the atmosphere than there is dimethylamine, but an accurate quantitative assessment is difficult due to the small number of amine measurements. The relative abundance of different amines compared to ammonia also varies significantly according to specific environmental conditions. For example, Sellegri et al. (2005) have measured almost the same atmospheric concentrations for trimethylamine and ammonia in boreal forest at SMEAR II station (Hari and Kulmala, 2005), whereas in a recent study in marine environment (Müller et al., 2009), concentrations of diethyl- and dimethylamine were observed to be three orders of magnitude smaller than that of ammonium, although the amines still contributed non-negligibly to the total detected nitrogen. However, in another marine environment study during high biological activity (Facchini et al., 2008), the same amines were measured to be considerably abundant in the sub-micrometer aerosol particles, again indicating their possible importance in the secondary organic aersol formation. Altogether, probably a realistic estimate for the difference in the concentrations is between 1 to 4 orders of magnitude. Using the formation free energies collected in the Table 2 with the Eq. (7), one can obtain qualitative estimates for the ratio of concentrations of $(H_2SO_4)_2\cdot(CH_3)_2NH$ to $(H_2SO_4)_2\cdot NH_3\cdot H_2O$. These results are presented in Table 3.

Table 3. Ratio of concentrations of clusters of two sulfuric acids with one dimethylamine to two sulfuric acids with one ammonia and one water, as a function of the dimethylamine to ammonia concentration ratio. Equilibrium steady-state conditions are assumed and T=298.15 K, P=1 atm and RH=50%.

$[(CH_3)_2NH]/[NH_3]$ ratio	$[(H_2SO_4)_2\cdot(CH_3)_2NH]/[(H_2SO_4)_2NH_3H_2O]$ ratio
1	1.2×10^{10}
0.1	1.2×10^{9}
0.01	1.2×10^{8}
0.001	1.2×10^{7}
0.0001	1.2×10^{6}
0.00001	1.2×10^{5}

Table 3 reveals that dimethylamine-containing two-acid clusters would clearly dominate the cluster distribution, even when the (gas-phase) amine concentration is only a thousandth or less of the ammonia concentration. Of course, the results in the Table 3 should be taken only as a rough estimate due to several approximations made in the calculation, as already mentioned during the discussion on hydration. Nevertheless, under the conditions where ammonia and the amine are competing as a nucleation enhancing agents, the amine-containing clusters are likely to prevail, at least until all the available amine is consumed in the process.

The atmospheric relevance of the results presented in this study is tied to the overall significance of ternary nucletion in the atmosphere, which is still a subject of ongoing research. According to some authors, the role of ternary nucleation of sulfuric acid, ammonia and water is negligible (Yu, 2006), whereas other approaches (Korhonen et al., 1999; Napari et al., 2002; Anttila et al., 2005) give varying predictions for the ternary nucleation rates. Jung et al. (2009) have shown that the ternary nucleation model of Napari et al. (2002) can be used as a basis of successful prediction of particle formation rates in Pittsburg, US.

However, rigorous ab initio based nucleation parameterizations for atmospherically relevant compounds are still to be constructed and a subtle caution should be maintained while drawing conclusions in the light of the current theoretical results for the nucleation rates. On the other hand, nucleation rates do not necessarily reveal all the details: aerosol particle formation might be a two-step process, involving formation of very stable molecular clusters with diameters below two nanometers and their subsequent growth to observable sizes under favourable conditions (Kulmala et al., 2000, 2007). In this scenario, amines, such as dimethylamine, are particularly good candidates for the nucleation enhancement and stabilization of the small atmospheric clusters.

4 Conclusions

We have investigated the hydration (by up to five water molecules) of clusters consisting of 1–2 sulfuric acid molecules with either an ammonia or a dimethylamine molecule by computational means. The formation energetics and structures of the abovementioned clusters were explored using quantum chemistry. Also, the equilibrium hydrate distributions for the plain one- and two-acid clusters, single acid clusters with either ammonia or dimethylamine, and clusters of two sulfuric acids with either one of the bases were calculated.

The results indicate that (a) dimethylamine enhances the growth of the cluster along the sulfuric acid axis much more effectively than ammonia when the number of water molecules in the cluster is either zero or greater than two, and (b) in all tropospherically reasonable conditions the two-acid clusters with dimethylamine remain almost completely unhydrated. Thus, it is very likely that dimethylamine assists sulfuric acid nucleation much more efficiently than ammonia in all tropospherical circumstances. However, calculations on larger clusters (containing both more acids and multiple bases) are still required to determine the size of the critical cluster in sulfuric acid – dimethylamine nucleation.

Acknowledgements. We thank the computing resources of CSC – IT Center for Science Ltd in Espoo, Finland, for computing time. This research was supported by the Academy of Finland (project numbers 1127372, 118433, 203675 and Center of Excellence program, project number 1118615) and OPGC (Observation de Physique de Globe de Clermont Ferrand).

Edited by: A. Wiedensohler

References

Ahlrichs, R., Bär, M., Horn, H., and Kölmel, C.: Electronic structure calculations on workstation computers: The program system turbomole, Chem. Phys. Lett., 162, 165–169, 1989.

Allison, I., Bindoff, N. L., Bindschadler, R. A., et al.: The Copenhagen Diagnosis: Updating the world on the Latest Climate Science, The University of New South Wales Climate Change Research Centre (CCRC), Sydney, Australia, 60 pp., 2009.

Al Natsheh, A., Nadykto, A. B., Mikkelsen, K. V., Yu, F., and Ruuskanen, J.: Sulfuric acid and sulfuric acid hydrates in the gas phase: a DFT investigation, J. Phys. Chem. A, 108, 8914–8929, 2004.

Anttila, T., Vehkamäki, H., Napari, I., and Kulmala, M.: Effect of ammonium bisulphate formation on atmospheric water-sulphuric acid-ammonia nucleation, Boreal Env. Res., 10, 511–523, 2005.

Anderson, K. E., Siepmann, J. I., McMurry, P. H., and VandeVondele, J.: Importance of the number of acid molecules and the strength of the base for double-ion formation in $(H_2SO_4)_m\cdot Base\cdot(H_2O)_6$ clusters, J. Am. Chem. Soc., 130, 14144–14147, 2008.

Ball, S. M., Hanson, D. R., Eisele, F. L., and McMurry, P. H.: Laboratory studies of particle nucleation: Initial results for H_2SO_4,

H_2O, and NH_3 vapors, J. Geophys. Res. D, 104, 23709–23718, 1999.

Bandy, A. R. and Ianni, J. C.: Study of the hydrates of H_2SO_4 using density functional theory, J. Phys. Chem. A, 102, 6533–6539, 1998.

Barsanti, K. C., McMurry, P. H., and Smith, J. N.: The potential contribution of organic salts to new particle growth, Atmos. Chem. Phys., 9, 2949–2957, doi:10.5194/acp-9-2949-2009, 2009.

Bernholdt, D. E. and Harrison, R. J.: Large-scale correlated electronic structure calculations: the RI-MP2 method on parallel computers, Chem. Phys. Lett., 250, 477–484, 1996.

Bzdek, B. R., Ridge, D. P., and Johnston, M. V.: Amine exchange into ammonium bisulfate and ammonium nitrate nuclei, Atmos. Chem. Phys., 10, 3495–3503, doi:10.5194/acp-10-3495-2010, 2010.

Ding, C.-G., Laasonen, K., and Laaksonen, A.: Two Sulfuric Acids in Small Water Clusters, J. Phys. Chem. A, 107, 8648–8658, 2003.

Dunning Jr., T. H., Peterson, K. A., and Wilson, A. K.: Gaussian basis sets for use in correlated molecular calculations. X. The atoms aluminum through argon revisited, J. Chem. Phys., 114, 9244–9253, 2001.

Frisch, M. J., Trucks, G. W., Schlegel, H. B., Scuseria, G. E., Robb, M. A., Cheeseman, J. R., Montgomery Jr., J. A., Vreven, T., Kudin, K. N., Burant, J. C., Millam, J. M., Iyengar, S. S., Tomasi, J., Barone, V., Mennucci, B., Cossi, M., Scalmani, G., Rega, N., Petersson, G. A., Nakatsuji, H., Hada, M., Ehara, M., Toyota, K., Fukuda, R., Hasegawa, J., Ishida, M., Nakajima, T., Honda, Y., Kitao, O., Nakai, H., Klene, M., Li, X., Knox, J. E., Hratchian, H. P., Cross, J. B., Bakken, V., Adamo, C., Jaramillo, J., Gomperts, R., Stratmann, R. E., Yazyev, O., Austin, A. J., Cammi, R., Pomelli, C., Ochterski, J. W., Ayala, P. Y., Morokuma, K., Voth, G. A., Salvador, P., Dannenberg, J. J., Zakrzewski, V. G., Dapprich, S., Daniels, A. D., Strain, M. C., Farkas, O., Malick, D. K., Rabuck, A. D., Raghavachari, K., Foresman, J. B., Ortiz, J. V., Cui, Q., Baboul, A. G., Clifford, S., Cioslowski, J., Stefanov, B. B., Liu, G., Liashenko, A., Piskorz, P., Komaromi, I., Martin, R. L., Fox, D. J., Keith, T., Al-Laham, M. A., Peng, C. Y., Nanayakkara, A., Challacombe, M., Gill, P. M. W., Johnson, B., Chen, W., Wong, M. W., Gonzalez, C., and Pople, J. A.: Gaussian 03, Revision C.02, , Gaussian, Inc., Wallingford CT, 2004.

Grev, R. S., Janssen, C. L., and Schaefer III, H. F.: Concerning zero-point vibrational energy corrections to electronic energies, J. Chem. Phys., 95, 5128–5132, 1991.

Facchini, M. C., Decesari, S., Rinaldi, M., Carbone, C., Finessi, E., Mircea, M., Fuzzi, S., Moretti, F., Tagliavini, E., Ceburnis, D., and O'Dowd, C. D.: Important source of marine secondary organic aerosol from biogenic amines, Environ. Sci. Technol., 42, 9116–9121, 2008.

Hanson, D. R. and Eisele, F. L.: Diffusion of H_2SO_4 in humidified nitrogen: hydrated H_2SO_4, J. Phys. Chem. A, 104, 1715–1719, 2000.

Hari, P. and Kulmala, M.: Station for Measuring Ecosystem–Atmosphere Relations (SMEAR II), Boreal Env. Res., 10, 315–322, 2005.

Ianni, J. C. and Bandy, A. R.: A density functional theory study of the hydrates of NH_3, H_2SO_4 and its implications for the formation of new atmospheric particles, J. Phys. Chem. A, 103, 2801–2811, 1999.

Iida, K., Stolzenburg, M., McMurry, P., Dunn, M. J., Smith, J. N., Eisele, F., and Keady, P.: Contribution of ion-induced nucleation to new particle formation: Methodology and its application to atmospheric observations in Boulder, Colorado, J. Geophys. Res., 111, D23201, doi:10.1029/2006JD007167, 2006.

The Intergovernmental Panel on Climate Change: Climate Change 2007: The Physical Science Basis, Cambridge University Press, New York, USA, 2007.

Jung, J., Fountoukis, C., Adams, P. J., and Pandis, S. N.: Simulation of in-situ ultrafine particle formation in the Eastern United States using PMCAMx-UF, in: Proceedings of the 18th International Conference on Nucleation and Atmospheric Aerosols, Prague, Czech Republic, 10–14 August 2009, 338–342, 2009.

Kavouras, I. G., Mihalopoulos, N., and Stephanou, E. G.: Secondary organic aerosol formation vs. primary organic aerosol emission: in situ evidence for the chemical coupling between monoterpene acidic photooxidation products and new particle formation over forests, Environ. Sci. Technol., 33, 1028–1037, 1999.

Kazil, J., Lovejoy, E. R., Barth, M. C., and O'Brien, K.: Aerosol nucleation over oceans and the role of galactic cosmic rays, Atmos. Chem. Phys., 6, 4905–4924, doi:10.5194/acp-6-4905-2006, 2006.

Korhonen, P., Kulmala, M., Laaksonen, A., Viisanen, Y., McGraw, R., and Seinfeld, J. H.: Ternary nucleation of H_2SO_4, NH_3, and H_2O in the atmosphere, J. Geophys. Res., 104, 26349–26353, 1999.

Kulmala, M., Pirjola, L., and Mäkelä, J. M.: Stable sulphate clusters as a source of new atmospheric particles, Nature, 404, 66–69, 2000.

Kulmala, M., Vehkamäki, H., Petäjä, T., Dal Maso, M., Lauri, A., Kerminen, V.-M., Birmili, W., and McMurry, P. H.: Formation and growth rates of ultrafine atmospheric particles: a review of observations, J. Aerosol Sci., 35, 143–176, 2004.

Kulmala, M., Lehtinen, K. E. J., and Laaksonen, A.: Cluster activation theory as an explanation of the linear dependence between formation rate of 3nm particles and sulphuric acid concentration, Atmos. Chem. Phys., 6, 787–793, doi:10.5194/acp-6-787-2006, 2006.

Kulmala, M., Riipinen, I., Sipilä, M., Manninen, H. E., Petäjä, T., Junninen, H., Dal Maso, M., Mordas, G., Mirme, A., Vana, M., Hirsikko, A., Laakso, L., Harrison, R. M., Hanson, I., Leung, C., Lehtinen, K. E. J., and Kerminen, V.-M.: Toward direct measurement of atmospheric nucleation, Science, 318, 89–92, 2007.

Kulmala, M., Riipinen, I., Nieminen, T., Hulkkonen, M., Sogacheva, L., Manninen, H. E., Paasonen, P., Petäjä, T., Dal Maso, M., Aalto, P. P., Viljanen, A., Usoskin, I., Vainio, R., Mirme, S., Mirme, A., Minikin, A., Petzold, A., Hõrrak, U., Plaß-Dülmer, C., Birmili, W., and Kerminen, V.-M.: Atmospheric data over a solar cycle: no connection between galactic cosmic rays and new particle formation, Atmos. Chem. Phys., 10, 1885–1898, doi:10.5194/acp-10-1885-2010, 2010.

Kurtén, T., Noppel, M., Vehkamäki, H., Salonen, M., and Kulmala, M.: Quantum chemical studies of hydrate formation of H_2SO_4 and HSO_4^-, Bor. Env. Res., 12, 431–453, 2007a.

Kurtén, T., Torpo, L., Ding, C.-G., Vehkamäki, H., Sundberg, M. R., Laasonen, K., and Kulmala, M.: A density functional study

on water-sulfuric acid-ammonia clusters and implications for atmospheric cluster formation, Geophys. Res., 112, D04210, doi:10.1029/2006JD007391, 2007b.

Kurtén, T., Torpo, L., Sundberg, M. R., Kerminen, V.-M., Vehkamäki, H., and Kulmala, M.: Estimating the NH3:H2SO4 ratio of nucleating clusters in atmospheric conditions using quantum chemical methods, Atmos. Chem. Phys., 7, 2765–2773, doi:10.5194/acp-7-2765-2007, 2007c.

Kurtén, T., Loukonen, V., Vehkamäki, H., and Kulmala, M.: Amines are likely to enhance neutral and ion-induced sulfuric acid-water nucleation in the atmosphere more effectively than ammonia, Atmos. Chem. Phys., 8, 4095–4103, doi:10.5194/acp-8-4095-2008, 2008.

Kurtén, T. and Vehkamäki, H.: Investigating Atmospheric Sulfuric Acid-Water-Ammonia Particle Formation Using Quantum Chemistry, Adv. Quant. Chem., 55, 407–427, 2008.

Larson, L. J., Largent, A., and Tao, F.-M.: Structure of the sulfuric acid-ammonia system and the effect of water molecules in the gas phase, J. Phys. Chem. A, 103, 6786–6792, 1999.

Manninen, H. E., Nieminen, T., Riipinen, I., Yli-Juuti, T., Gagné, S., Asmi, E., Aalto, P. P., Petäjä, T., Kerminen, V.-M., and Kulmala, M.: Charged and total particle formation and growth rates during EUCAARI 2007 campaign in Hyytiälä, Atmos. Chem. Phys., 9, 4077–4089, doi:10.5194/acp-9-4077-2009, 2009.

Merrick, J. P., Moran, D., and Radom, L.: An Evaluation of Harmonic Vibrational Frequency Scale Factors, J. Phys. Chem. A , 111, 11683–1170, 2007.

Miehlich, B., Savin, A., Stoll, H., and Preuss, H.: Results obtained with the correlation energy density functionals of becke and Lee, Yang and Parr, Chem. Phys. Lett., 157, 200–206, 1989.

Murphy, S. M., Sorooshian, A., Kroll, J. H., Ng, N. L., Chhabra, P., Tong, C., Surratt, J. D., Knipping, E., Flagan, R. C., and Seinfeld, J. H.: Secondary aerosol formation from atmospheric reactions of aliphatic amines, Atmos. Chem. Phys., 7, 2313–2337, doi:10.5194/acp-7-2313-2007, 2007.

Müller, C., Iinuma, Y., Karstensen, J., van Pinxteren, D., Lehmann, S., Gnauk, T., and Herrmann, H.: Seasonal variation of aliphatic amines in marine sub-micrometer particles at the Cape Verde islands, Atmos. Chem. Phys., 9, 9587–9597, doi:10.5194/acp-9-9587-2009, 2009.

Mäkelä, J. M., Yli-Koivisto, S., Hiltunen, V., Seidl, W., Swietlicki, E., Teinilä, K., Sillanpää, M., Koponen, I. K., Paatero, J., Rosman, K., and Hämeri, K.: Chemical composition of aerosol during particle formation events in boreal forest, Tellus B, 53, 380–393, 2001.

Møller, C. and Plesset, M. S.: Note on an approximation treatment for many-electron systems, Phys. Rev., 46, 618–622, 1934.

Nadykto, A. B. and Yu, F.: Strong hydrogen bonding between atmospheric nucleation precursors and common organics, Chem. Phys. Lett., 435, 14–18, 2007.

Napari, I., Noppel, M., Vehkamaäki, H., and Kulmala, M.: An improved model for ternary nucleation of sulfuric acid-ammonia-water, J. Chem. Phys., 116, 4221–4227, 2002.

Noppel, M., Vehkamäki, H., and Kulmala, M.: An improved model for hydrate formation in sulfuric acid-water nucleation, J. Chem. Phys., 116, 218–228, 2002.

Ortega, I. K., Kurtén, T., Vehkamäki, H., and Kulmala, M.: The role of ammonia in sulfuric acid ion induced nucleation, Atmos. Chem. Phys., 8, 2859–2867, doi:10.5194/acp-8-2859-2008, 2008.

Re, S., Osamura, Y., and Morokuma, K.: Coexistence of neutral and ion-pair clusters of hydrated sulfuric acid $H_2SO_4(H_2O)_n$ (n=1–5) – a molecular orbital study, J. Phys. Chem. A, 103, 3535–3547, 1999.

Riipinen, I., Sihto, S.-L., Kulmala, M., Arnold, F., Dal Maso, M., Birmili, W., Saarnio, K., Teinilä, K., Kerminen, V.-M., Laaksonen, A., and Lehtinen, K. E. J.: Connections between atmospheric sulphuric acid and new particle formation during QUEST IIIIV campaigns in Heidelberg and Hyytil, Atmos. Chem. Phys., 7, 1899–1914, doi:10.5194/acp-7-1899-2007, 2007.

Scott, A. P. and Radom, L.: Harmonic vibrational frequencies: an evaluation of Hartree-Fock, Møller-Plesset, quadratic configuration interaction, density functional theory, and semiempirical scale factors, J. Phys. Chem., 100, 16502–16513, 1996.

Seinfeld, J. H. and Pandis, S. N.: Atmospheric Chemistry and Physics: from Air Pollution to Climate Change, John Wiley & Sons, New York, USA, 764–765, 1998.

Sellegri, K., Hanke, M., Umann, B., Arnold, F., and Kulmala, M.: Measurements of organic gases during aerosol formation events in the boreal forest atmosphere during QUEST, Atmos. Chem. Phys., 5, 373–384, doi:10.5194/acp-5-373-2005, 2005.

Sihto, S.-L., Kulmala, M., Kerminen, V.-M., Dal Maso, M., Petäjä, T., Riipinen, I., Korhonen, H., Arnold, F., Janson, R., Boy, M., Laaksonen, A., and Lehtinen, K. E. J.: Atmospheric sulphuric acid and aerosol formation: implications from atmospheric measurements for nucleation and early growth mechanisms, Atmos. Chem. Phys., 6, 4079–4091, doi:10.5194/acp-6-4079-2006, 2006.

Smith, J. N., Dunn, M. J., VanReken, T. M., Iida, K., Stolzenburg, M. R., McMurry, P. H., and Huey, L. G.: Chemical composition of atmospheric nanoparticles formed from nucleation in Tecamac, Mexico: Evidence for an important role for organic species in nanoparticle growth, Geophys. Res. Lett., 35, L04808, doi:10.1029/2007GL032523, 2008.

Smith, J. N., Barsanti, K. C., Friedli, H. R., Ehn, M., Kulmala, M., Collins, D. R., Scheckman, J. H., Williams, B. J., and McMurry, P. H.: Observations of aminium salts in atmospheric nanoparticles and possible climatic implications, Proceedings of the National Academy of Sciences of the United States of America, 107, 6632–6639, doi:10.1073/pnas.0912127107, 2010.

Smith, W., Yong, C. W., and Rodger, P. M.: DL_POLY: Application to molecular simulation, Molec. Simulat., 28, 385–471, 2002.

Soler, J. M., Artacho, E., Gale, J. D., Garcia, A., Junquera, J., Ordejon, P., and Sanchez-Portal, D.: The SIESTA method for ab initio order-N materials simulation, J. Phys.-Condens. Mat., 14, 2745–2779, 2002.

Spracklen, D. V., Carslaw, K. S., Kulmala, M., Kerminen, V.-M., Mann, G. W., and Sihto, S.-L.: The contribution of boundary layer nucleation events to total particle concentrations on regional and global scales, Atmos. Chem. Phys., 6, 5631–5648, doi:10.5194/acp-6-5631-2006, 2006.

Torpo, L., Kurtén, T., Vehkamäki, H., Sundberg, M. R., Laasonen, K., and Kulmala, M.: The significant role of ammonia in atmospheric nanoclusters, J. Phys. Chem. A, 111, 10671–10674, 2007.

Wang, L., Khalizov, A. F., Zheng, J., Xu, W., Ma, Y., Lal, V., and Zhang, R.: Atmospheric nanoparticles formed from heterogeneous reactions of organics, Nature Geosci., 3, 238–242,

doi:10.1038/NGEO778, 2010.

Weber, R. J., Marti, J. J., McMurry, P. H., Eisele, F. L., Tanner, D. J., and Jefferson, A.: Measured atmospheric new particle formation rates: Implications for nucleation mechanisms, Chem. Eng. Commun., 151, 53–64, 1996.

Weber, R. J., Marti, J. J., McMurry, P. H., Eisele, F. L., Tanner, D. J., Jefferson, A.: Measurements of new particle formation and ultrafine particle growth rates at a clean continental site, J. Geophys. Res., 102, 4375–4385, 1997.

Yu, F.: Effect of ammonia on new particle formation: a kinetic H_2SO_4-H_2O-NH_3 nucleation model constrained by laboratory measurements, J. Geophys. Res., 111, D01204, doi:10.1029/2005JD005968, 2006.

Yu, F. and Turco, R. P.: Ultrafine aerosol formation via ion-induced nucleation, Geophys. Res. Lett., 27, 883–886, 2000.

Yu, F. and Turco, R.: Case studies of particle formation events observed in boreal forests: implications for nucleation mechanisms, Atmos. Chem. Phys., 8, 6085–6102, doi:10.5194/acp-8-6085-2008, 2008.

Paper III

Chemical Physics 428 (2014) 164–174

Contents lists available at ScienceDirect

Chemical Physics

journal homepage: www.elsevier.com/locate/chemphys

On the stability and dynamics of (sulfuric acid)(ammonia) and (sulfuric acid)(dimethylamine) clusters: A first-principles molecular dynamics investigation

V. Loukonen [a,*], I-F.W. Kuo [b], M.J. McGrath [c,1], H. Vehkamäki [a]

[a] Department of Physics, University of Helsinki, P.O. Box 64, FI-00014 University of Helsinki, Finland
[b] Lawrence Livermore National Laboratory, Chemical Sciences Division, Livermore, CA 94550, USA
[c] Department of Biophysics, Graduate School of Science, Kyoto University, Kyoto 606-8502, Japan

ARTICLE INFO

Article history:
Received 11 September 2013
In final form 19 November 2013
Available online 1 December 2013

Keywords:
Weakly bound molecular clusters
First-principles molecular dynamics
Electric dipole moment
Sulfuric acid
Atmospheric new-particle formation

ABSTRACT

The main pathway of new-particle formation in the atmosphere is likely to begin from small sulfuric acid clusters stabilized by other compounds, such as ammonia or amines. Here, we present the results of first-principles molecular dynamics simulations probing the stability and dynamics of (sulfuric acid)(ammonia/dimethylamine) clusters with two, three and four sulfuric acid molecules and a varying number of the bases. In each of the eight simulated clusters, an energetic equilibrium was reached and 35 ps of equilibrium data was collected in the $NVT(T = 300\ \mathrm{K})$ ensemble. The clusters exhibited pronounced thermal motion including rotations of the molecules within the clusters. Regardless of the continuous movement, the clusters stayed bound together. The calculated electric dipole moments were found to be sensitive to the thermal motion and consequently, large fluctuations were observed. In addition, the vibrational spectra for all the clusters were determined, indicating that the thermal motion differs from purely harmonic motion.

1. Motivation

Currently, one of the most pressing research problems the scientific community faces is the formation and growth of atmospheric aerosol particles. For example, some of these tiny particles take part in the processes deteriorating the quality of air, directly affecting the daily lives of millions of people [1]. On a grander scale, aerosol particles are intimately tied to the climate and climate change via different radiative processes [2]. The numerous and interconnected feedback mechanisms, ranging over several orders of magnitude in space and time, make aerosol particle formation and its consequences very elusive to study, both experimentally and theoretically [3]. Here, we adapt bottom-up approach to tackle the phenomenon: we present results from first-principles molecular dynamics simulations of atmospheric sulfuric acid clusters – thus concentrating on the smallest space and time regimes of sub-nanometer and -nanosecond.

The main driving agent of new-particle formation in the atmosphere is sulfuric acid [4,5]. However, the measured ambient concentrations of sulfuric acid are several orders of magnitude too small for it to alone explain the observed new-particle formation events and the acid alone does not account for most of the further aerosol particle growth either [6,7]. Traditionally, the explanation for the observations has been sought from some combination of sulfuric acid, water and ammonia "nucleating particles" [8]. The role of ions has also been extensively discussed [9,10]. However, state-of-the-art laboratory measurements concluded that sulfuric acid particle formation enhanced by ammonia and ions cannot explain the boundary-layer formation events [11]. Recently, the participation of various amines in the process has drawn a lot of attention. Theoretical studies, motivated by filter sample findings [12], first suggested that amines, such as dimethylamine, stabilize the smallest sulfuric acid clusters much more strongly than the standard candidate ammonia, and thus possibly enhance the particle formation more effectively [13,14]. The suggestion was later strengthened by various experiments, and further experimental and theoretical work has studied the clusters of sulfuric acid and amines [15–22]. The current paper continues this line of research: we focus on the dynamics and stability of sulfuric acid–ammonia and sulfuric acid–dimethylamine clusters.

The bulk of the previous theoretical studies have been static structure optimization calculations [23]. In such calculations, one typically tries to find the global minimum energy cluster as a function of the molecular coordinates, that is, to find the arrangement of the molecules in the cluster which minimizes the electronic

* Corresponding author. Tel.: +358 503182219.
E-mail address: ville.loukonen@helsinki.fi (V. Loukonen).
[1] Present address: Laboratoire des Sciences de la Climat et l'Environment, 91191 Gif-sur-Yvette, France.

0301-0104/$ - see front matter © 2013 Elsevier B.V. All rights reserved.
http://dx.doi.org/10.1016/j.chemphys.2013.11.014

ground state energy. Once such a cluster is found, all the molecular vibrations are often assumed to be harmonic. In addition, the clusters are most often assumed to rotate rigidly and the translational degrees of freedom are taken to be those of an isolated ideal gas particle. The partition function is then constructed under these assumptions, yielding various thermodynamical quantities via the machinery of statistical mechanics. This scheme includes the temperature and entropy into the electronic structure calculations, thus effectively interpolating the results from $T = 0$ K to, say, $T = 300$ K. The main shortcoming of the scheme is the lack of detailed and non-ideal descriptions of the kinetic energy contributions. To address this issue and to obtain insight on how the small clusters behave when the temperature and the kinetic energy are explicitly taken into account, we performed first-principles molecular dynamics (FPMD) simulations. One prior attempt has been performed to use FPMD on atmospheric (sulfuric acid)(base) clusters [24]. In that investigation, the threshold of proton transfer in hydrated sulfuric acid clusters (up to two acid molecules with six water molecules) with various bases was studied. The results differed partly from standard quantum chemical results [14], possibly due to the dynamical effects, demonstrating that dynamics of atmospheric sulfuric acid clusters should be studied in more detail.

Here, we extend the body of atmospherically relevant FPMD simulations in both size and simulation time: the largest cluster studied here contains four sulfuric acid and four dimethylamine molecules, and equilibrium data was collected for all the clusters for 35 ps (the simulation details are given in Section 2). To achieve this, one compromise had to be made: the exclusion of water. Although in the atmosphere there are several orders of magnitude more water than sulfuric acid, ammonia or dimethylamine, not much is currently known about the hydration state of the clusters formed by the latter molecules. Agreeably, FPMD would be a good method to investigate the role of water in the clusters, especially as water is often lost from small clusters during detection in the experiments. However, the inclusion of water molecules would increase the computational cost and complexity significantly, and thus it is left for future studies. Furthermore, as the main goal of the present paper is to study the dynamics and stability of sulfuric acid clusters, the exclusion of water might be a good first order approximation as the binding of sulfuric acid with water is considerably weaker than with ammonia or dimethylamine.

2. Simulations

We performed Born–Oppenheimer based first-principles molecular dynamics simulations, where the atomic nuclei evolve in time according to the classical equations of motion. However, the forces driving the dynamics are calculated from electronic structure theory [25,26]. All the simulations were performed using the CP2K program package (www.cp2k.org) and the forces were calculated within Kohn–Sham density functional theory as implemented in the Quickstep [25] module of CP2K. We used the PBE functional [27], which has been previously shown to work well for polar hydrogen-bonding liquids [28,29] and recently in the context of atmospheric clusters [30,31]. The density functional was used with a dual basis set method [26]: a doubly polarized triple-ζ Gaussian-type basis set in real-space and a plane-wave basis set with a cut-off of 600 Ry in the momentum-space. Norm-conserving GTH pseudo-potentials were used for the core electrons [32]. The convergence criteria for the wavefunction was 10^{-7} Hartrees. The size of the simulation box was $20 \times 20 \times 20$ Å^3 in all of the simulations.

Once the forces were obtained, the system was propagated in time with a timestep of 0.5 fs in the canonical *NVT* ensemble. The temperature was set to the ambient $T = 300$ K where every degree of freedom was controlled by individual Nosé–Hoover chain thermostats [33] with a coupling constant of 2000 cm^{-1}. The canonical ensemble was chosen as we wanted to observe how the small clusters behave under constant temperature. Especially, we were interested to see how the presumably stable clusters responded when the system possessed kinetic energy at $T \neq 0$ K conditions. Guided by a recent quantum chemical study [18], which extensively searched for the most stable molecular clusters, we chose six (sulfuric acid)$_m$(base)$_n$ clusters (with $m = 2, 3, 4$) separately with the two base molecules, ammonia and dimethylamine (henceforth, sulfuric acid will be abbreviated as SA, ammonia as Amm and dimethylamine as DMA). In this size range, the (SA)$_m$(Amm)$_n$ clusters with $n = m - 1$, and the clusters of (SA)$_m$(DMA)$_n$ with $n = m$ were found to be the most stable ones [18]. In addition to these six clusters, we included the clusters of (SA)$_3$(Amm)$_3$ and (SA)$_2$(DMA)$_1$ into this study, as the stability of these clusters was very close to the most stable ones [18], and further, it extended our data set in a way that we were able to directly compare the roles of the base molecules in the clusters of (SA)$_2$(base)$_1$ and (SA)$_3$(base)$_3$.

We took the initial geometries from the literature [18] and optimized the clusters with the level of theory used in the simulations. While it is true in general that the minima found with different methods are not necessarily the same, here this matter is of secondary importance: the optimized initial clusters were only used as starting points for the equilibration simulations. To be able to draw meaningful physical conclusions based on the simulations, the clusters need to be first equilibrated. Thus, only after the clusters had successfully reached an energetic equilibrium, 35 ps production run simulations were performed. All the analysis is based on the production runs. The results of the simulations are presented in the following section: first, we discuss the energetic and structural properties observed in the simulations, after which we focus on the electric dipole moments and on the vibrational–rotational spectra.

3. Results and discussion

3.1. Energetics and structural considerations

One of the motivating questions behind this investigation was to find out how the presumably stable atmospheric small clusters behave if the temperature is taken into account explicitly. One fundamental way to answer this question is to look at the energetics of the clusters. In Figs. 1 and 2 one can see the potential energy as a function of time over the whole trajectory for all the studied ammonia- and amine-containing clusters, respectively. There are at least two interesting features to notice.

First, an energetic equilibrium is reached in all of the clusters. Typically, this happened within a few picoseconds. The only cluster not to equilibrate within ten picoseconds, was the cluster of (SA)$_4$(Amm)$_3$. Curiously, even 45 ps was not enough to relax the structure. Intrigued by this, the simulation was continued. The cluster finally reached an equilibrium after ~55 ps. To ascertain this, and to collect equilibrium data for the cluster, the simulation was continued for another 35 ps.

In general, the bonding patterns in the studied clusters are largely dictated by proton transfers from sulfuric acid molecules to the base molecules. The proton transfers create ion pairs within the electrically neutral clusters and the resulting hydrogen bonds are relatively strong. In all of the initial starting structures, the base molecules had accepted one proton from the acids. In other words, all the ammonia molecules NH_3 were in the form of NH_4^+ and all the dimethylamine molecules $(CH_3)_2NH$ were in the form of $(CH_3)_2NH_2^+$, that is, as ammonium and dimethylaminium ions,

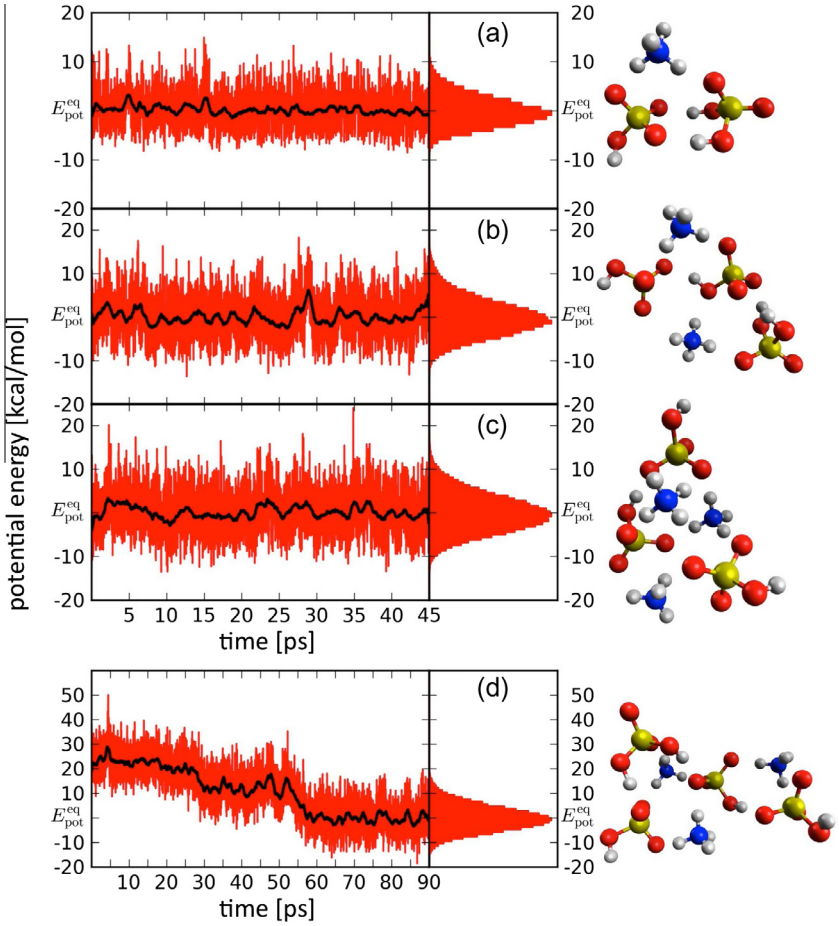

Fig. 1. Potential energy as a function of time for the ammonia-containing clusters at the temperature $T = 300$ K: (a) $(SA)_2(Amm)_1$, (b) $(SA)_3(Amm)_2$, (c) $(SA)_3(Amm)_3$, (d) $(SA)_4(Amm)_3$. The histograms show the potential energy distributions during the equilibrium simulations (from 10 ps to 45 ps), where E_{pot}^{eq} is the mean value of the potential energy at equilibrium. The black curve shows a sliding average of the potential energy with a 1 ps resolution. Note that for the cluster of $(SA)_4(Amm)_3$ the time axis is longer; for this cluster the equilibrium period is from 55 ps to 90 ps. The balls-and-sticks figures show the structures of the clusters at the time 27.5 ps (for the $(SA)_4(Amm)_3$ cluster at 72.5 ps); sulfur atoms are pictured in yellow, oxygen in red, nitrogen in blue, carbon in grey and hydrogen in white. (For interpretation of the references to colour in this figure caption, the reader is referred to the web version of this article.)

respectively. Correspondingly, there were an equal amount of sulfuric acid molecules H_2SO_4 as bisulfate ions HSO_4^- in the clusters. The importance of the proton transfers for the stability of the these clusters has been seen in a number of previous first-principles studies [13,14,18,19,24]. Indeed, the high reactivity of sulfuric acid is probably one of the main reasons why it has such an important role in atmospheric new-particle formation.

Besides $(SA)_4(Amm)_3$, the other two clusters which did not equilibrate immediately were $(SA)_3(DMA)_3$ and $(SA)_4(DMA)_4$. The structural changes in any of these clusters during the equilibration period were not large; in fact, the structural reorganization was rather subtle. However, these minute changes in geometries do have a significant effect in the potential energy (cf. Figs. 1 and 2). This highlights the advantageous features of molecular dynamics. Even for these relatively small molecular clusters, it is already a very challenging task to find the minimum energy geometries at $T = 0$ K. Guessing the cluster structures for $T = 300$ K is yet more difficult, if not impossible, without real dynamical simulations. It should be stressed that during the equilibration there were no proton transfers – the changes in the potential energy arise from molecules finding more optimal bonding patterns.

Secondly, the potential energy is constantly oscillating in all of the clusters. Furthermore, the maximum magnitude of the oscillation is ~10 kcal/mol and is not dependent on the cluster composition or whether the equilibrium is reached or not. Indeed, this is what one would expect: the kinetic energy at the temperature of $T = 300$ K keeps the molecules constantly moving. This thermal motion shows as oscillation in the potential energy, and produces distributions centered around the equilibrium values (cf. distributions in Figs. 1 and 2 and the numerical values in Table 1). The temperature distributions over the entire trajectories are shown in Fig. 3. The obtained distributions are centered at the target temperature of $T = 300$ K confirming that the thermostatting is working properly. It is also noteworthy that none of the temperature distributions show multiple peaks – this is in accordance with the notion that the magnitude of the potential energy oscillation is the same throughout the simulation runs.

The potential energy distributions during the equilibrium simulations provoke interesting considerations. From a cluster point-of-view the physical interpretation is clear: at the temperature of $T = 300$ K there exists a distribution of molecular geometries for each of the studied clusters – likely to be true in general also. One might argue, that in some sense the concept of "global minimum energy structure" is not too meaningful at ambient temperatures; obtaining thermodynamical quantities via the usual machinery of statistical physics from the global minimum energy structures within the harmonic approximation may lead to substantial errors as the kinetic energy contribution is not explicitly considered. In Table 1 the potential energies E_{pot}^{eq} from the simulations are shown relative to the potential energies calculated at the

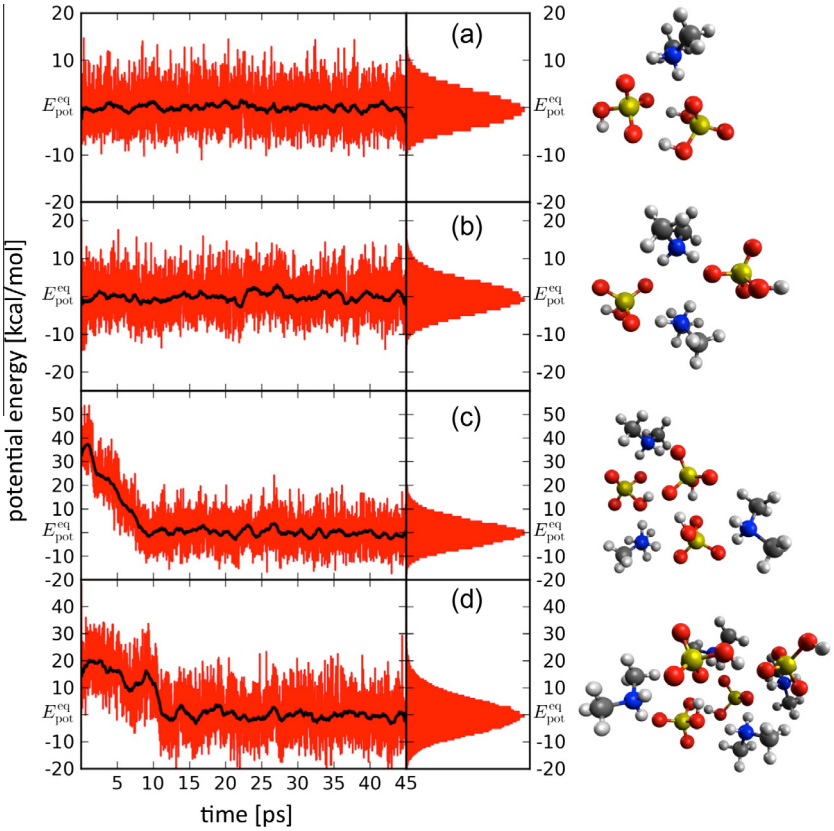

Fig. 2. Potential energy as a function of time for the amine-containing clusters at the temperature $T = 300$ K: (a) $(SA)_2(DMA)_1$, (b) $(SA)_2(DMA)_2$, (c) $(SA)_3(DMA)_3$ and (d) $(SA)_4(DMA)_4$. The histograms show the potential energy distributions during the equilibrium simulations (from 10 ps to 45 ps), where E^{eq}_{pot} is the mean value of the potential energy at equilibrium. The black curve shows a sliding average of the potential energy with a 1 ps resolution. The balls-and-sticks figures show the structures of the clusters at the time 27.5 ps; sulfur atoms are pictured in yellow, oxygen in red, nitrogen in blue, carbon in grey and hydrogen in white. (For interpretation of the references to colour in this figure caption, the reader is referred to the web version of this article.)

Table 1
Mean values of the potential E^{eq}_{pot} and kinetic energy E^{eq}_{kin} after equilibration (last 35 ps of the simulations). The potential energy values are relative to the potential energies of the corresponding optimized structures at $T = 0$ K.

Cluster	E^{eq}_{pot} [kcal/mol]	E^{eq}_{kin} [kcal/mol]
$(SA)_2(Amm)_1$	14.4 ± 3.0	16.0 ± 3.1
$(SA)_3(Amm)_2$	20.9 ± 4.2	25.9 ± 3.9
$(SA)_3(Amm)_3$	25.7 ± 4.3	29.5 ± 4.2
$(SA)_4(Amm)_3$	7.4 ± 5.1	35.8 ± 4.5
$(SA)_2(DMA)_1$	20.6 ± 3.5	21.4 ± 3.6
$(SA)_2(DMA)_2$	27.8 ± 4.2	30.4 ± 4.3
$(SA)_3(DMA)_3$	15.0 ± 5.4	45.6 ± 5.2
$(SA)_4(DMA)_4$	19.0 ± 6.5	60.8 ± 6.0

same level of theory at $T = 0$ K. Table 1 also contains the kinetic energies E^{eq}_{kin} obtained from the simulations. Comparing the values of these two quantities reveals that $E^{eq}_{pot} \neq E^{eq}_{kin}$, indicating that there is anharmonicity in the energetics of the clusters in dynamical equilibrium at $T = 300$ K.

However, an accurate assessment of the dynamical effects and the anharmonicity on the various thermodynamical quantities, such as the formation free energies, is extremely difficult. In this particular study there were no drastic differences in the cluster structures during the simulation compared to the stable static geometries. This might be partly due to the nature of the clusters. As already mentioned, the proton transfers and the subsequent hydrogen bonding patterns between the ion pairs seem to quite decisively dictate the geometries of the clusters. Colloquially, the clusters are looser during the simulations – in particular, the intermolecular bond lengths and angles are continuously evolving. The magnitude of the fluctuation in the distances was moderate and rather uniform throughout the simulations. Fig. 4 shows the radii of gyrations (the average distance from the center of mass), the center-of-mass radii (the largest distance from the center of mass) and the physical radii (half of the largest separation between the atoms) for all the clusters. One can see that the physical dimensions are rather stable.

The physical size of the clusters bears some significance in the growth kinetics. Modeling approaches where the collisions between the molecules and/or clusters are not explicitly considered depend on the bulk values of the molecular and cluster sizes. For example, in kinetic modeling ([34, e.g.]) the colliding molecules and clusters are often assumed to be spherical "liquid droplets" and typically the hard-spheres collision cross sections are used to approximate the collision rates. The hard-spheres collision cross section is proportional to the square of the sum of the radii of the colliding molecules or clusters and thus it is desirable to use as realistic radii as possible. The simulations presented here enable a comparison between the first-principles molecular dynamics radii and the bulk radii. The "liquid drop model" radii together with (hypothetical) electrical mobility radii are shown in Fig. 4. The electrical mobility radius approximates the size at which several instruments would detect the clusters [35]. Comparing the liquid drop model radii to the physical and center-of-mass radii obtained from the simulations reveals that the liquid drop radii differ from these by an average 0.6 Å and 0.9 Å, respectively. In terms of hard-spheres collision cross sections, in the worst case the differences in radii turn into a discrepancy factor of 1.8 in the collisions

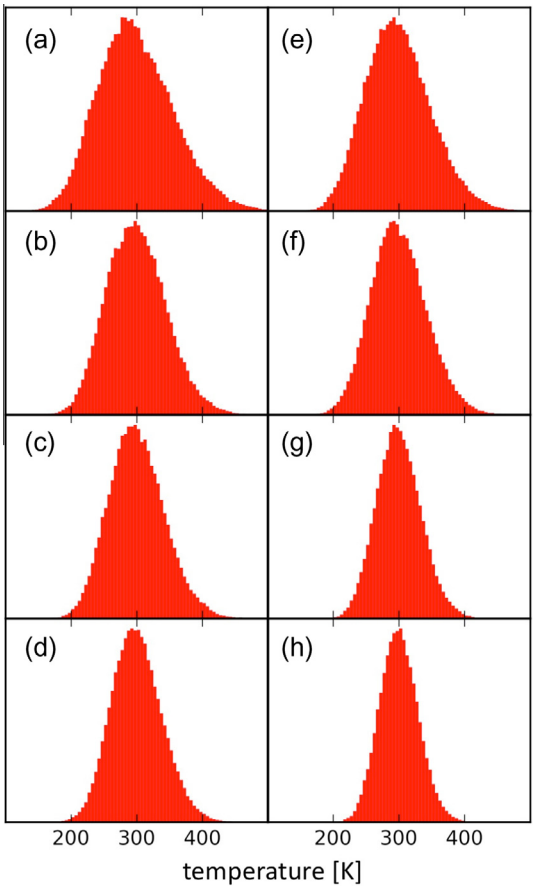

Fig. 3. Temperature distributions of all the studied clusters for the whole length of the simulations. (a) $(SA)_2(Amm)_1$, (b) $(SA)_3(Amm)_2$, (c) $(SA)_3(Amm)_3$, (d) $(SA)_4(Amm)_3$, (e) $(SA)_2(DMA)_1$, (f) $(SA)_2(DMA)_2$, (g) $(SA)_3(DMA)_3$ and (h) $(SA)_4(DMA)_4$.

between the clusters examined here. The bulk approach with an error smaller than a factor of two is a fairly good approximation for the collision cross sections. However, it should be kept in mind that for real molecules and clusters the electronic interactions have larger range than the sharp boundary of a liquid droplet, and it is likely that more crucial uncertainties arise from other aspects of the collision process, such as the sticking factor or cluster rearrangement and fragmentation after collisions.

In addition to showing the fluctuation in the size of the clusters, more information can be extracted from Fig. 4. Comparing the radii of gyrations to the physical radii, one can see how the mass is distributed in the clusters. For example, the physical radii of the two smallest clusters, $(SA)_2(Amm)_1$ and $(SA)_2(DMA)_1$, are roughly equal. However, the radii of gyrations reveal that the mass in $(SA)_2(DMA)_1$ is more dispersed, yielding thus a larger radius of gyration. Conversely, the radii of gyration of the $(SA)_3(DMA)_3$ and $(SA)_4(DMA)_4$ clusters are very similar, but the physical radius of the $(SA)_4(DMA)_4$ is clearly larger. However, the mass must be distributed in a similar fashion in these clusters (cf. the molecular structures in Fig. 2).

A more detailed cluster point-of-view can be obtained by studying radial distribution functions (RDFs). For the molecular clusters in this study, the most interesting RDFs are those between the sulfur atoms and the ones between the sulfur and the nitrogen atoms. The former yields information on how the sulfuric acid molecules coordinate each other and the latter how the acids and bases are coordinated in the clusters. These RDFs for all the studied clusters can be seen in Fig. 5. Fig. 5 shows how the oscillation in energy translates into oscillation in distances; spikes of the stable static structures (shown in Fig. 5 in black) turn into distributions, showing that the distances can, on the average, either increase or decrease when the clusters undergo thermal motion. In addition, the asymmetry in the clusters of $(SA)_3(Amm)_2$ and $(SA)_4(Amm)_3$ – caused by one intact sulfuric acid molecule – can be clearly seen in the sulfur–sulfur RDFs. Interestingly, adding one ammonia molecule to the former cluster leads to a tighter geometry, as can be seen in the $(SA)_3(Amm)_3$ sulfur–sulfur RDF. However, even with the same numbers of acid and base molecules this cluster is not geometrically symmetric, unlike its amine-containing counterpart, cf. (c) and (g) in Fig. 5. In the $(SA)_3(DMA)_3$ cluster each of the amines is coordinated by two acids. In the corresponding ammonia cluster, two of the ammonia molecules are coordinated by three acid molecules and the one remaining base is coordinated by two

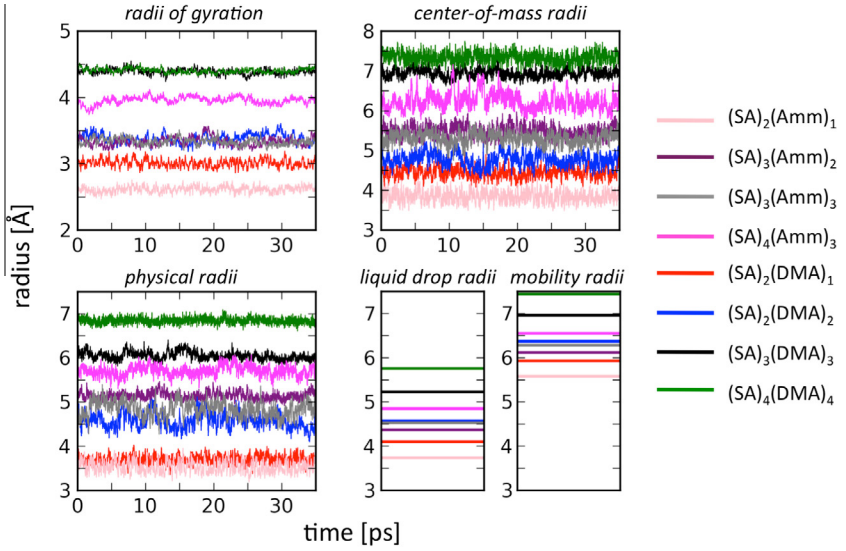

Fig. 4. The radii of gyration, the center-of-mass radii and the physical radii for all the studied clusters (see definitions in the text). The radii are given in Ångströms and the time corresponds to the last 35 ps of the simulation runs. For comparison, the liquid drop model radii r_{ldm} and the hypothetical electrical mobility radii [35], $r_{mobi} = (r_{ldm} + 1.5\text{Å})\left(1 + \frac{28.8\ u}{m_{cluster}}\right)^{1/2}$ where u is the atomic mass unit, are shown as well. The bulk densities needed for r_{ldm} and r_{mobi} are taken from the CRC Handbook of Chemistry and Physics [36].

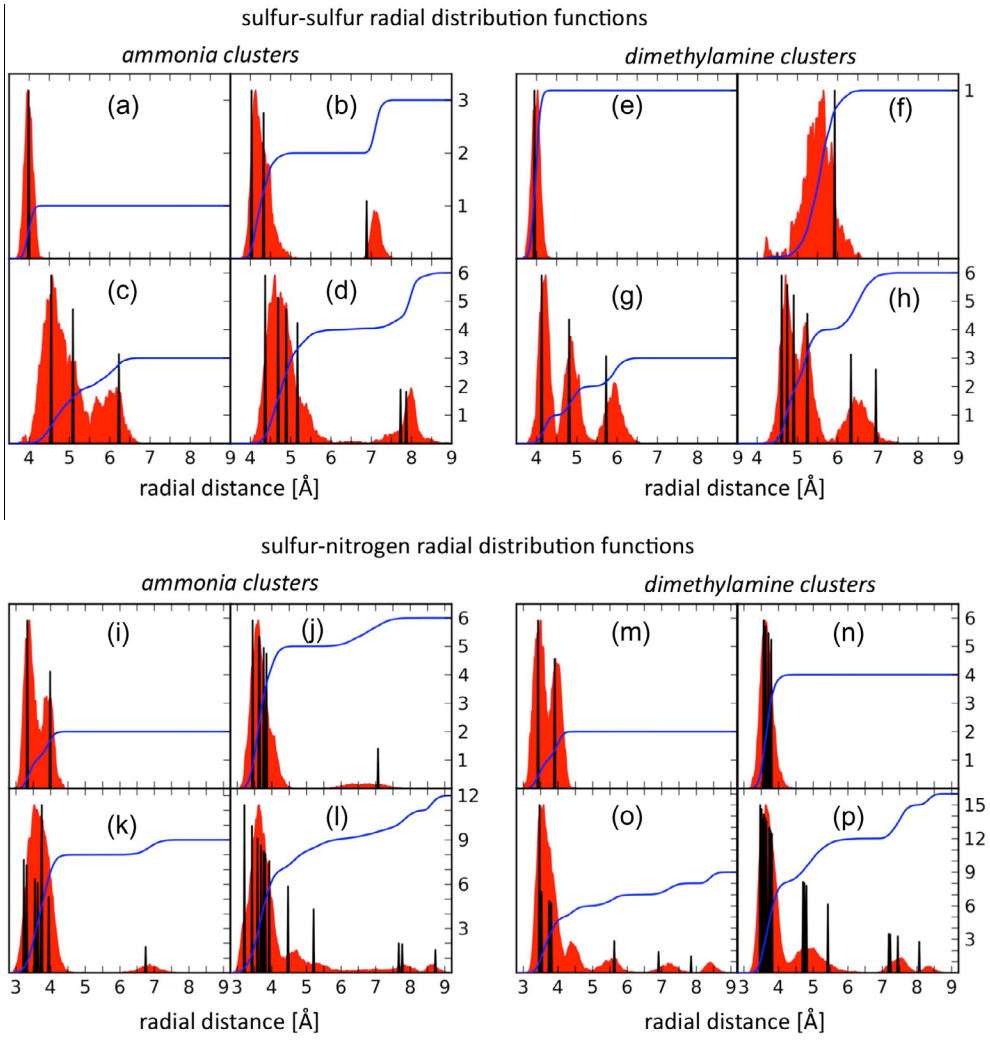

Fig. 5. The sulfur–sulfur and sulfur–nitrogen radial distribution functions (RDFs) of all the studied clusters are shown in red (in arb. units). For comparison, the RDFs of the optimized, static clusters are plotted in black. The blue curves show the coordination numbers (CNs). The CNs measure how many pairs of S–S and S–N atoms are within the radial distance (indicated on the right-hand side ordinate). The static geometries were obtained by optimizing the cluster structures, taken from the equilibrium simulations, at the same level of theory as used in the simulations. (a)&(i) $(SA)_2(Amm)_1$, (b)&(j) $(SA)_3(Amm)_2$, (c)&(k) $(SA)_3(Amm)_3$, (d)&(l) $(SA)_4(Amm)_3$, (e)&(m) $(SA)_2(DMA)_1$, (f)&(n) $(SA)_2(DMA)_2$, (g)&(o) $(SA)_3(DMA)_3$ and (h)&(p) $(SA)_4(DMA)_4$. (For interpretation of the references to colour in this figure caption, the reader is referred to the web version of this article.)

acids. Even though both of the base molecules are able to accept one proton, the number of hydrogen bonds they can participate in is different. Within the clusters ammonia can form up to four bonds, whereas dimethylamine only two. This fact is already significant in the small clusters studied here, but the importance is likely to grow with the size of the clusters. From the structures of the clusters in Fig. 2, one can see that the amine-containing clusters are quite "closed" – what sticks out are the inert methyl groups, especially in $(SA)_3(DMA)_3$ and $(SA)_4(DMA)_4$ clusters. On the other hand, in the ammonia clusters there are "free" hydrogens, potentially available for bonding (cf. Fig. 1).

The simulations also revealed some unexpected dynamical structural behavior. After the clusters had reached equilibrium bonding patterns, these patterns did not change. However, the individual atoms participating in the hydrogen bonds did change. In other words, the molecules in the clusters did not only exhibit thermal vibrations, but also rotations. These concerted rotations were confined by the equilibrium bonding patterns and the symmetry of the molecules. In the ammonia-containing clusters, the rotating species were mainly the singly-protonated ammonium ions, which are very symmetric. In the dimethylamine clusters the rotating molecules were the singly-deprotonated bisulfate ions, where the three free oxygen atoms are symmetric with respect to the center sulfur atom. These rotations can be seen as abrupt changes of the participating atoms in the N–H···O bond distances in Figs. 6 and 7, where the former shows this bond fluctuation in the cluster of $(SA)_3(Amm)_2$ and the latter in the cluster of $(SA)_2(DMA)_2$.

Regardless of the oscillation, vibration and rotation, during the simulations there were no signs of clusters breaking up. Nor were there any signs of donated protons transferring back to bisulfate ions from either of the base molecules. This is one of the most important results of the current paper as the stability of the clusters depends on the proton transfers. Consequently, it is very unlikely that any molecule involved in the proton-transfer-induced ion pair would leave the cluster, and accordingly, this was not observed. In particular for the clusters with an equal number of acids and bases, this suggests that the smallest unit to evaporate would be $(SA)_1(base)_1$. However, also this type of cluster break-up seems to be hindered by the geometry of the studied clusters: both the acid and base molecules are coordinated by more than just one molecule of the other kind. This holds for the other clusters as well:

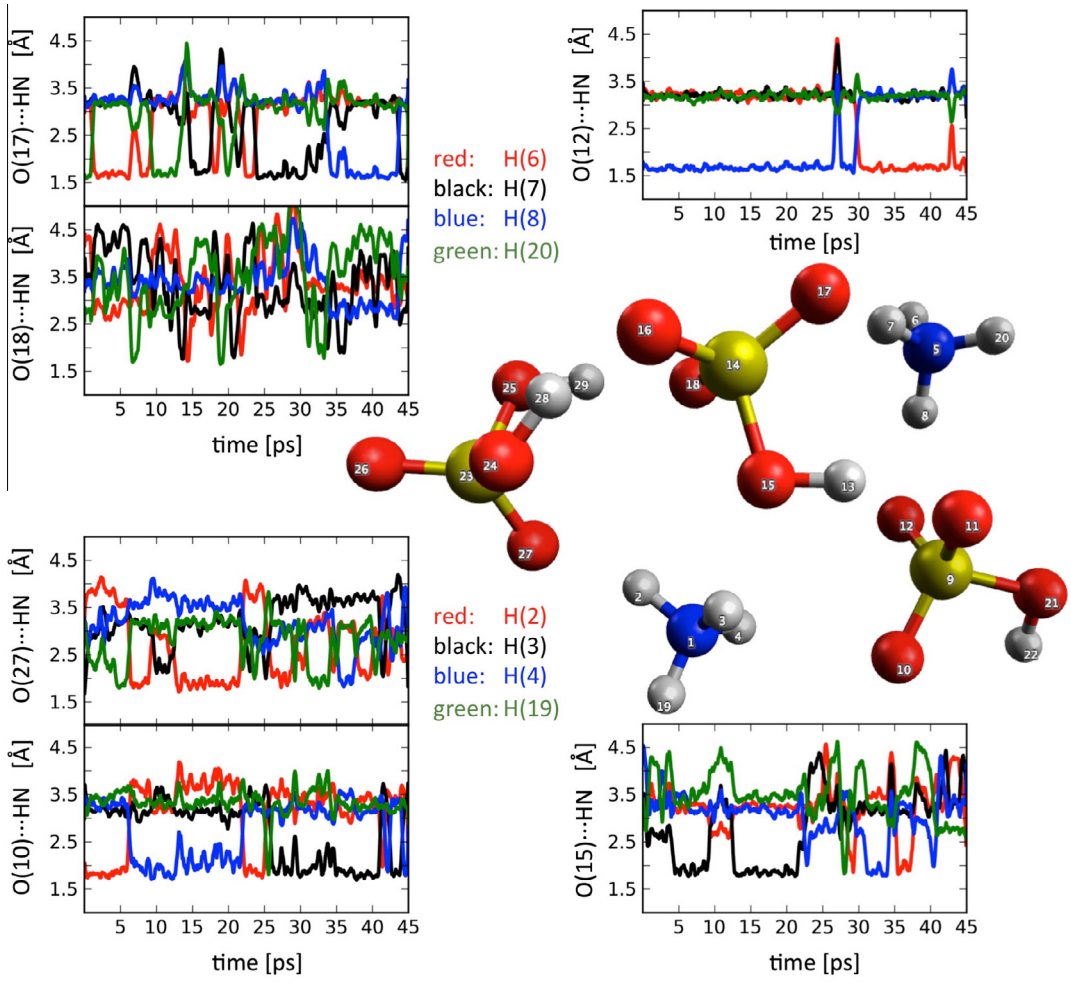

Fig. 6. H-bond fluctuation in the cluster of $(SA)_3(Amm)_2$. The graphs show some of the distances from the hydrogens of the two NH_4^+ molecules to the oxygen atoms of the surrounding bisulfate/sulfuric acid molecules, demonstrating the dynamical nature of the hydrogen bonding in the clusters. Notice that the bonding pattern is conserved regardless of the molecular rotations.

in the clusters of $(SA)_n(base)_{n-1}$ the intact sulfuric acid molecule is always coordinated by more than just one molecule. The high-level of coordination is not unexpected, as we are intentionally studying very stable cluster configurations. It should be noted that most of the studied clusters are not direct collision products of sulfuric acid, ammonia, dimethylamine molecules or even $(SA)_1(base)_1$ units. Rather, the initial clusters were configurations of the constituent molecules which minimize the potential energy at temperature of $T = 0$ K. The results presented in this section show that the clusters seem to be stable at the temperature of $T = 300$ K as well – the thermal energy keeps the molecules vibrating and rotating, but is not enough to break the clusters or significantly transform the geometries away from the very stable static structures.

Molecular dynamics simulations performed in the *NVT* ensemble allow the assessment of the isochoric heat capacity C_V via potential energy fluctuations:

$$C_V = \langle (\Delta E_{pot}^{eq})^2 \rangle / k_B T^2, \quad (1)$$

where $\langle (\Delta E_{pot}^{eq})^2 \rangle$ is the variance of the potential energy during the equilibrium simulations, k_B is the Boltzmann constant and T the temperature. The heat capacities of all the studied clusters are given in Table 2. The uncertainty in the heat capacities is difficult to estimate and it should be kept in mind that the C_V calculated from an *NVT* simulation depends on the thermostat settings. To obtain a crude estimate how the length of the simulation period affects the C_V values, we divided the equilibrium period of 35 ps into blocks of six different sizes: 5 ps, 5.85 ps, 7 ps, 8.75 ps, 11.76 ps and 17.5 ps, thus fitting into the equilibrium period six, five, four, three and two times, respectively. We then evaluated the heat capacities and obtained standard deviations within each block size. Finally, we took the weighted average of the standard deviations as the uncertainty for the final heat capacity, evaluated using the whole equilibrium simulation.

The heat capacities of the ammonia-containing clusters do not show particular systematics with regard to the system size. In contrast, the heat capacity of the amine clusters increases with increasing cluster size. At least partly this is explained by the larger size of the dimethylamine molecule in comparison with the ammonia molecule. Table 2 also contains the heat capacities for all the clusters obtained via structure optimization and the rigid rotor–harmonic oscillator approximation at two different levels of theory: PBE density functional with polarized triple-ζ-Gaussian-type basis set and B3LYP hybrid functional [37] with CBSB7 basis set [38]. The former method is very close to the one used here in the FPMD simulations and the latter has been previously used in several atmospheric cluster studies [18,19,21]. All the static calculations were performed with Gaussian 09 program suite [39] and the cluster structures for the optimizations were taken from the equilibrium simulations.

It is interesting to compare the first-principles molecular dynamics simulations results with the static values. The static heat

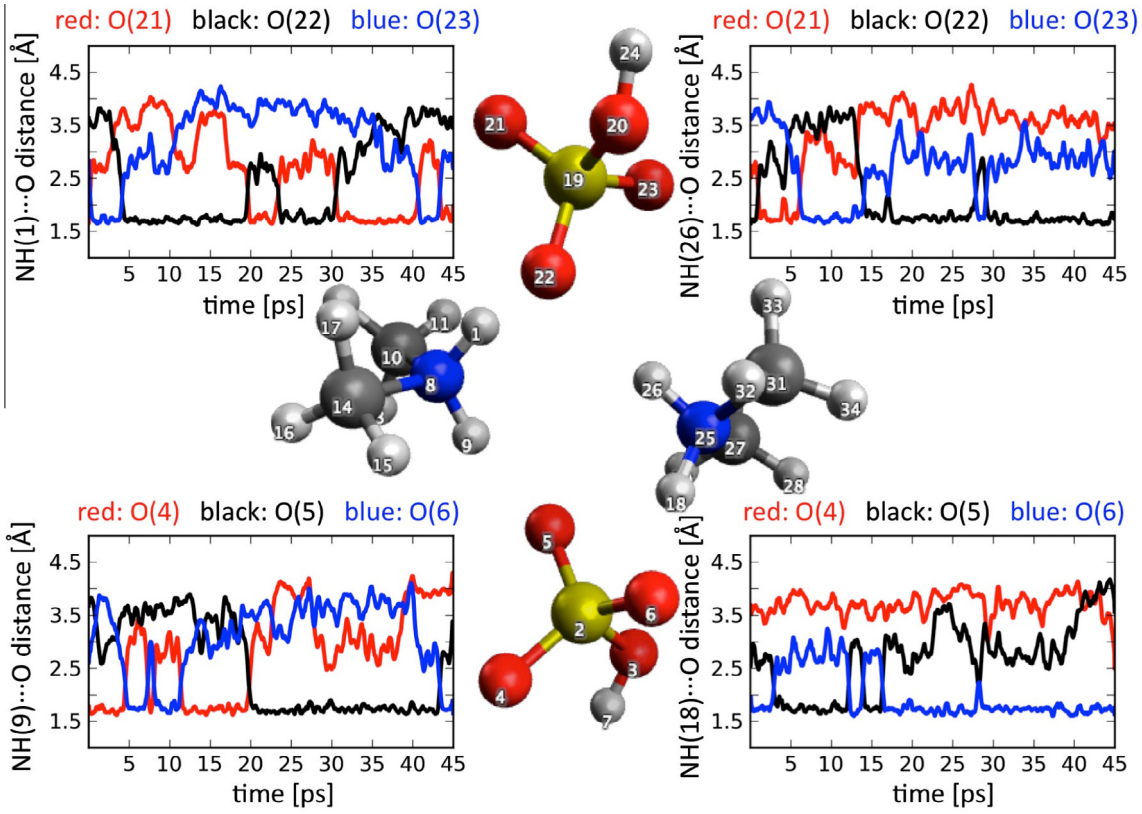

Fig. 7. H-bond fluctuation in the cluster of $(SA)_2(DMA)_2$. The graphs show how the four hydrogen bonds between the sulfuric acid and dimethylamine molecules evolve in time. Notice that the bonding pattern is conserved regardless of the molecular rotations.

Table 2
Heat capacities $\frac{C_V}{\text{molecule}}$ [$\frac{\text{cal}}{\text{mol}}$/K] from the first-principles molecular dynamics simulations at the temperature $T = 300$ K (the column "FPMD"). For comparison, heat capacities from static calculations at two different levels of theory are also shown (see text).

Cluster	FPMD	PBE/TZVP	B3LYP/CBSB7
$(SA)_2(Amm)_1$	17.1 ± 0.9	16.4	15.9
$(SA)_3(Amm)_2$	20.0 ± 2.4	16.0	15.6
$(SA)_3(Amm)_3$	17.3 ± 1.0	15.0	14.7
$(SA)_4(Amm)_3$	20.6 ± 0.7	16.0	15.6
$(SA)_2(DMA)_1$	23.1 ± 1.0	19.4	18.8
$(SA)_2(DMA)_2$	24.3 ± 1.0	19.6	19.1
$(SA)_3(DMA)_3$	27.0 ± 0.9	19.4	18.9
$(SA)_4(DMA)_4$	29.7 ± 2.5	19.7	19.2

capacities are quite uniform within the both sets of clusters – both methods yielding 3–4 kcal/mol larger C_V for the amine clusters and neither capturing the increasing trend for the amine-containing clusters. The main contribution to the static heat capacities comes from the vibrational frequencies, here assumed to be harmonic. Clearly, to capture the thermal movement of the clusters in equilibrium one needs to go beyond the harmonic approximation. This is in concert with the earlier observation that there is anharmonicity in the energetics of the clusters (cf. Table 1) and further, the anharmonicity grows with the system size.

3.2. Dipole moments and vibrational spectra

The interactions between the clusters presented are notoriously weak. In particular in the case of electrically neutral clusters there are no chemical reactions besides proton transfer and the strongest bond between the species is the hydrogen bond. In this landscape the van der Waals interactions become important. For example, it is probable that the electric dipole moment has a role in the collisions between neutral clusters. However, not much is known about the dipoles of the clusters under study. To address this, we have calculated the time-evolution of the electric dipole moments for all the clusters under study.

The first-principles molecular dynamics simulations yielded phase-space trajectories for all the atomic nuclei. We took "snapshots" of these trajectories with an interval of 5 fs and found an approximative location for the negative charge using maximally localized Wannier function centers [40,41]. Knowing the locations of the positive and negative charges, we were able to calculate the electric dipole moments. The dipole moments of all the studied clusters are shown in Fig. 8; the ammonia-containing clusters are on the left pane and the dimethylamine-containing clusters on the right.

Again, there are at least two interesting features in Fig. 8. There is fast, large-amplitude oscillation around the momentary mean values. But unlike in the case of potential energy, here also the mean values are oscillating, although with slower frequency and smaller magnitude. The reason for this undulatory behavior is the same as for the potential energy and bond distance oscillation: thermal molecular movement. However, it seems that the dipole moment is more sensitive than the potential energy to molecular movement. For example, the thermal rotations taking place within the equilibrium bonding patterns do not show up in the potential energy (cf. Figs. 1, 2, 6 and 7), but these rotations are likely to contribute to the fluctuations seen in the electric dipoles (cf. Fig. 8).

The equilibrium values of the electric dipole moments are summarized in Table 3. The cluster data set is too limited in order to draw general systematic conclusions about the dipole moments. However, it is interesting to notice that the electric dipole

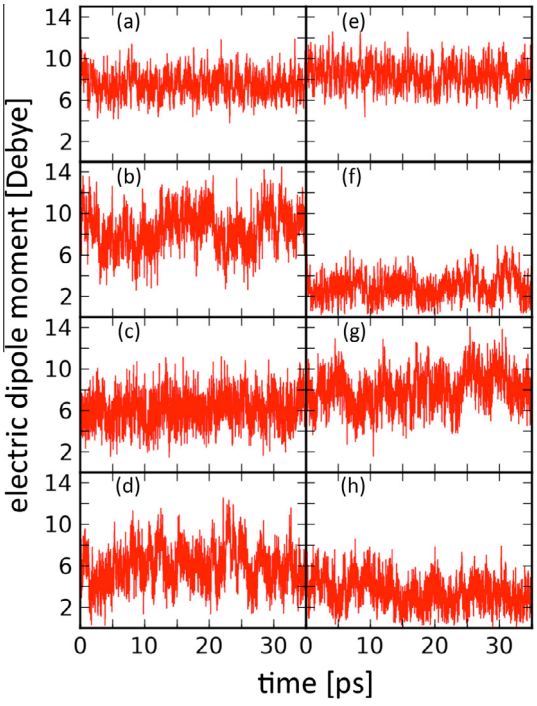

Fig. 8. Electric dipole moments of the studied clusters as a function of time. The time axis corresponds to the last 35 ps of the simulations. (a) $(SA)_2(Amm)_1$, (b) $(SA)_3(Amm)_2$, (c) $(SA)_3(Amm)_3$, (d) $(SA)_4(Amm)_3$, (e) $(SA)_2(DMA)_1$, (f) $(SA)_2(DMA)_2$, (g) $(SA)_3(DMA)_3$ and (h) $(SA)_4(DMA)_4$.

moments of dimethylamine-containing clusters with an even number of acids and bases are considerably smaller than those with an odd number of bases, probably due to symmetry in clusters. The ammonia-clusters do not show similar characteristics.

The electric dipole moment is related to the vibrational–rotational spectrum of the clusters. The thermal fluctuation seen in the dipoles is bound to also have an effect on the spectra of the clusters. To obtain the IR absorption power spectrum $I(\omega)$, we Fourier transformed the autocorrelation function of the electric dipole moment $M(t)$ [42]:

$$I(\omega) \propto \omega \tanh(\beta\hbar\omega/2) \int dt\ e^{-i\omega t} \langle M(t)M(0)\rangle_{eq}, \qquad (2)$$

where $1/\beta = k_B T$ and $k_B, \hbar$ are the Boltzmann and Planck constants, respectively, and T is the temperature. The angular brackets denote the autocorrelation function of the electric dipole moment $M(t)$ taken over the equilibrium simulation with a maximum time-shift of 17.5 ps.

The spectra $I(\omega)$ for all the clusters is shown in Fig. 9. One should note that 35 ps of equilibrium simulation is rather short period for full spectrum analysis; thus the lower-end of the spectra shown here tends to be noisy. Also, the 5 fs interval for evaluating the dipoles limits the high-frequency end of the spectrum, and furthermore, the thermostat coupling constant of 2000 cm^{-1} makes the higher-end of the spectra less reliable. Indeed, the spectra are not shown here out of spectroscopic interest, but rather because they provide yet another view on the thermal molecular motion. The harmonic vibrational spectra are also shown for comparison. Fig. 9 reveals immediately that IR spectroscopy in general is not the most useful tool to study the clusters of sulfuric acid with ammonia or dimethylamine; all the vibrations are centered at two regions, one from the very low end up to 1750 cm^{-1} and another centered below 3000 cm^{-1}. This renders the spectra practically indistinguishable from one another. However, pertinent to the current paper are the differences in the FPMD and harmonic spectra. These differences are a manifestation of the difference in the two approaches, using static structures or performing molecular dynamics simulations. Importantly, in the former approach the inclusion of all the thermal quantities is typically done via the harmonic vibrational frequencies – how well these represent true vibrations is directly related to the reliability of the entropic contribution to the free energies. As can be seen from Fig. 9, the two types of spectra are not identical, but on the other hand, the spectra are not completely different either. The spectra from FPMD simulations are more disperse and consist of numerous peaks, whereas the harmonic spectra consist of sharp and well-defined peaks. As stated in Section 3.1, in the simulations at $T = 300$ K the molecules are under constant thermal motion. All of this motion constitutes

Table 3
Mean values of the electric dipole moments from the first-principles molecular dynamics simulations, corresponding to the last 35 ps of simulations in Figs. 1 and 2. The electric dipole moments are calculated with an interval of 5 fs.

Cluster	Electric dipole moment [Debye]
$(SA)_2(Amm)_1$	7.6 ± 1.1
$(SA)_3(Amm)_2$	8.5 ± 1.9
$(SA)_3(Amm)_3$	6.1 ± 1.5
$(SA)_4(Amm)_3$	5.9 ± 1.8
$(SA)_2(DMA)_1$	8.5 ± 1.2
$(SA)_2(DMA)_2$	2.9 ± 1.2
$(SA)_3(DMA)_3$	8.1 ± 1.7
$(SA)_4(DMA)_4$	3.6 ± 1.4

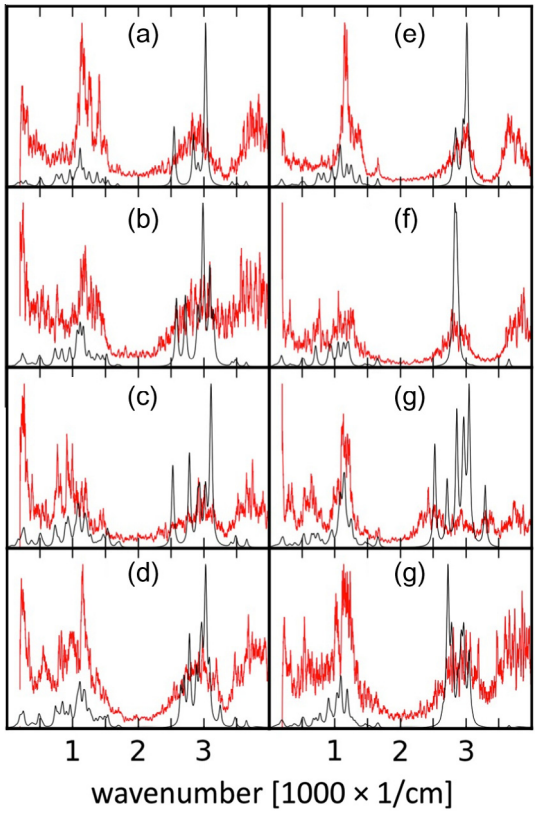

Fig. 9. The IR absorption spectra for all the studied clusters. The spectra in red are obtained from the first-principles molecular dynamics simulations as described in the text. The spectra shown in black are calculated from single static structures within the harmonic approximation using Gaussian 09 program suite [39] at the PBE/TZVP level of theory. (a) $(SA)_2(Amm)_1$, (b) $(SA)_3(Amm)_2$, (c) $(SA)_3(Amm)_3$, (d) $(SA)_4(Amm)_3$, (e) $(SA)_2(DMA)_1$, (f) $(SA)_2(DMA)_2$, (g) $(SA)_3(DMA)_3$ and (h) $(SA)_4(DMA)_4$. (For interpretation of the references to color in this figure legend, the reader is referred to the web version of this article.)

the vibrational spectrum of the cluster in question – including the thermal rotations within the clusters, which are beyond the harmonic approach. However, in this particular study, the proton transfer patterns strongly lock the cluster geometries, and the molecular motion takes place around these dynamical equilibrium geometries. Fig. 9 shows that this motion is not harmonic. In other words, in FPMD simulations the atomic nuclei are not "sitting in harmonic wells" but move more dynamically.

4. Conclusions

We have performed first-principles molecular dynamics simulations to obtain insight into the dynamics and stability of small (sulfuric acid)(ammonia/dimethylamine) clusters. The studied clusters represent prototype examples of stabilized atmospheric sulfuric acid clusters, and as such their properties are important for the formation and further growth of atmospheric aerosol particles. Based on the FPMD simulations, the following conclusions can be drawn:

(a) the kinetic energy at $T = 300$ K keeps the molecules constantly moving – as a consequence, a whole distribution of cluster geometries become relevant, rather than just one minimum energy cluster configuration;
(b) regardless of this movement, the clusters stay bound together – there are no signs of protons transferring back to sulfuric acid molecules from the base molecules or the intact sulfuric acid molecules leaving the clusters;
(c) the electric dipole moments are sensitive to the molecular movement and show large fluctuations; and
(d) the vibrational–rotational spectra of the clusters clearly differ from the harmonic one – demonstrating that the thermal molecular movement in FPMD simulations is not harmonic.

It is worth emphasizing that the initial cluster configurations were products of configuration space sampling and optimization routines, not simple agglomerates of direct molecular collisions. This is an important detail, as the simulations here show that the studied clusters are also rather stable when the effect of kinetic energy is explicitly considered. Now, the interesting question is: do these stable clusters exist in the atmosphere? Or perhaps more accurately, do these stable clusters dominate the cluster configuration distribution for a given cluster composition? To answer these questions is beyond the scope of the present paper. However, the results presented here are intimately related to these issues. For example, when a cluster of one sulfuric acid and one dimethylamine molecule forms, one proton transfer most probably takes place. The potential energy of the complex decreases significantly, thus increasing the kinetic energy. It is plausible that the collisions with the carrier gas take away the excess kinetic energy from the cluster, after which it would evolve as the larger clusters simulated in this paper. However, the formation dynamics of the larger clusters are much more uncertain. As shown here, the bonding patterns of the clusters are rather stable, but for example to go from the cluster of $(SA)_2(DMA)_2$ to $(SA)_3(DMA)_3$ cluster, or from $(SA)_3(DMA)_3$ to $(SA)_4(DMA)_4$, requires breaking the bonding patterns and rearranging the molecules. Typically, it has been assumed that the rearrangement is instantaneous and barrierless. The FPMD simulation results presented here suggest that this might not be the case. From a more applicative point-of-view, these issues would serve to effectively lower the stability of the clusters in terms of formation free energy, as calculated by the standard quantum chemical procedure. Also, the observed distribution of cluster configurations at the temperature of $T = 300$ K and the increasing anharmonicity with growing cluster size are likely to work in the same direction. These interesting questions shall be the focus of the future investigations.

Acknowledgments

This work was financially supported by the Maj and Tor Nessling Foundation (project #2011200), the Academy of Finland (Center of Excellence program project #1118615, LASTU program project #135054) and the European Research Council (project ERC-StG 257360-MOCAPAF). We also thank the Livermore Computing and the Grand Challenge scientific computing program and the CSC – IT Center for Science Ltd for kindly providing computer resources. Part of this work was performed under the auspices of the US Department of Energy under contract DE-AC52–07NA27344.

Appendix A. Supplementary data

Supplementary data associated with this article can be found, in the online version, at http://dx.doi.org/10.1016/j.chemphys.2013.11.014.

References

[1] D.T. Shindell, H. Levy II, M.D. Schwarzkopf, L.W. Horowitz, J.-F. Lamarque, G. Faluvegi, J. Geophys. Res. 113 (2008) D11109.
[2] M.B. Baker, T. Peter, Nature 451 (2008) 299.
[3] M. Kulmala, A. Asmi, H.K. Lappalainen, U. Baltensperger, J.-L. Brenguier, M.C. Facchini, H.-C. Hansson, Ø. Hov, C.D. O'Dowd, U. Pöschl, A. Wiedensohler, R. Boers, O. Boucher, G. de Leeuw, H.A.C. Denier van der Gon, J. Feichter, R. Krejci, P. Laj, H. Lihavainen, U. Lohmann, G. McFiggans, T. Mentel, C. Pilinis, I. Riipinen, M. Schulz, A. Stohl, E. Swietlicki, E. Vignati, C. Alves, M. Amann, M. Ammann, S. Arabas, P. Artaxo, H. Baars, D.C.S. Beddows, R. Bergström, J.P. Beukes, M. Bilde, J.F. Burkhart, F. Canonaco, S.L. Clegg, H. Coe, S. Crumeyrolle, B. D'Anna, S. Decesari, S. Gilardoni, M. Fischer, A.M. Fjaeraa, C. Fountoukis, C. George, L. Gomes, P. Halloran, T. Hamburger, R.M. Harrison, H. Herrmann, T. Hoffmann, C. Hoose, M. Hu, A. Hyvärinen, U. Hõrrak, Y. Iinuma, T. Iversen, M. Josipovic, M. Kanakidou, A. Kiendler-Scharr, A. Kirkevåg, G. Kiss, Z. Klimont, P. Kolmonen, M. Komppula, J.-E. Kristjánsson, L. Laakso, A. Laaksonen, L. Labonnote, V.A. Lanz, K.E.J. Lehtinen, L.V. Rizzo, R. Makkonen, H.E. Manninen, G. McMeeking, J. Merikanto, A. Minikin, S. Mirme, W.T. Morgan, E. Nemitz, D. O'Donnell, T.S. Panwar, H. Pawlowska, A. Petzold, J.J. Pienaar, C. Pio, C. Plass-Duelmer, A.S.H. Prévôt, S. Pryor, C.L. Reddington, G. Roberts, D. Rosenfeld, J. Schwarz, Ø. Seland, K. Sellegri, X.J. Shen, M. Shiraiwa, H. Siebert, B. Sierau, D. Simpson, J.Y. Sun, D. Topping, P. Tunved, P. Vaattovaara, V. Vakkari, J.P. Veefkind, A. Visschedijk, H. Vuollekoski, R. Vuolo, B. Wehner, J. Wildt, S. Woodward, D.R. Worsnop, G.-J. van Zadelhoff, A.A. Zardini, K. Zhang, P.G. van Zyl, V.-M. Kerminen, K. S Carslaw, S.N. Pandis, Atmos. Chem. Phys. 11 (2011) 13061.
[4] M. Kulmala, H. Vehkamäki, T. Petäjä, M. Dal Maso, A. Lauri, V.-M. Kerminen, W. Birmili, P.H. McMurry, Aerosol Sci. 35 (2004) 143.
[5] M. Sipilä, T. Berndt, T. Petäjä, D. Brus, J. Vanhanen, F. Stratmann, J. Patokoski, R.L. Mauldin III, A.-P. Hyvärinen, H. Lihavainen, M. Kulmala, Science 327 (2010) 1243.
[6] R. Zhang, Science 328 (2010) 1366.
[7] C. Kuang, I. Riipinen, S.-L. Sihto, M. Kulmala, A.V. McCormick, P.H. McMurry, Atmos. Chem. Phys. 10 (2010) 8469.
[8] M. Kulmala, L. Pirjola, J.M. Mäkelä, Nature 404 (2000) 66.
[9] F. Yu, R.P. Turco, J. Geophys. Res. 106 (2001) 4797.
[10] H.E. Manninen, T. Nieminen, E. Asmi, S. Gagné, S. Häkkinen, K. Lehtipalo, P. Aalto, M. Vana, A. Mirme, S. Mirme, U. Hõrrak, C. Plass-Dülmer, G. Stange, G. Kiss, A. Hoffer, N. Törő, M. Moerman, B. Henzing, G. de Leeuw, M. Brinkenberg, G.N. Kouvarakis, A. Bougiatioti, N. Mihalopoulos, C. O'Dowd, D. Ceburnis, A. Arneth, B. Svenningsson, E. Swietlicki, L. Tarozzi, S. Decesari, M.C. Facchini, W. Birmili, A. Sonntag, A. Wiedensohler, J. Boulon, K. Sellegri, P. Laj, M. Gysel, N. Bukowiecki, E. Weingartner, G. Wehrle, A. Laaksonen, A. Hamed, J. Joutsensaari, T. Petäjä, V.-M. Kerminen, M. Kulmala, Atmos. Chem. Phys. 10 (2010) 7907.
[11] J. Kirkby, J. Curtius, J. Almeida, E. Dunne, J. Duplissy, S. Ehrhart, A. Franchin, S. Gagné, L. Ickes, A. Kürten, A. Kupc, A. Metzger, F. Riccobono, L. Rondo, S. Schobesberger, G. Tsagkogeorgas, D. Wimmer, A. Amorim, F. Bianchi, M. Breitenlechner, A. David, J. Dommen, A. Downard, M. Ehn, R.C. Flagan, S. Haider, A. Hansel, D. Hauser, W. Jud, H. Junninen, F. Kreissl, A. Kvashin, A. Laaksonen, K. Lehtipalo, J. Lima, E.R. Lovejoy, V. Makhmutov, S. Mathot, J. Mikkilä, P. Minginette, S. Mogo, T. Nieminen, A. Onnela, P. Pereira, T. Petäjä, R. Schnitzhofer, J.H. Seinfeld, M. Sipilä, Y. Stozhkov, F. Stratmann, A. Tomé, J. Vanhanen, Y. Viisanen, A. Vrtala, P.E. Wagner, H. Walther, E. Weingartner, H. Wex, P.M. Winkler, K.S. Carslaw, D.R. Worsnop, U. Baltensperger, M. Kulmala, Nature 476 (2011) 429.

[12] J.M. Mäkelä, S. Yli-Koivisto, V. Hiltunen, W. Seidl, E. Swietlicki, K. Teinilä, M. Sillanpää, I.K. Koponen, J. Paatero, K. Rosman, K. Hämeri, Tellus 53B (2001) 380.
[13] T. Kurtén, V. Loukonen, H. Vehkamäki, M. Kulmala, Atmos. Chem. Phys. 8 (2008) 4095.
[14] V. Loukonen, T. Kurtén, I.K. Ortega, H. Vehkamäki, A.A.H. Pádua, K. Sellegri, M. Kulmala, Atmos. Chem. Phys. 10 (2010) 4961.
[15] J.N. Smith, K.C. Barsanti, H.R. Friedli, M. Ehn, M. Kulmala, D.R. Collins, J.H. Scheckman, B.J. Williams, P.H. McMurry, Proc. Natl. Acad. Sci. 107 (2010) 6634.
[16] B.R. Bzdek, D.P. Ridge, M.V. Johnston, Atmos. Chem. Phys. 10 (2010) 3495.
[17] J. Zhao, J.N. Smith, F.L. Eisele, M. Chen, C. Kuang, P.H. McMurry, Atmos. Chem. Phys. 11 (2011) 10823.
[18] I.K. Ortega, O. Kupiainen, T. Kurtén, T. Olenius, O. Wilkman, M.J. McGrath, V. Loukonen, H. Vehkamäki, Atmos. Chem. Phys. 12 (2012) 225.
[19] O. Kupiainen, I.K. Ortega, T. Kurtén, H. Vehkamäki, Atmos. Chem. Phys. 12 (2012) 3591.
[20] J.H. Zollner, W.A. Glasoe, B. Panta, K.K. Carlson, P.H. McMurry, D.R. Hanson, Atmos. Chem. Phys. 12 (2012) 4399.
[21] P. Paasonen, T. Olenius, O. Kupiainen, T. Kurtén, T. Petäjä, W. Birmili, A. Hamed, M. Hu, L.G. Huey, C. Plass-Duelmer, J.N. Smith, A. Wiedensohler, V. Loukonen, M.J. McGrath, I.K. Ortega, A. Laaksonen, H. Vehkamäki, V.-M. Kerminen, M. Kulmala, Atmos. Chem. Phys. 12 (2012) 9113.
[22] M. Chen, M. Titcombe, J. Jiang, C. Jen, C. Kuang, M.L. Fischer, F.L. Eisele, J.I. Siepmann, D.R. Hanson, J. Zhao, P.H. McMurry, Proc. Natl. Acad. Sci. 109 (2012) 18713.
[23] T. Kurtén, H. Vehkamäki, Adv. Quantum Chem. 55 (2008) 407.
[24] K.E. Anderson, J.I. Siepmann, P.H. McMurry, J. VandeVondele, J. Am. Chem. Soc. 130 (2008) 14144.
[25] J. VandeVondele, M. Krack, F. Mohamed, M. Parrinello, T. Chassaing, J. Hutter, Comput. Phys. Commun. 167 (2005) 103.
[26] G. Lippert, J. Hutter, M. Parrinello, Mol. Phys. 92 (1997) 477.
[27] J.P. Perdew, K. Burke, M. Ernzerhof, Phys. Rev. Lett. 77 (1996) 3865.
[28] M.J. McGrath, J.I. Siepmann, I.-F.W. Kuo, C.J. Mundy, Mol. Phys. 104 (2006) 3619.
[29] I.-F.W. Kuo, C.J. Mundy, M.J. McGrath, J.I. Siepmann, J. Phys. Chem. C 112 (2008) 15412.
[30] J. Elm, M. Bilde, K.V. Mikkelsen, J. Chem. Theory Comput. 8 (2012) 2071.
[31] H.R. Leverentz, J.I. Siepmann, D.G. Truhlar, V. Loukonen, H. Vehkamäki, J. Phys. Chem. A 117 (2013) 3819.
[32] S. Goedecker, M. Teter, J. Hutter, Phys. Rev. B 54 (1996) 1703.
[33] D.J. Tobias, G.L. Martyna, M.L. Klein, J. Phys. Chem. 97 (1993) 12959.
[34] M.J. McGrath, T. Olenius, K. Ortega, V. Loukonen, P. Paasonen, T. Kurtén, M. Kulmala, H. Vehkamäki, Atmos. Chem. Phys. 12 (2012) 2345.
[35] M. Ehn, H. Junninen, S. Schobesberger, H.E. Manninen, A. Franchin, M. Sipilä, T. Petäjä, V.-M. Kerminen, H. Tammet, A. Mirme, S. Mirme, U. Hõrrak, M. Kulmala, D.R. Worsnop, Aerosol Sci. Technol. 45 (2011) 522.
[36] W.M. Haynes (Ed.), CRC Handbook of Chemistry and Physics, ninety fourth ed., (Internet Version 2014), CRC Press/Taylor and Francis, Boca Raton, FL.
[37] A.D. Becke, J. Chem. Phys. 98 (1993) 5648.
[38] J.A. Montgomery, M.J. Frisch, J.W. Ochterski, J. Chem. Phys. 110 (1999) 2822.
[39] Gaussian 09, Revision A.1, M.J. Frisch, G.W. Trucks, H.B. Schlegel, G.E. Scuseria, M.A. Robb, J.R. Cheeseman, G. Scalmani, V. Barone, B. Mennucci, G.A. Petersson, H. Nakatsuji, M. Caricato, X. Li, H.P. Hratchian, A.F. Izmaylov, J. Bloino, G. Zheng, J.L. Sonnenberg, M. Hada, M. Ehara, K. Toyota, R. Fukuda, J. Hasegawa, M. Ishida, T. Nakajima, Y. Honda, O. Kitao, H. Nakai, T. Vreven, J.A. Montgomery, Jr., J.E. Peralta, F. Ogliaro, M. Bearpark, J.J. Heyd, E. Brothers, K.N. Kudin, V.N. Staroverov, R. Kobayashi, J. Normand, K. Raghavachari, A. Rendell, J.C. Burant, S.S. Iyengar, J. Tomasi, M. Cossi, N. Rega, J.M. Millam, M. Klene, J.E. Knox, J.B. Cross, V. Bakken, C. Adamo, J. Jaramillo, R. Gomperts, R.E. Stratmann, O. Yazyev, A.J. Austin, R. Cammi, C. Pomelli, J.W. Ochterski, R.L. Martin, K. Morokuma, V.G. Zakrzewski, G.A. Voth, P. Salvador, J.J. Dannenberg, S. Dapprich, A.D. Daniels, Farkas, J.B. Foresman, J.V. Ortiz, J. Cioslowski, D.J. Fox, Gaussian Inc, Wallingford CT, 2009.
[40] G.H. Wannier, Phys. Rev. 52 (1937) 191.
[41] P.L. Silvestrelli, M. Bernasconi, M. Parrinello, Chem. Phys. Lett. 277 (1997) 478.
[42] B. Guillot, J. Chem. Phys. 95 (1991) 1543.

Paper IV

Molecular Physics, 2014
http://dx.doi.org/10.1080/00268976.2013.877167

RESEARCH ARTICLE

From collisions to clusters: first steps of sulphuric acid nanocluster formation dynamics

Ville Loukonen[a,*], Nicolai Bork[a,b] and Hanna Vehkamäki[a]

[a]*Department of Physics, University of Helsinki, Helsinki, Finland;* [b]*Department of Chemistry, H. C. Ørsted Institute, University of Copenhagen, Copenhagen, Denmark*

(*Received 9 September 2013; accepted 12 December 2013*)

The clustering of sulphuric acid with base molecules is one of the main pathways of new-particle formation in the Earth's atmosphere. First step in the clustering process is likely the formation of a (sulphuric acid)$_1$(base)$_1$(water)$_n$ cluster. Here, we present results from direct first-principles molecular dynamics collision simulations of (sulphuric acid)$_1$(water)$_{0,1}$ + (dimethylamine) → (sulphuric acid)$_1$(dimethylamine)$_1$(water)$_{0,1}$ cluster formation processes. The simulations indicate that the sticking factor in the collisions is unity: the interaction between the molecules is strong enough to overcome the possible initial non-optimal collision orientations. No post-collisional cluster break up is observed. The reasons for the efficient clustering are (i) the proton transfer reaction which takes place in each of the collision simulations and (ii) the subsequent competition over the proton control. As a consequence, the clusters show very dynamic ion pair structure, which differs from both the static structure optimisation calculations and the equilibrium first-principles molecular dynamics simulations. In some of the simulation runs, water mediates the proton transfer by acting as a proton bridge. In general, water is able to notably stabilise the formed clusters by allocating a fraction of the released clustering energy.

Keywords: molecular collisions; first-principles molecular dynamics; atmospheric new-particle formation

1. Background

The significance of sulphuric acid (H_2SO_4, henceforth SA) in atmospheric new-particle formation has been well established [1,2]. Similarly, the need for other participating species in the initial clustering and during the subsequent growth processes is well documented in the literature [3]. However, the exact details of the new-particle formation process are still to be revealed. Recently, an acid–base stabilisation mechanism involving dimethylamine ($(CH_3)_2NH$, henceforth DMA) as the base molecule has been discussed in some detail [4–8]. In essence, the crux of the argument is that SA and DMA form very stable clusters due to proton transfer reactions which are assumed to take place in the process. In addition to calculations performed on various levels of computational sophistication, the argument is strengthened by experimental studies on the enhancing effect of the amines on the new-particle formation [9–12].

A vast majority of the recent theoretical investigations on atmospheric new-particle formation are based on the standard electronic structure calculations procedure (for details, see [13]). In this scheme, one typically seeks the most stable molecular cluster at the temperature $T = 0$ K and then extrapolates to ambient temperatures using the harmonic oscillator–rigid rotor approximation (HORRA). This also entails the assumption of the thermodynamical equilibrium. However, molecular clustering is a very dynamic non-equilibrium phenomenon, and it is debatable to what extent it can be approximated relying on equilibrium concepts. For example, the described standard procedure simplifies the entire statistical mechanical phase space into one or few energetically favourable cluster configurations. This is a drastic approximation and it is known to worsen with increasing temperature and complexity of the system [14,15]. Typically, the approximation is applied only out of computational necessity – sophisticated phase-space sampling methods [16–18] often require at least $\mathcal{O}(10^6)$ energy evaluations per cluster, which is a very significant computational burden, especially at an *ab initio* level. Free energy calculations based on the standard electronic structure procedure are further challenged by the HORRA. Similarly with the previous approximation, the HORRA also worsens as the complexity and temperature of the system grow [14,15,19]. Ideally, theoretical investigations of molecular clustering would take into account both of the described non-ideal contributions. Essentially, this means solving the quantum many-body dynamics for both the electrons and atomic nuclei present in the system. Even with the full power of the current high-performance supercomputers, this goal is still far unattainable. Thus, a practical scientist must seek for a more affordable method to study the phenomenon – a method that is hopefully

* Corresponding author. Email: ville.loukonen@helsinki.fi

not ridden with the discussed approximations. Besides Monte Carlo approaches, one such method is the molecular dynamics simulation.

On a larger scale force-field molecular dynamics simulations have been successfully used to obtain insight into various dynamic physical quantities and features such as the mass accommodation factor [20,21], collision cross-sections [22,23] and post-collisional relaxation of small clusters [24,25]. Unfortunately, the force-field molecular dynamics simulations provide only crude approximations if used to study the first steps of SA-driven new-particle formation due to the very high reactivity of the acid. Thus, one is forced to use a method which is able to account for the changes in the electronic structure of the system on the fly. One method meeting the discussed criteria is the first-principles molecular dynamics (FPMD) simulation. Recently, the applicability of the FPMD simulation to study atmospherically relevant collision processes was demonstrated [26], and here we take the first steps towards investigating the molecular-level dynamics behind the SA clustering process.

We present results from direct FPMD collision simulations for the clustering of (SA) + (DMA) → (SA)(DMA) and (SA)(water) + (DMA) → (SA)(DMA)(water). In atmospheric conditions, most of the SA is most likely hydrated by at least one water molecule [27,28]. This follows from the fact that there are typically 10^{10} times more water than sulphuric acid molecules in the atmosphere. Although the bonding of water with SA is considerably weaker than that with DMA, it is thus essential to study the role of water during the initial clustering.

Above all, this straightforward approach allows the investigation of the sticking factor: can non-optimal collision geometry hinder or prevent the clustering – or can water block the reaction? Furthermore, FPMD simulations reveal the dynamics of the collision: does the proton transfer always happen – or can the transferred proton transfer back to the acid?

These questions are answered in detail in Section 3. First, the technical simulation details are given in Section 2. Discussion concerning the consequences of the results then closes the paper in Section 4.

2. Collision simulations

To probe the dynamics of the (SA)(DMA) and the (SA)(DMA)(water) cluster formation, we performed 12 direct head-on collisions for both the clusters. By varying the starting geometries, we tried to accommodate all the relevant head-on collision possibilities (see Supplemental data Figure S2 and Figure S3 for all the initial collision geometries). Due to the high computational cost (see below), we were only able to study head-on collisions.

The collisions were performed using the Born–Oppenheimer FPMD simulation method with the CP2K program package [29]. We applied the Perdew–Burke–Ernzerhof (PBE) density functional [30] with the dispersion correction D3 devised by Grimme [31]. Recent benchmarking studies [32,33] found the PBE functional to perform quite well for various sulphuric acid containing clusters, especially when used with the dispersion correction. We used an augmented doubly polarised triple-ζ Gaussian-type basis set in the real space together with a plane-wave basis set of cut-off 400 Ry in the momentum space [34]. Norm-conserving Goedecker–Teter–Hutter (GTH) pseudo-potentials were used for the core electronic states [35], and the convergence criterion for the wave-function was 10^{-7} Hartrees. The collisions were performed in a simulation box of $20 \times 20 \times 20$ Å^3, where periodic boundary conditions were not applied in any direction. The Poisson equation was solved according to the scheme by Martyna and Tuckerman [36]. The collisions were run in the *NVE* ensemble.

In all the simulations, a time step of 0.5 fs was used. On the average, we were able to perform one simulation time step in about 0.4 CPU-hours. Given this high computational burden, we chose the initial collision velocities to be roughly twice the relative velocity between the species according to the Maxwell–Boltzmann distribution at a temperature of $T = 300$ K to be able to perform as many collisions as possible and to run the simulations sufficiently long after the collisions. Sensitivity testing revealed that the elevated collision velocities did not change the collision dynamics, but made the molecules collide faster, as desired. The (SA)+(DMA) collisions were let to run for 5 picoseconds (ps) and the (SA)(water)+(DMA) collision for 7 ps.

In addition to the collisions, we also performed equilibrium FPMD simulations for the two clusters, (SA)(DMA) and (SA)(DMA)(water) (cf. Section 3.4). These simulations were performed with the same technical details and at the same level of theory as the collisions, except now in the *NVT* ensemble at a temperature of $T = 300$ K. Each degree of freedom was controlled by a Nosé–Hoover chain thermostat with a coupling constant of 2000 cm^{-1} [37]. The initial cluster configurations were taken from the literature [5] and first optimised with the level of theory used here. Then, the clusters were equilibrated for 3 ps and the data were collected during production runs of 8 ps.

3. Results of the collision simulations

3.1. *Sticking factor = 1*

Perhaps the first thing to observe in the collisions of molecules is whether or not the species stick together – do the molecules bond in such a way they can be said to form a small cluster? If the sticking factor for the (SA) + (DMA) collision significantly differs from unity, it is likely to alter the clustering efficiency, as the formation of the (SA)(DMA) cluster seems to be the very first step in the

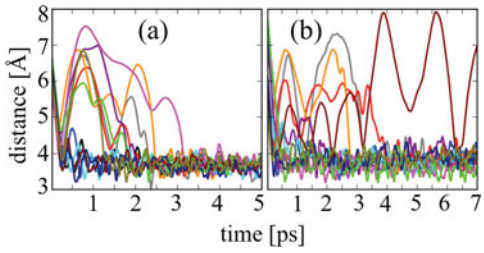

Figure 1. The distance between the centre-of-mass (SA) and centre-of-mass (DMA) in the simulation runs. (a) (SA) + (DMA) → (SA)(DMA) collisions; (b) (SA)(water) + (DMA) → (SA)(DMA)(water) collisions. The distances are given in Å and the time in ps. One (SA)(water)+(DMA) collision took longer (∼9 ps) to find a sticking configuration (see text). Here the centres-of-mass exclude the hydrogens. For more quantitative inspection, a larger figure with a legend is provided in Supplemental data Figure S1.

DMA-enhanced SA clustering process [7]. A suitable metric for the sticking can be obtained from the simulations by monitoring the positions of the centres-of-mass of the molecules. In Figure 1, the distance between the centre-of-mass of the SA and the centre-of-mass of the DMA is shown for each simulation run: in the graph (a) for the (SA) + (DMA) → (SA)(DMA) collisions and in the graph (b) for the (SA)(water) + (DMA) → (SA)(DMA)(water) collisions. Figure 1(a) reveals immediately that there is no significant steric hindrance in the (SA) + (DMA) collisions: non-optimal collision geometry is always overcome within roughly 3 ps. Six of the total 12 collisions lead directly to a cluster within 1 ps. In the other half of the collisions, structural rearrangement is needed before the cluster formation. See Supplemental data Figure S2 for the initial collision geometries.

Very similar conclusions can be drawn from the (SA)(water) + (DMA) collisions. Eleven of the total 12 collisions result in sticking within 4 ps, nine of these already within 2 ps. However, one collision simulation did not stick during the 7 ps of simulation. As the initial structure of the collision in question intuitively looks particularly susceptible for proton transfer, the simulation was continued. After 9 ps, also this simulation led to a bound cluster (see Supplemental data Figure S1 for the sticking and Figure S3 for the initial collision geometries).

Although an FPMD simulation is a very powerful method, care must be taken in the physical interpretation of the results. Inadequate phase-space sampling may lead to an unsatisfactory description of the underlying dynamics. Fortunately, the head-on collisions under investigation here appear to be an on/off system. Besides showing that there is no steric hindrance in the cluster formation, this is demonstrated in Figure 1: after the collisions the molecules stay bound together as a cluster. In neither set of the simulations do the molecules break back to separated monomers (or into a monomer and a dimer). This is due both to the strong ion-enhanced hydrogen bonding, which results from the proton transfer, and to the large enough number of accessible degrees of freedom, which are able to accommodate the energy released in the clustering process.

3.2. *Proton transfer happens always*

In all of the collision simulations, a proton transfer takes place, both in the runs with and without water. The instant in time the proton transfer takes place is highlighted by the maroon vertical lines running through all the subplots in Figures 2 and 3. The dynamics of the transfer are shown by the red curves in the uppermost graphs of each subplot in Figures 2 and 3. These curves show the difference between the distance from the transferred proton to the oxygen it is initially bound (R_{OH}) and to the nitrogen (R_{NH}) which captures it,

$$R_{trans} = R_{OH} - R_{NH}. \quad (1)$$

Thus, the proton transfer is defined to happen when the R_{trans} becomes positive. After the proton transfer, the R_{OH} tracks the distance from the transferred proton to the closest of the SA's oxygens, which is not necessarily the same oxygen it was initially bound to. All the proton transfers in the (SA)+(DMA) collisions and most of the transfers in the (SA)(water) + (DMA) collisions are direct: the proton transfers directly from the SA's oxygen to the DMA's nitrogen atom. However, in five of the collisions including water, the molecular arrangement was such that the direct transfer was not favourable. Basically, the nitrogen's lone pair electrons were too far from both of the SA's hydrogens to induce the reaction. In these cases, the water molecule acts as a proton bridge and the reaction proceeds via Grotthuss-type mechanism. The water transfers a proton to the DMA at the same time as it receives another proton from the SA (cf. Figure 4). The reaction proceeds very rapidly, within 100 fs. Effectively, the water stays as a neutral molecule, just mediating the ion pair formation. After the proton transfer, the electrostatic attraction between HSO_4^- and $(CH_3)_2NH_2^+$ pulls the ions in contact, pushing the water farther away. In Figure 3(b), the evolution of the proton bridge process is shown by the orange curve in the uppermost subplots: the curve shows the differences in the distances measured from the transferred proton similarly to the R_{trans}, but here between the water and the DMA (all the proton bridge processes are shown similarly in Supplemental data Figure S3).

3.3. *The release of energy in the proton transfer is significant*

The potential and the kinetic energies of the (SA) + (DMA) simulations are shown in Figure 2 and for the (SA)(water) + (DMA) collisions in Figure 3: in each subplot the black curve in the middle panel shows the potential energy of the

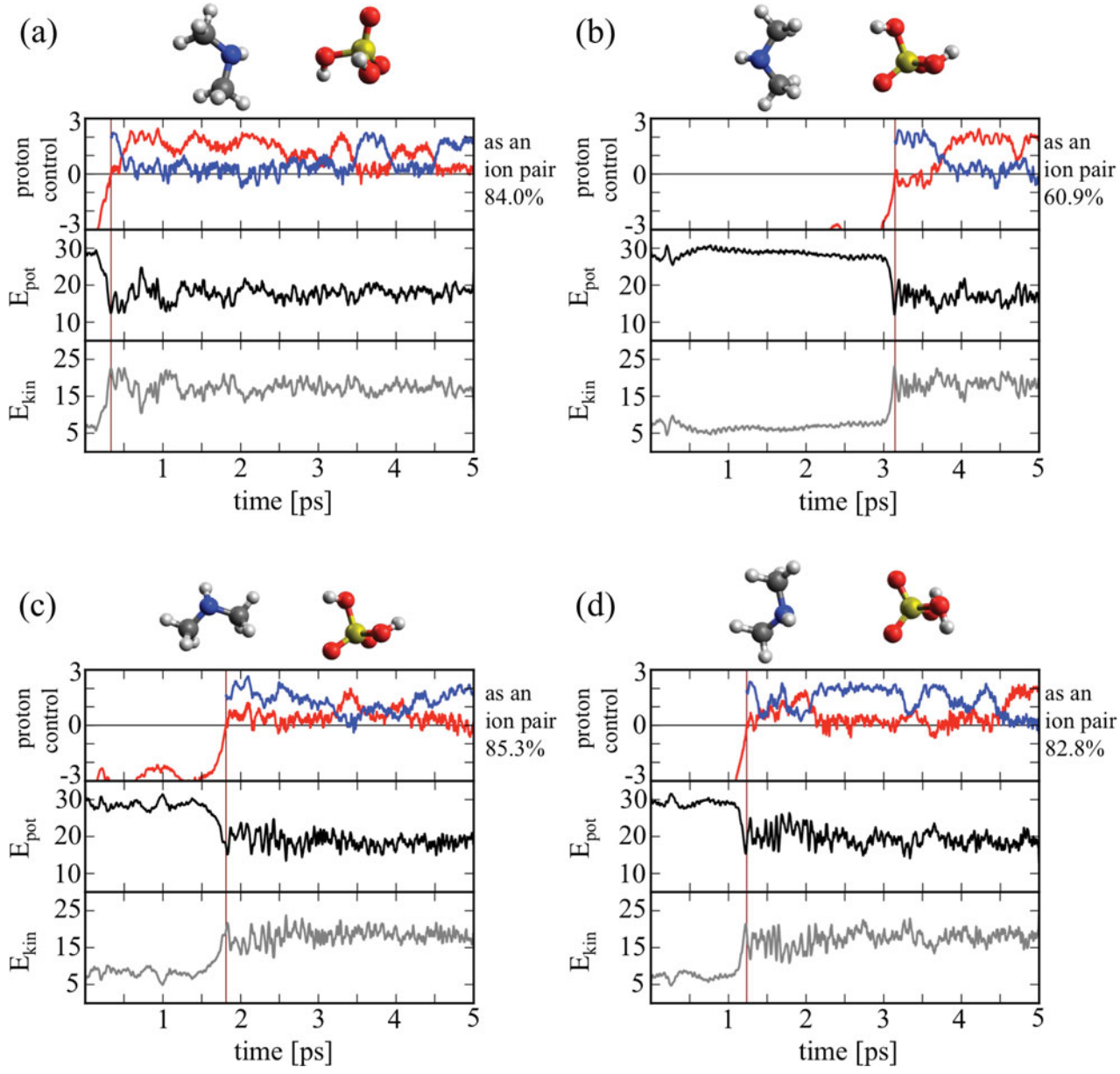

Figure 2. Proton control and the energetics for representative (SA) + (DMA) → (SA)(DMA) collisions. In each graph, the uppermost panel shows the proton control. The red curve (initially negative) shows the proton transfer distance R_{trans} and the blue curve (beginning at the proton transfer; denoted by the vertical lines) corresponds to hydrogen bonding competition R_{comp} in Å (see Equations (1) and (2)). When both the red and blue curves are positive, the system is an ion pair; the percentages of the simulation time the cluster spends as an ion pair after the initial proton transfer are given next to the proton control graphs. The middle panel shows the evolution of the potential energy E_{pot} and the bottommost panel the evolution of the kinetic energy E_{kin} of the whole system. The energies are given in units of kcal/mol. The E_{pot} is measured with respect to the optimised cluster at $T = 0$ K, and the E_{kin} is the total kinetic energy of the system in the centre-of-mass frame. For each run, the initial molecular collision geometry is shown; sulphur atoms are depicted in yellow, oxygens in red, nitrogens in blue, carbons in grey and hydrogens in white.

whole system; the corresponding kinetic energy is shown in the bottommost panel by the grey curve. The potential energy consists of both the intra- and inter-molecular contributions, and is given with reference to the optimised ground-state energies of the clusters at $T = 0$ K. The kinetic energy is given with respect to the centre-of-mass of the cluster. There is a distinctive drop in the potential energy when the proton transfer happens. Coinciding with this, the kinetic energy of the system naturally increases. The average change in the energy caused by the proton transfer in the (SA) + (DMA) collisions is 8.6 ± 1.8 kcal/mol and in the (SA)(water) + (DMA) collisions, 8.0 ± 2.3 kcal/mol

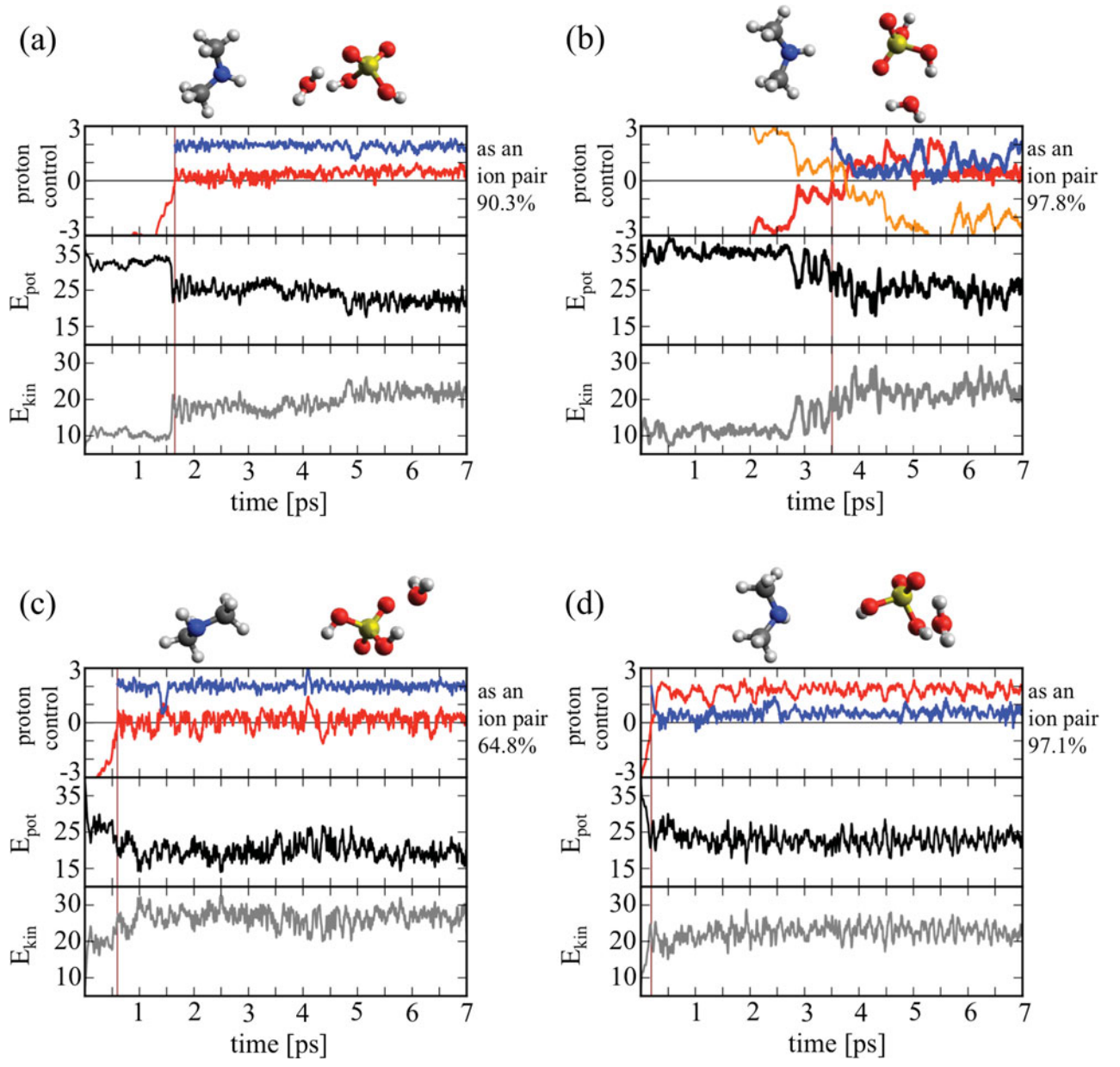

Figure 3. Proton control and the energetics for representative (SA)(water) + (DMA) → (SA)(DMA)(water) collisions. In each graph, the uppermost panel shows the proton control. The red curve (initially negative) shows the proton transfer distance R_{trans} and the blue curve (beginning at the proton transfer; denoted by the vertical lines) corresponds to hydrogen bonding competition R_{comp} in Å (see Equations (1) and (2)). When both the red and blue curves are positive, the system is an ion pair; the percentages of the simulation time the cluster spends as an ion pair after the initial proton transfer are given next to the proton control graphs. In graph (b), the orange curve (initially positive) shows the proton bridge mechanism. The middle panel shows the evolution of the potential energy E_{pot} and the bottommost panel the evolution of the kinetic energy E_{kin} of the whole system. The energies are given in units of kcal/mol. The E_{pot} is measured with respect to the optimised cluster at $T = 0$ K, and the E_{kin} is the total kinetic energy of the system in the centre-of-mass frame. For each run, the initial molecular collision geometry is shown; sulphur atoms are depicted in yellow, oxygens in red, nitrogens in blue, carbons in grey and hydrogens in white.

(averaged over all the runs). This is a considerable amount of energy in the context of small hydrogen-bonded clusters. The released energy keeps the clusters kinetically exited, but importantly is not enough to break the clusters back into monomers (or into a monomer and a dimer), as can be seen in Figures 1, 2 and 3. Also, from the potential and kinetic energy curves in Figures 2 and 3, one can see that in most of the simulation runs the oscillation in the energy relaxes in roughly 1 ps after the proton transfer as more of the accessible degrees of freedom become exited.

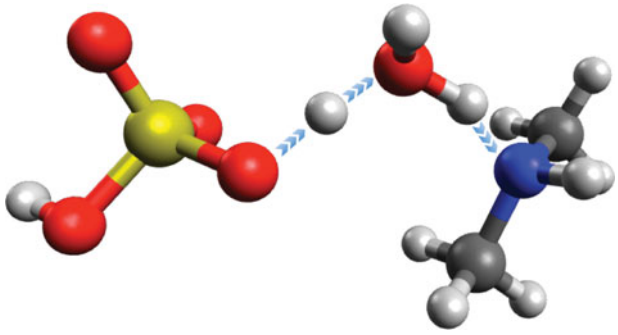

Figure 4. One example of water acting as a proton bridge and mediating the ion pair formation. The proton initially held by the SA is transferring to the water molecule, and one of the water's protons is starting to transfer to the DMA. Colours are as in Figures 2 and 3. The depicted frame corresponds to the simulation run shown in Supplemental data Figure S3(e) at the time 3.058 ps.

On a microscopic scale, the kinetic energy translates into molecular movement. Here, the kinetic energy in the newly formed clusters is bound to have an effect on the bonding. However, the further fate of the clusters is difficult to predict based solely on the presented simulations. After the formation of the studied clusters in the atmosphere, the vast overwhelming majority of the subsequent collisions the clusters undergo will be with inert carrier gas molecules. Assuming a sulphuric acid concentration of 10^6 per cm^3, the clusters collide with the acid monomer roughly once in 4 minutes, whereas they will encounter a carrier gas molecule once in 80 ps under 1 atm pressure and a temperature of 300 K. Dedicated collision simulations investigating the energy transfer between the newly formed clusters and the carrier gas would give valuable insight into the relaxation timescale – however, such simulations are beyond the scope of the current paper.

3.4. *Proton control differs from the equilibrium*

The efficient clustering between DMA and SA (and water) results from the initial proton transfer from SA to DMA and from the subsequent competition over the control of the two protons involved in the bonding. In addition to showing the proton transfer distances R_{trans}, the uppermost graphs in Figures 2 and 3 also show the proton control competition between the SA and DMA. The blue curves in the subplots show the difference in distances from the proton initially bound to DMA to DMA's nitrogen (R'_{NH}) and to SA's closest oxygen atom (R'_{OH}):

$$R_{\text{comp}} = R'_{\text{OH}} - R'_{\text{NH}}. \quad (2)$$

Defined in this way, the positive values correspond to DMA controlling the proton, similarly to the proton transfer distances R_{trans}, shown in red in the same graphs. A combination of these curves thus gives the total picture of the proton control: when both the curves are positive at the same time, DMA controls both protons and consequently, the cluster is an ion pair. Instances where either R_{trans} or R_{comp} is negative correspond to nominally neutral molecules bound by one or more hydrogen bonds. In Figures 2 and 3, the percentage of the time the clusters spend as ion pairs after the initial transfer is given next to the proton control graphs for each collision simulation.

The first aspect to notice is the very dynamic nature of the bonding between the molecules. The proton transfer and the following bonding is far from static. On the average, the (SA)(DMA) cluster is an ion pair 76% ± 8% of the time after the initial proton transfer. The static structure optimisation calculations also predict proton transfer in the (SA)(DMA) clusters [4,5] as reported in the current paper. However, by the nature of these static calculations, no dynamical effects are taken into account. Consequently, all further analysis based on the static calculations implicitly assumes that the cluster of (SA)(DMA) spends 100% of the time as an ion pair. In light of the results presented here, this assumption might be a significant source of error, for example, in the free energy calculations. On the other hand, the cluster analysis based on the structure optimisation calculations typically assumes also that the thermodynamic equilibrium prevails. To obtain insight into the behaviour of the clusters in equilibrium, we simulated the clusters in the *NVT* ensemble at $T = 300$ K, starting directly from the minimum energy structures (cf. simulation details in Section 2). The energetics and proton control of these simulations are shown in Figure 5. In the case of the (SA)(DMA) cluster, the 8 ps equilibrium simulations reveal that the cluster spends 93% of the time as an ion pair (cf. Figure 5(a)). Two interesting conclusions can be drawn. First, the assumption that the cluster of (SA)(DMA) is always an ion pair is not valid and is likely to induce errors in the energetics based on the static calculations, especially if only the most stable configuration is taken into account. Second, the proton control dynamics of the (SA)(DMA) cluster differ significantly between the collision and equilibrium simulations. The reason for this is the released energy in the proton transfer which turns into kinetic energy. To reach equilibrium, the cluster needs to dispose the extra energy. Likely, this will happen via collisions with the carrier gas, as discussed in Section 3.3.

The inclusion of one water molecule changes the proton control dynamics. Based on the collision simulations, the (SA)(DMA)(water) cluster is an ion pair 88% ± 12% of the time after the initial proton transfer. Clearly, water is able to stabilise the ion pair dynamics. The water molecule provides additional degrees of freedom which can allocate some of the kinetic energy within the system. The change in the proton control percentage from the (SA)(DMA) case is quite significant. This can be also distinctively seen by comparing the proton control graphs in Figures 2 and 3: the R_{trans} and R_{comp} curves are much smoother and the oscillation is more restrained in the case of (SA)(DMA)(water) clusters.

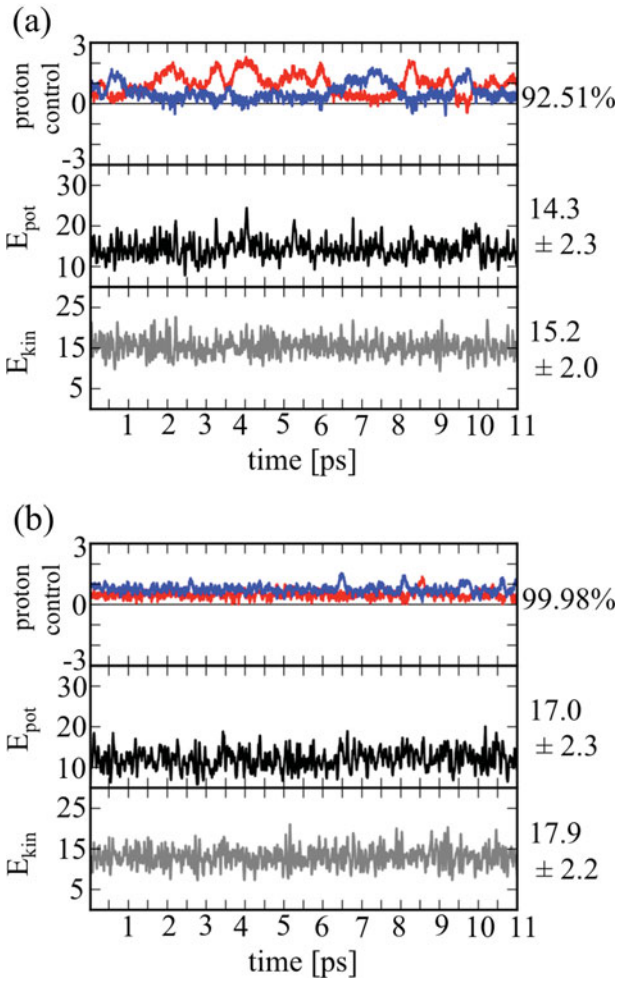

Figure 5. Proton control (in Å) and the energetics (in kcal/mol) of the equilibrium simulations at the temperature of $T = 300$ K; (a) (SA)(DMA), (b) (SA)(DMA)(water). The potential energies E_{pot} are given with respect to the optimised structures. The first 3 ps of the simulations were used to equilibrate the clusters and data was collected during the last 8 ps. The mean values (with standard deviations) are given next to the energies from the last 8 ps together with the proton control percentages. Here the proton control curves (blue and red) show the differences in the distances from the two protons to the DMA's nitrogen and to the closest oxygen atom of the SA or water. As in Figures 2 and 3, positive values correspond to the DMA controlling the protons.

The stabilising effect of water is even more pronounced in the equilibrium simulation at $NVT(T = 300$ K) (cf. Figure 5(b)). The equilibrium simulation agrees well with the static calculations with regard to the proton control, giving 99.98% ion pair percentage for the cluster, as also the static structure optimisation calculations predict the proton transfer [5]. According to the results presented here, we can conclude that the (SA)(DMA)(water) cluster has an ion pair structure under thermodynamical equilibrium at $T =$ 300 K. However, to obtain equilibrium after the collisional formation, the cluster still needs to dispose some of the extra energy, similarly to the (SA)(DMA) cluster. It should also be stressed that although the ion pair percentage of the (SA)(DMA)(water) cluster in equilibrium simulations is practically the same as in the static calculations, there are features in the cluster energetics which go beyond the static approach. For example, Figure 5 shows that the average potential and kinetic energies are not equal in the equilibrium simulation, indicating that the vibrational motion of the clusters is not harmonic [15]. The same applies also to the (SA)(DMA) cluster.

4. Conclusions and discussion

The reported direct FPMD collision simulations present the first steps in deeper and more detailed understanding of atmospheric clustering. The simulations indicate that the proton transfer will always take place in the head-on collisions between SA and DMA, resulting in relatively strongly bound clusters. The presence of one water molecule or non-optimal initial collision geometry is not enough to hinder the reaction. The released energy in the proton transfer keeps the clusters kinetically exited, leading to ion pair cluster structures differing from equilibrium considerations. The existence of water is observed to stabilise the cluster as it can accommodate a portion of the kinetic energy. The stabilising effect of water is in agreement with the previous equilibrium FPMD simulations [15], where already the cluster of $(SA)_2(DMA)_1$ was seen to be an ion pair 100% of the simulation time. Together, these simulation results suggest that the ion pair structure is likely to be conserved when the system possesses an ample amount of degrees of freedom. This in turn implies that the possible cluster reorganisation after collisions happens via ion pairs, and that fragmentation is more likely cluster process than SA monomer evaporation – given that there are enough base molecules to accommodate the proton transfer.

The presented direct collision simulations also indirectly hint at the importance of the entropic contributions to the formation free energies. The observed dynamical nature of the ion pairs is likely to have a contribution to the formation energetics – a contribution which is beyond the reach of the standard electronic structure calculations with the HORRA. Instead, formation free energies based on more complete phase-space sampling with anharmonic motion are called for. For example, thermodynamic integration or metadynamics with FPMD simulations as a physics engine fulfil these requirements; these possibilities will be explored in the future endeavours.

Acknowledgements

We gratefully acknowledge the financial support by the Maj and Tor Nessling Foundation (project #2011200), the Academy of Finland (Center of Excellence program, project #1118615, and LASTU program, project #135054), the European Research Council (project #257360 MOCAPAF) and the Villum Foundation. We also thank the CSC – IT Center for Science Ltd. and the University of Helsinki for providing computational resources.

Supplemental data

Supplemental data for this article can be accessed here.

References

[1] M. Kulmala, H. Vehkamäki, T. Petäjä, M. Dal Maso, A. Lauri, V.-M. Kerminen, W. Birmili, and P.H. McMurry, Aerosol Sci. **35**, 143 (2004).

[2] C. Kuang, P.H. McMurry, A.V. McCormick, and F.L. Eisele, J. Geophys. Res. **113**, D10209 (2008).

[3] R. Zhang, Science **328**, 1366 (2010).

[4] T. Kurtén, V. Loukonen, H. Vehkamäki, and M. Kulmala, Atmos. Chem. Phys. **8**, 4095 (2008).

[5] V. Loukonen, T. Kurtén, I.K. Ortega, H. Vehkamäki, A.A.H. Pádua, K. Sellegri, and M. Kulmala, Atmos. Chem. Phys. **10**, 4961 (2010).

[6] J.W. DePalma, B.R. Bzdek, D.J. Doren, and Murray V. Johnston, J. Phys. Chem. A **116**, 1030 (2012).

[7] M.J. McGrath, T. Olenius, I.K. Ortega, V. Loukonen, P. Paasonen, T. Kurtén, M. Kulmala, and H. Vehkamäki, Atmos. Chem. Phys. **12**, 2345 (2012).

[8] I.K. Ortega, O. Kupiainen, T. Kurtén, T. Olenius, O. Wilkman, M.J. McGrath, V. Loukonen, and H. Vehkamäki, Atmos. Chem. Phys. **12**, 225 (2012).

[9] J.N. Smith, K.C. Barsanti, H.R. Friedli, M. Ehn, M. Kulmala, D.R. Collins, J.H. Scheckman, B.J. Williams, and P.H. McMurry, Proc. Natl. Acad. Sci. **107**, 6634 (2010).

[10] J. Zhao, J.N. Smith, F.L. Eisele, M. Chen, C. Kuang, and P.H. McMurry, Atmos. Chem. Phys. **11**, 10823 (2011).

[11] J.H. Zollner, W.A. Glasoe, B. Panta, K.K. Carlson, P.H. McMurry, and D.R. Hanson, Atmos. Chem. Phys. **12**, 4399 (2012).

[12] J. Almeida, S. Schobesberger, A. Kürten, I.K. Ortega, O. Kupiainen–Määttä, A.P. Praplan, A. Adamov, A. Amorim, F. Bianchi, M. Breitenlechner, A. David, J. Dommen, N.M. Donahue, A. Downard, E. Dunne, J. Duplissy, S. Ehrhart, R.C. Flagan, A. Franchin, R. Guida, J. Hakala, A. Hansel, M. Heinritzi, H. Henschel, T. Jokinen, H. Junninen, M. Kajos, J. Kangasluoma, H. Keskinen, A. Kupc, T. Kurtén, A.N. Kvashin, A. Laaksonen, K. Lehtipalo, M. Leiminger, J. Leppä, V. Loukonen, V. Makhmutov, S. Mathot, M.J. McGrath, T. Nieminen, T. Olenius, A. Onnela, T. Petäjä, F. Riccobono, I. Riipinen, M. Rissanen, L. Rondo, T. Ruuskanen, F.D. Santos, N. Sarnela, S. Schallhart, R. Schnitzhofer, J.H. Seinfeld, M. Simon, M. Sipilä, Y. Stozhkov, F. Stratmann, A. Tomé, J. Tröstl, G. Tsagkogeorgas, P. Vaattovaara, Y. Viisanen, A. Virtanen, A. Vrtala, P.E. Wagner, E. Weingartner, H. Wex, C. Williamson, D. Wimmer, P. Ye, T. Yli-Juuti, K.S. Carslaw, M. Kulmala, J. Curtius, U. Baltensperger, D.R. Worsnop, H. Vehkamäki, and J. Kirkby, Nature **502**, 359 (2013).

[13] T. Kurtén and H. Vehkamäki, Adv. Quant. Chem. **55**, 407 (2008).

[14] S. Kathmann, G. Schenter, and B. Garrett, J. Phys. Chem. C **111**, 4977 (2007).

[15] V. Loukonen, I-F.W. Kuo, M.J. McGrath, and H. Vehkamäki, Chem. Phys. **428**, 164 (2014).

[16] B. Chen and J.I. Siepmann, J. Phys. Chem. B **104**, 8725 (2000).

[17] B. Chen, J.I. Siepmann, and M.L. Klein, J. Phys. Chem. A **109**, 1137 (2005).

[18] S.M. Kathmann, G.K. Schenter, B.C. Garrett, B. Chen, and J.I. Siepmann, J. Phys. Chem. C **113**, 10354 (2009).

[19] S.M. Kathmann, G.K. Schenter, and B.C. Garrett, J. Chem. Phys. **116**, 5046 (2002).

[20] X. Ma, P. Chakraborty, B.J. Henz, and M.R. Zachariah, Phys. Chem. Chem. Phys. **13**, 9374 (2011).

[21] J. Julin, M. Shiraiwa, R.E.H. Miles, J.P. Reid, U. Pöschl, and I. Riipinen, J. Phys. Chem. A **117**, 410 (2013).

[22] J. Lengyel, J. Kočišek, V. Poterya, A. Pysanenko, P. Svrčková, M. Fárník, D.K. Zaouris, and J. Fedor, J. Chem. Phys. **137**, 034304 (2012).

[23] I. Napari and H. Vehkamäki, J. Chem. Phys. **120**, 165 (2004).

[24] I. Napari and H. Vehkamäki, J. Chem. Phys. **124**, 024303 (2006).

[25] I. Napari and H. Vehkamäki, J. Chem. Phys. **125**, 094313 (2006).

[26] N. Bork, V. Loukonen, and H. Vehkamäki, J. Phys. Chem. A **117**, 3143 (2013).

[27] T. Kurtén, M. Noppel, H. Vehkamäki, M. Salonen, and M. Kulmala, Boreal Env. Res. **12**, 431 (2007).

[28] B. Temelso, T.E. Morrell, R.M. Shields, M.A. Allodi, E.K. Wood, K.N. Kirschner, T.C. Castonguay, K.A. Archer, and G.C. Shields, J. Phys. Chem. A **116**, 2209 (2012).

[29] Freely available from www.cp2k.org under the GPL license.

[30] J.P. Perdew, K. Burke, and M. Ernzerhof, Phys. Rev. Lett. **77**, 3865 (1996).

[31] S. Grimme, J. Comput. Chem. **27**, 1787 (2006).

[32] J. Elm, M. Bilde, and K.V. Mikkelsen, J. Chem. Theory Comput. **8**, 2071 (2012).

[33] H.R. Leverentz, J.I. Siepmann, D.G. Truhlar, V. Loukonen, and H. Vehkamäki, J. Phys. Chem. A **117**, 3819 (2013).

[34] G. Lippert, J. Hutter, and M. Parrinello, Mol. Phys. **92**, 477 (1997).

[35] S. Goedecker, M. Teter, and J. Hutter, Phys. Rev. B **54**, 1703 (1996).

[36] G.J. Martyna and Mark E. Tuckerman, J. Chem. Phys. **110**, 2810 (1999).

[37] D.J. Tobias, G.L. Martyna, and M.L. Klein, J. Phys. Chem. **97**, 12959 (1993).